INVESTIGATION OF VISCOUS LINE VORTICES WITH AND WITHOUT THE INJECTION OF CORE TURBULENCE

Andrew D. Zalay, et al

Rochester Applied Science Associates, Incorporated

Prepared for:

Office of Naval Research

February 1974

UNCLASSIFIED

Security Classification

AD-785256

DOCUMENT CONTROL DATA - R & D

(Security classification of title, body of abstract and indexing annotation must be entered when the overall report is classified)

1. ORIGINATING ACTIVITY (Corporate author)
Rochester Applied Science Associates, Inc.
140 Allens Creek Road
Rochester, New York 14618

2a. REPORT SECURITY CLASSIFICATION
UNCLASSIFIED

2b. GROUP
N/A

3. REPORT TITLE

INVESTIGATION OF VISCOUS LINE VORTICES WITH AND WITHOUT THE INJECTION OF CORE TURBULENCE

4. DESCRIPTIVE NOTES (Type of report and inclusive dates) FINAL REPORT
15 February 1973 - 14 February 1974

5. AUTHOR(S) (First name, middle initial, last name)
Andrew D. Zalay
Richard P. White, Jr.
John C. Balcerak

6. REPORT DATE	7a. TOTAL NO. OF PAGES	7b. NO. OF REFS
February 1974	159	35

8a. CONTRACT OR GRANT NO	9a. ORIGINATOR'S REPORT NUMBER(S)
N00014-71-C-0226	74-01
b. PROJECT NO.	
c.	9b. OTHER REPORT NO(S) (Any other numbers that may be assigned this report)
d.	

10. DISTRIBUTION STATEMENT
Approved for Public Release; Distribution Unlimited
Reproduction in whole or part is permitted for any purpose of the United States Government

11. SUPPLEMENTARY NOTES	12. SPONSORING MILITARY ACTIVITY
	OFFICE OF NAVAL RESEARCH AERODYNAMICS CODE 411 ARLINGTON, VIRGINIA 22217

13. ABSTRACT

An experimental research program was conducted to investigate the general characteristics of a line vortex trailed from a three-dimensional lifting surface, and to determine how its general velocity distribution, turbulence level, turbulent frequency content, and dissipation rates are affected by the injection of a jet of turbulent air and by a fixed turbulence generator. Three component hot-wire surveys indicated that injection of the vortex core reduced the peak tangential velocity, established a strong axial flow component, increased the core diameter, altered the turbulence spectrum, and enhanced the turbulence level in the viscous core. Correlation of these observed vortex parameters with existing vortex decay models demonstrated that the injection of a trailing vortex leads to a significant enhancement of the natural decay process. Scaling and application of the vortex injection technique to full-scale aircraft suggested that with 2% of the total available thrust, the vortex injection system may reduce the aircraft separation criteria, dictated by the vortex wake hazard, by an order of magnitude.

DD FORM 1 NOV 1473 REPLACES DD FORM 1473, 1 JAN 64, WHICH IS OBSOLETE FOR ARMY USE.

UNCLASSIFIED

Security Classification

14. KEY WORDS	LINK A		LINK B		LINK C	
	ROLE	WT	ROLE	WT	ROLE	WT
HOT WIRE MEASUREMENTS						
TIP VORTEX						
TURBULENCE						
SWIRLING FLOW						
VORTEX DISSIPATION						
VORTEX FLOW						

RASA REPORT 74-01

INVESTIGATION OF VISCOUS LINE VORTICES WITH AND WITHOUT THE INJECTION OF CORE TURBULENCE

February 1974

By
Andrew D. Zalay
Richard P. White
John C. Balcerak

Prepared under Contract No. N00014-71-C-0226
NR 215-170

For

OFFICE OF NAVAL RESEARCH
AERODYNAMICS CODE 411
DEPARTMENT OF THE NAVY
Arlington, Virginia 22217

By

ROCHESTER APPLIED SCIENCE ASSOCIATES, INC.
140 Allens Creek Road, Rochester, New York 14618
716/271-3450

ib

FOREWORD

The work described in this report was performed by Rochester Applied Science Associates, Inc. for the Department of the Navy, Office of Naval Research, Arlington, Virginia, under Contract Number N00014-71-C-0226. The research program was undertaken under the technical cognizance of Mr. Thomas Wilson.

Appreciation is extended by the authors to Dr. Martin Lessen, Yates Memorial Professor of Engineering, Department of Mechanical and Aerospace Sciences at the University of Rochester and his graduate students Frederick Paillet and Pawan Jit Singh for making available the results of their numerical trailing vortex stability calculations.

The authors also wish to express their appreciation to Dr. Kevin Johnson at RASA for his valuable assistance in the acquisition and data reduction phase and to Mr. Donald Gross and his staff at the University of Maryland Wind Tunnel Facility for their valuable assistance during the wind tunnel tests.

ABSTRACT

An experimental research program was conducted to investigate the general characteristics of a line vortex trailed from a three-dimensional lifting surface, and to determine how its general velocity distribution, turbulence level, turbulent frequency content, and dissipation rates are affected by the injection of a jet of turbulent air and by a fixed turbulence generator. Three component hot-wire surveys indicated that injection of the vortex core reduced the peak tangential velocity, established a strong axial flow component, increased the core diameter, altered the turbulence spectrum, and enhanced the turbulence level in the viscous core. Correlation of these observed vortex parameters with existing vortex decay models demonstrated that the injection of a trailing vortex leads to a significant enhancement of the natural decay process. Scaling and application of the vortex injection technique to full-scale aircraft suggested that with 2% of the total available thrust, the vortex injection system may reduce the aircraft separation criteria, dictated by the vortex wake hazard, by an order of magnitude.

TABLE OF CONTENTS

		Page
FOREWORD		ii
ABSTRACT		iii
LIST OF SYMBOLS		v
LIST OF TABLES		viii
LIST OF ILLUSTRATIONS		ix
I.	INTRODUCTION	1
II.	DESCRIPTION OF MODELS AND INSTRUMENTATION	5
	A. Models	5
	B. Instrumentation	6
	C. Calibration	10
III.	WIND TUNNEL TESTS	12
IV.	DISCUSSION OF RESULTS	14
	A. Typical hot-wire velocity measurements	15
	B. Velocity distribution of the trailing vortex	18
	C. Turbulent velocity distribution of the trailing vortex	29
	D. Correlation with theoretical and empirical models	41
	E. Velocity distribution of the trailing vortex based on vorticity meter surveys	49
	F. Scaling and application of vortex injection system to flight vehicles	55
V.	CONCLUSIONS	65
VI.	RECOMMENDATIONS	71
VII.	REFERENCES	72
APPENDIX		141

LIST OF SYMBOLS

A	area of jet, ft^2
A_1, A_2, A_3	constants
AR	aspect ratio
a_1	Townsend parameter (equal to 0.15)
B_1, B_2, B_3	constants
C, C_1, C_2, C_3	constants, ft/sec volts
C_D	drag coefficient, D/qS
C_{D_i}	induced drag coefficient, $C_L^2/\pi AR$
C_L	lift coefficient, L/qS
C_ℓ	section lift coefficient, L/qc
c	chord, in.
$dC_\ell/d\alpha$	slope of the lift curve, 1/radians
D	drag force, lbs
k	calibration constant for vorticity meter, k = 27.8 sec/ft
L	Prandtl mixing length, in.
$\dot{m}$	mass flow from injection nozzle, lb/sec
m	constant
n	wave number
R	radius of helicopter rotor, in.
r	radial distance, in.
r_c	radius of vortex core, in.
q	dynamic pressure, lb/ft^2
$\sqrt{q^2}$	rms turbulent velocity, ft/sec
S	projected wing lifting area, ft^2
s	semispan of wing, ft
T	thrust, lb
U_∞	freestream velocity, ft/sec
U_j	jet exit velocity, ft/sec

V_{x_1}, V_{y_1}, V_{z_1}	voltage output from x, y, z anemometers, volts
V_{x_2}, V_{y_2}, V_{z_2}	voltage output from x, y, z linearizers, volts
V_{x_3}, V_{y_3}, V_{z_3}, V_{t_3}	voltage output from the transformation computer in the x, y, z coordinate system and the total component $V_{t_3} = \sqrt{V_{x_3} + V_{y_3}^2 + V_{z_3}^2}$, volts
v_x'', v_y'', v_z''	velocity perpendicular to the hot-wire elements, ft/sec
v_x', v_y', v_z'	velocity in a coordinate system oriented along the hot-wire elements, ft/sec
v_x, v_y, v_z	velocity in the wind tunnel coordinate system, ft/sec
v_r, v_θ, v_z	velocity in a cylindrical coordinate system with the origin located at the center of the vortex core, ft/sec
v_{t_3}	total velocity component, ft/sec $v_{t_3} = \sqrt{v_x^2 + v_y^2 + v_z^2}$
$v_{\theta m}$, $v_{\theta max}$	peak tangential velocity of trailing vortex, v_θ measured at $r=r_c$, ft/sec
v_{zm}, $v_{z\ max}$	peak axial velocity of trailing vortex, v_z measured at r=0, ft/sec
w	upwash velocity, ft/sec
x, x_1	distance along x coordinate, ft/sec
α	angle of attack, deg
α_R	root angle of attack, deg
Γ	circulation strength, ft^2/sec
Γ_c	core circulation strength, $\Gamma_c=\Gamma(r=r_c)$, ft^2/sec
Γ_o	total circulation strength, $\Gamma=\Gamma(r=\infty)$, ft^2/sec

ν	kinematic viscosity, ft^2/sec
ν_T	turbulent eddy kinematic viscosity, ft^2/sec
ξ	vorticity, 1/sec
ρ	density of air, ρ=0.00238 slugs
η	vorticity meter calibration factor, ratio of rotational velocity of vanes to fluid

LIST OF TABLES

Table		Page
1.	Summary of Wind Tunnel Trailing Vortex Test Conditions	76
2.	Summary of General Trailing Vortex Parameters Measured by Hot-Wire Surveys	77
3.	Survey of Published Trailing Vortex Characteristics	79

LIST OF ILLUSTRATIONS

Figure		Page
1.	21-inch chord semispan model as installed in the University of Maryland Wind Tunnel with closeup photograph of injection nozzle	80
2.	Sketch of the sonic tip vortex injection nozzle for the 21-inch chord semispan model	81
3.	8-inch chord semispan model as installed in the University of Maryland Wind Tunnel with tip spoiler configuration	82
4.	Sketch of the sonic tip vortex injection nozzle for the 8-inch chord semispan model	83
5.	Sketch of the tip spoiler for the 8-inch chord semispan model	84
6.	Block diagram of triaxial hot-wire system	85
7.	Sketch of triaxial hot-wire probe coordinate system	86
8.	Variable speed traverse mechanism installed in wind tunnel - upstream view	87
9.	Sample oscillograph record of hot-wire vortex traverse for the unmodified 21-inch chord semispan model $z/c = 6.5$, $U_\infty = 150$ ft/sec, $\alpha_R = 8.5°$	88
10.	Sample oscillograph record of hot-wire vortex traverse for the 21-inch chord semispan model with the 1/2 inch diameter sonic jet, $\dot{m} = 0.12$ lb/sec, $z/c = 6.5$, $U_\infty = 150$ ft/sec, $\alpha_R = 8.5°$	89
11.	Mean velocity distribution of the the trailing vortex for the 21-inch chord unmodified model, $z/c = 6.5$, $U_\infty = 150$ ft/sec, $\alpha_R = 8.5°$	90
12.	Mean velocity distribution of the trailing vortex for the 21-inch chord model with the 1/2-inch diameter sonic nozzle the $\dot{m} = 0.12$ lb/sec, $z/c = 6.5$, $U_\infty = 150$ ft/sec, $\alpha_R = 8.5°$	91

LIST OF ILLUSTRATIONS

Figure		Page
13.	Mean velocity distribution of the trailing vortex for the 21-inch chord model with the 5/8-inch diameter sonic nozzle, $\dot{m}$ = 0.18 lb/sec, z/c = 6.5, U_∞ = 150 ft/sec, α_R = 8.5°	92
14.	Mean velocity distribution of the trailing vortex for the 8-inch chord unmodified model, z/c = 6.5, U_∞ = 175 ft/sec, α = 12°	93
15.	Mean velocity distribution of the trailing vortex for the 8-inch chord model with the 5/16-inch diameter sonic nozzle, $\dot{m}$ = 0.06 lb/sec, z/c = 6.5, U_∞ = 175 ft/sec, α = 12°	94
16.	Mean velocity distribution of the trailing vortex for the 8-inch chord model with the 3/8-inch diameter sonic nozzle, $\dot{m}$ = 0.07 lb/sec, z/c = 6.5, U_∞ = 175 ft/sec, α = 12°	95
17.	Mean velocity distribution in the wake of the 8-inch chord model with the 3/8-inch diameter nozzle, $\dot{m}$ = 0.07 lb/sec, z/c = 6.5, U_∞ = 175 ft/sec, α = 0	96
18.	Mean velocity distribution of the trailing vortex for the 8-inch chord unmodified model, z/c = 16.5, U_∞ = 175 ft/sec, α = 12°	97
19.	Mean velocity distribution of the trailing vortex for the 8-inch chord model with the 3/8-inch diameter sonic nozzle, $\dot{m}$ = 0.07 lb/sec, z/c = 16.5, U_∞ = 175 ft/sec, α = 12°	98
20.	Mean velocity distribution of the trailing vortex for the 8-inch chord model with the tip spoiler, z/c = 6.5, U_∞ = 175 ft/sec, α = 12°	99
21.	Mean velocity distribution of the trailing vortex for the 8-inch chord model with the tip spoiler, z/c = 16.5, U_∞ = 175 ft/sec, α = 12°	100
22.	Mean velocity distribution of the trailing vortex for the 8-inch chord model with the 3/8-inch diameter nozzle with subsonic injection, T = 0.3 lb, z/c = 6.5, U_∞ = 175 ft/sec, α = 12°	101

LIST OF ILLUSTRATIONS

Figure		Page
23.	Mean velocity distribution of the trailing vortex for the 8-inch chord model with 3/8-inch diameter nozzle with subsonic injection T = 1.1 lb, z/c = 6.5, U_∞ = 175 ft/sec, α = 12°	102
24.	Unsteady total velocity component observed during hot-wire traverse across the core of the trailing vortex for the 8-inch chord model at z/c = 6.5, α = 12°, U_∞ = 175 ft/sec, (vertical scale 3 ft/sec per division)	103
25.	Unsteady total velocity component observed during hot-wire traverses across the core of the trailing vortex for the 8-inch chord model at z/c = 16.5, U_∞ = 175 ft/sec, α = 12° (vertical scale 3 ft/sec per division)	105
26.	Unsteady total velocity component observed with stationary hot-wire probe positioned in the center of the trailing vortex core for the 21-inch chord model z/c = 6.5, U_∞ = 150 ft/sec, α_R = 8.5° (vertical scale 2.6 ft/sec per division)	107
27.	Distribution of turbulence in the core of the trailing vortex for the 21-inch chord semispan model, z/c = 6.5, U_∞ = 175 ft/sec, α_R = 8.5°	108
28.	Distribution of turbulence in the core of trailing vortex for the 8-inch chord semi-span model, U_∞ = 175 ft/sec, α = 12°	109
29.	Sample of the digitized total velocity component of the trailing vortex for the 8-inch chord model, z/c = 6.5, U_∞ = 175 ft/sec, α = 12°, top to bottom; ambient free stream velocity, unmodified vortex, vortex with 3/8-inch diameter sonic nozzle, and vortex with tip spoiler. Vertical scale is the same for each of the figures	110

LIST OF ILLUSTRATIONS

Figure		Page
30.	Sample of the digitized total velocity component of the trailing vortex for the 8-inch chord model, z/c = 16.5, U_∞ = 175 ft/sec, α = 12°, top to bottom; unmodified vortex, vortex with the 3/8-inch diameter sonic nozzle, and vortex with tip spoiler. Vertical scale is the same for each of the figures.	111
31.	Sample of the digitized total velocity component of the trailing vortex for the 21-inch chord model, z/c = 6.5, U_∞ = 150 ft/sec, α = 8.5° top to bottom; unmodified vortex and vortex with the 1/2 and the 5/8-inch diameter sonic nozzles. Vertical scale is the same for each of the figures.	112
32.	Turbulent velocity spectrum of the trailing vortex core for the 8-inch chord model, z/c = 6.5, U_∞ = 175 ft/sec, α = 12°	113
33.	Turbulent velocity spectrum of the trailing vortex core for the 8-inch chord model, z/c = 16.5, U_∞ = 175 ft/sec, α = 12°	114
34.	Turbulent velocity spectrum of the trailing vortex core for the 21-inch chord model, z/c = 6.5, U_∞ = 150 ft/sec, α_R = 8.5	115
35.	Dimensionless tangential velocity profile of the trailing vortex for the 21-inch chord model with and without sonic injection at z/c = 6.5, U_∞ = 150 ft/sec, α_R = 8.5	116
36.	Dimensionless tangential velocity profile of the trailing vortex for the 8-inch chord model with and without sonic injection and tip spoiler at z/c = 6.5, U_∞ = 175 ft/sec, α = 12°	117
37.	Dimensionless tangential velocity profile of the trailing vortex for the 8-inch chord model with and without sonic injection and tip spoiler at z/c = 16.5, U_∞ = 175 ft/sec, α = 12°	118
38.	Comparison of observed trailing vortex swirl parameters with viscous jet-vortex stability theory of Lessen et al (References 28, 29)	119

LIST OF ILLUSTRATIONS

Figure		Page
39.	Survey of trailing vortex by vorticity meter for unmodified 21-inch chord model z/c = 6.5, U_∞ = 150 ft/sec, α_R = 8.5°	120
40.	Survey of trailing vortex by vorticity meter for the 21-inch chord model with the 1/2-inch diameter sonic nozzle, $\dot{m}$ = 0.12 lb/sec, z/c = 6.5, U_∞ = 150 ft/sec, α_R = 8.5°	121
41.	Survey of trailing vortex by vorticity meter for the 21-inch chord model with the 5/8-inch diameter sonic nozzle, $\dot{m}$ = 0.18 lb/sec, z/c = 6.5, U_∞ = 150 ft/sec, α_R = 8.5°	122
42.	Comparison of the trailing vortex vorticity distribution as measured by the vorticity meter and as calculated from hot-wire data for the unmodified 21-inch chord model, z/c = 6.5, U_∞ = 150 ft/sec, α_R = 8.5°	123
43.	Comparison of trailing vortex circulation distribution as calculated from hot-wire and vorticity meter measurements for the unmodified 21-inch chord model z/c = 6.5, U_∞ = 150 ft/sec, α_R = 8.5°	124
44.	Comparison of trailing vortex tangential velocity distribution as measured by hot-wire system and as calculated from the vorticity meter data for the unmodified 21-inch chord model, z/c = 6.5, U_∞ = 150 ft/sec, α_R = 8.5°	125
45.	Comparison of trailing vortex vorticity distribution as measured by vorticity meter and as calculated from hot-wire data for the 21-inch chord model with the 1/2-inch diameter sonic nozzle, $\dot{m}$ = 0.12 lb/sec, z/c = 6.5, U_∞ = 150 ft/sec, α_R = 8.5°	126
46.	Comparison of trailing vortex circulation distribution as calculated from hot-wire and vorticity meter measurements for the 21-inch chord model with the 1/2-inch diameter sonic nozzle $\dot{m}$ = 0.12 lb/sec, z/c = 6.5, U_∞= 150 ft/sec, α_R = 8.5°	127

LIST OF ILLUSTRATIONS

Figure		Page
47.	Comparison of trailing vortex tangential velocity distribution as measured by hot-wire system and as calculated from the vorticity meter data for the 21-inch chord model with the 1/2-inch diameter sonic nozzle, $\dot{m}$ = 0.12 lb/sec, z/c = 6.5, U_∞ = 150 ft/sec, α_R = 8.5°	128
48.	Comparison of trailing vortex vorticity distribution as measured by vorticity meter and as calculated from hot-wire data for the 21-inch chord model with the 5/8-inch diameter sonic nozzle $\dot{m}$ = 0.18 lb/sec, z/c = 6.5, U_∞ = 150 ft/sec, α_R = 8.5°	129
49.	Comparison of trailing vortex circulation distribution as calculated from hot-wire and vorticity meter measurements for the 21-inch chord model with the 5/8-inch diameter sonic nozzle, $\dot{m}$ = 0.18 lb/sec, z/c = 6.5, U_∞ = 150 ft/sec, α_R = 8.5°	130
50.	Comparison of trailing vortex tangential velocity distribution as measured by hot-wire system and as calculated from the vorticity meter data for the 21-inch chord model with the 5/8-inch diameter sonic nozzle, $\dot{m}$ = 0.18 lb/sec, z/c = 6.5, U_∞ = 150 ft/sec, α_R = 8.5°	131
51.	Effect of turbulent mass injection on the vortex wake hazard behind fixed-wing aircraft	132
52.	Interaction of the trailing vortex from the 21-inch chord semispan model with a two-dimensional airfoil at z/c = 6.5, U_∞ = 150 ft/sec, α = 0°	133
53.	Core radius of the trailing vortex for the 21-inch and the 8-inch chord semispan models at z/c = 6.5 as a function of jet thrust	134
54.	Peak tangential velocity of the trailing vortex for the 21-inch and the 8-inch chord semispan models at z/c = 6.5 as a function of jet thrust . .	135

LIST OF ILLUSTRATIONS

Figure		Page
55.	Effect of blade vortex interaction on helicopter blade loads (Ref. 34)	136
56.	Effect of blade vortex interaction on helicopter acoustic signature (Ref. 34)	137
57.	Pressure time history of predicted rotational noise for a UH-1D rotor system, Γ_o = 550 ft^2/sec (Ref. 34)	138
58.	Pressure time history of predicted rotational noise for a UH-1D rotor system, Γ_o = 225 ft^2/sec. (Ref. 34)	139
59.	Effect of tip vortex core size on helicopter noise due to blade/vortex interaction (from Ref. 35)	140

I. INTRODUCTION

The acoustic and dynamic problems caused by the interaction of a concentrated line vortex trailed from the tip of a helicopter rotor with a following blade has been well-known since the inception of the helicopter. More recently, the "upset" problem caused by a smaller airplane running into the strong vortex generated by a larger aircraft has come to the forefront in the fixed-wing industry due to an increasing number of such incidences. Rochester Applied Science Associates, Inc. (RASA) has been conducting a comprehensive on-going research program of trailing vortices shed from three-dimensional lifting surfaces to determine a means by which the wake hazard, induced loads, and impulsive acoustic signatures can be minimized and to study the effects of vortex control on the aerodynamic performance of fixed and rotating wing aircraft.

In 1969, under ONR sponsorship, RASA conducted a theoretical analysis (Reference 1) to investigate the feasibility of injecting the forming vortex with a turbulent jet of air in order to excite latent instability modes and to promote mixing and turbulent diffusion, so that the concentrated vortex structure could be disrupted and premature decay induced. This preliminary analysis indicated that an effective control of vortex characteristics could be achieved through vortex injection, and a series of wind tunnel tests were conducted to demonstrate the validity of the concept, and to improve the system for application to flight hardware (References 2-6).

Under these research efforts, balance measurements, vorticity meter surveys, and flow-visualization tests were conducted for a range of vortex characteristics including variations in circulation strength, age, and downstream location, as well as for various mass injection parameters. On basis of vortex-meter measurements of the downstream vorticity distribution with and without the injection of core turbulence, optimum tip vortex

injection schemes were developed in terms of the proper injection angle, mass flow rate, and the jet thrust required to disrupt the concentrated vortex core into a less intense, more diffuse profile characteristic of an "aged" vortex.

The vorticity meter measurements and flow-visualization tests demonstrated that a rapid decay of the concentrated vortex was achieved on the order of 6.5 chord lengths downstream of the wing model by means of tip vortex injection at relatively modest rates of mass flow. While the vorticity-meter and flow-visualization data consistently demonstrated the effectiveness of utilizing a turbulent jet to enhance vortex decay, the data provided no information regarding the three-dimensional vortex flow field in terms of the radial and axial velocity components and the turbulence levels. Therefore, a complete comparison could not be made of the observed and theoretically predicted vortex instability phenomena beyond a study of the circulation strength of the vortex core. In addition, questions arose regarding the accuracy of the vorticity meter, particularly in detecting weak vortex fields, and additional data was sought to reinforce the findings of earlier investigators (References 7 and 8) in terms of the demonstrated capabilities and limitations of the vorticity meter. The present basic experimental research program was undertaken to resolve these general problems and to consolidate and summarize the four years of progress made by RASA in developing tip vortex injection as a means of enhancing the decay of the tip vortices behind three-dimensional lifting surfaces. Real time measurements of the basic characteristics of a trailing vortex including the velocity distribution, turbulence level, and dissipation rates were sought to reinforce and broaden the vortex decay trends observed earlier by vorticity measurements alone. Specific program objectives included; (1) verification that the continuous turbulent input from an unstable jet directed into the vortex

core caused rapid dissipation of the concentrated line vortex by measurement of the basic vortex characteristics with and without the influence of axial flow and injected turbulence; (2) measurements of the effects of a passive turbulence generator to determine the degree to which it can dissipate a trailing vortex by imparting a fixed amount of turbulence per unit of time; (3) comparison of the effects of vortex injection and passive turbulence generator in terms of enhancing the decay of the vortex structure; (4) comparison of hot-wire and vorticity meter measurements of trailing vortex phenomena; (5) investigation of the vortex core turbulence levels, distribution, and frequency content for the unmodified and the modified vortices in the light of current vortex decay models such as those of Baldwin, Lessen, et al; and (6) conclusions which could be drawn from the results of the investigation in terms of comparisons between vortex decay theory and data, the efficiency of vortex injection techniques, and possible applications for full-scale flight vehicles.

The present research effort was organized so that meaningful data could be obtained, analyzed, and compared with existing theoretical and empirical models in order to meet the above objectives.

To investigate the effects of scaling, wind tunnel tests were conducted on two models; a 21-inch chord rectangular semispan model with a full-span aspect ratio of 5.6 and an 8-inch chord model having a full-span aspect ratio of 7.3. The trailing vortex of the 21-inch chord model was surveyed by both the triaxial hot-wire system and the vorticity meter to establish the degree of correlation between these two different measuring techniques. The trailing vortex of the 8-inch chord model was surveyed by the hot-wire system at both 6.5 and 16.5 chord lengths

downstream to establish the effect of downstream distance on the mean and the turbulent velocity distribution of the trailing vortex. Two different size sonic injection nozzles were used with each model to investigate the influence of mass flow on the restructuring of the trailing vortex. For one nozzle, a range of pressure ratios was tested to show the effect of jet thrust on the mean and the turbulent velocity distribution of the trailing vortex.

II. DESCRIPTION OF MODELS AND INSTRUMENTATION

A. Models

Two wind tunnel models were tested in the program; (1) a 21-inch chord, 59-inch semispan rectangular airfoil with an NACA 0012 profile and with a linear twist of 0.35 deg/ft aft; (2) an untwisted, 8-inch chord, 29-inch semispan rectangular airfoil with an NACA 0015 profile.

The 21-inch chord model was fabricated from an outboard section of a UH-1D helicopter rotor blade and was used under a previous experimental research program conducted by RASA (Reference 5). The blade was modified to provide an injection system for the tip vortex using the D-spar as an air supply line and to facilitate its mounting in the University of Maryland Wind Tunnel. The injection system at the tip of the model was contained in a short wooden section which was bolted to the blade section and provided for various nozzle configurations. In this program, 1/2-inch and 5/8-inch diameter convergent sonic nozzles were used to inject the tip vortex. The nozzle exits were on the upper surface of the airfoil at the three-quarter chord portion and the nozzles were oriented at 9.5° with respect to the chord line. A photograph of the 21-inch chord semispan model as it appeared installed in the wind tunnel is shown in Figure 1 and a schematic diagram of the injection nozzle is shown in Figure 2.

The 8-inch chord semispan model was a modified version of the model which was tested by RASA at NSRDC in an earlier research effort sponsored by ONR (Reference 2). Modifications to the model under this program were made to; (1) adapt the model to the air-supply line and balance table of the University of Maryland Wind Tunnel; (2) replace an existing vortex injection slot with circular convergent sonic nozzles geometrically scaled to the nozzles on the 21-inch chord model; and (3) to provide for the mounting of a removable tip spoiler.

The 8-inch chord model was fabricated from a solid block of aluminum. The model had a 5/8-inch diameter hole bored through at the quarter chord which served as the air supply line. The injection system at the tip of the model was also contained in a short wooden section which was bolted to the main section to provide for various nozzle configurations. In this program, 3/8-inch and 5/16-inch diameter convergent sonic nozzles were used to inject the tip vortex. The nozzle exits were located on the upper surface of the airfoil at the three quarter chord position and the nozzles were oriented at 12° with respect to the chordline. The model was also fitted with a removable section without a nozzle and this section had provisions for mounting a tip spoiler. The design of the tip spoiler was based on that used by NASA (Reference 10). The spoiler had a height of 12% of the wing chord, a span of 4% of the wing semispan, and was located on the suction side of the airfoil at the quarter-chord position just inboard of the tip. A photograph of the 8-inch chord model as it appeared mounted in the wind tunnel with the tip spoiler is shown in Figure 3. A sketch of the tip vortex injection nozzle and the tip spoiler is shown in Figures 4 and 5.

B. Instrumentation

A triaxial hot-wire system was used to measure the instantaneous velocities in the vortex field. The system consisted of a three-element probe, and an anemometer and a linearizer for each element. An analog computer was used to transform the velocities from the probe coordinate system to the wind tunnel coordinate system. The output signals, comprised of the three components of velocity and the resultant velocity, were read out on an oscillograph and monitored on a storage oscilloscope. The oscillatory component of the resultant velocity was tape-recorded. A block diagram of the hot-wire instrumentation system is shown in Figure 6.

Each element of the hot-wire probe consisted of a platinum plated tungsten wire 5 μm in diameter. The sensitive wire length

was approximately 1.25mm. which resulted in measurements being averaged over a region approximately 2mm. in diameter. The three elements of the wire were arranged in an orthogonal array offset with respect to the body of the probe by an angle of 54.7° as shown in Figure 7.

The output signal from each of the three anemometers reflecting changes in velocity were linearized and matched for equal sensitivity by adjusting the gain of the linearizers. The output signals from the linearizers were then inputed into an analog computer which transformed the velocities from the coordinate system normal to the probe elements into a wind axis coordinate system, which gave the velocity components parallel to the longitudinal, vertical, and lateral axis of the wind tunnel. The output signals from the computer were amplified by a CEC low-gain amplifier and recorded on an oscillograph. Provisions were made to parallel the signal output from the computer for monitoring on a storage oscilloscope and for recording the high frequency signal associated with turbulence on a single-channel AM magnetic tape recorder.

The output of the anemometers consisted of three voltages, V_{x_1}, V_{y_1}, and V_{z_1}, which can be related to the actual velocity components, $v_x"$, $v_y"$, and $v_z"$, perpendicular to each of the three hot-wire elements by King's law according to the following formula.

$$V_{x_1} = \sqrt{A_1 + B_1 (v_x")^m}$$

$$V_{y_1} = \sqrt{A_2 + B_2 (v_y")^m}$$

$$V_{z_1} = \sqrt{A_2 + B_2 (v_z")^m}$$

The variables A, B, and m were determined experimentally from the observed output voltages of the anemometers for a range of calibration velocities.

The linearizer established a linear function between the output voltages from the three separate linearizers and the input velocities across the three hot-wire elements, respectively. The three linearized signals were matched for equal sensitivity by selecting values for K_1, K_2, and K_3 so that when $v_x" = v_y" = v_z"$ = constant = C_1 then $V_{x_2} = V_{y_2} = V_{z_2}$ = constant = C_2. Equal sensitivity for all probe elements were dictated by the operating characteristics of the analog computer for proper transformation of the velocity components.

The role of the analog transformation computer was to transpose the three linearized signals from a coordinate system normal to the probe into the wind tunnel coordinate system according to the relationship given in the Appendix. Four output signals were generated by the transformation computer. V_{x_3}, V_{y_3}, V_{z_3}, and V_{t_3} which represented the linearized hot-wire signals in the wind tunnel x, y, z coordinate system and the total component defined as

$$V_{t_3} = \sqrt{V_{x_3}^2 + V_{y_3}^2 + V_{z_3}^2}$$

The four output signals from the analog computer were fed into a CEC amplifier for conditioning and then recorded by a CEC light-pen oscillograph. Two 400 Hz sinusoidal reference calibration signals were also recorded on the CEC oscillograph. The CEC oscillograph was equipped with 7-323 galvonometers which had a sensitivity of 2.56 volts per inch trace deflection over a range 0-400 Hz. The sensitivity of the output signals from the tangential and radial components of velocity was set at twice the value of the axial and total components of velocity by the CEC amplifier.

The total velocity vector which was recorded by the oscillograph was paralleled so that the high frequency oscillatory component of the total velocity could also be recorded on a single-

channel AM magnetic tape recorder. The tape recorder was calibrated by a 4000 Hz sinusoidal reference signal with amplitudes of 0.037, 0.047, 0.148, and 0.296 volts rms. The frequency response of the tape recorder was good to within 2 db over the range of 240-18,000 Hz at a nominal tape speed of 1.5 ips.

The upper frequency response of the system was not limited by the capabilities of anemometer (0-30,000 Hz) but rather by the capabilities of the tape recorder (240-18,000 Hz) and by the frequency response of the galvonometers in the light pen oscillograph (0-400 Hz). The system was designed so that the three components of velocity associated with the vortex flow could be recorded by the light pen oscillograph while the higher frequency turbulent velocity components could be recorded on magnetic tape for off-line analysis.

In addition to the hot-wire system, vorticity measurements were also carried out in the trailed tip vortex by means of an AEA[1] vortex meter. The vorticity meter was mounted in the same position and on the same traverse mechanism as the hot-wire probe. The rotational speed of the vorticity meter was read out on an electronic counter and the signal was monitored on an oscilloscope. The vorticity meter was calibrated before and after each traverse sequence by mounting the calibration collar on the sensor and recording the output rpm as a function of tunnel velocity at 50, 100, 150, and 200 ft/sec. A more detailed description of the vorticity meter system can be found in References 2-5 and 7 and 8.

A traverse mechanism was used to sweep the triaxial hot-wire probe through the core of the trailing vortex at a speed of approximately 20 inches/second. The traverse mechanism is shown from an upstream view in Figure 8. The alternating black and white stripes on the bottom of the support rail were used in conjunction with a light emitting diode as a position indicating system for the surveys. A square-wave signal generated by the photoelectric position indicator traversing across the alternating black and white stripes provided a continuous record which could be used to

[1]Aero Engineering Associates, State College, Pennsylvania

determine the location of the hot-wire probe to an accuracy of ±0.01-inch. The data readout systems at the University of Maryland Wind Tunnel were used to record the model angle of attack, tunnel conditions, and balance data. The mass flow of the injected air was computed from measurements of the pressures and temperatures across a sharp-edge orifice. The static pressure at the orifice was read out on a mercury manometer, the pressure drop across the orifice was read out on an alcohol manometer, and the temperature at the orifice was monitored by a thermocouple and read out on a potentiometer.

C. Calibration

The hot wire anemometer system was calibrated using a pitot static tube which was positioned near the hot-wire probe in the diffuser section of the wind tunnel. These pitot tube velocity measurements were required because of the decrease in velocity between the test section and at the downstream location of the probe at the mouth of the diffuser. The hot-wire anemometer was calibrated against the alcohol manometer which had an accuracy of ± 1%. When the hot-wire probe was located in the upstream position in the test-section region, it was calibrated against the central manometer system at the University of Maryland Wind Tunnel which had an accuracy of ± 1%. Corrections to the hot-wire calibrations were not required to account for errors in velocity arising from fluctuations in temperature or density in the wind tunnel test section because these variations were within the allowable range specified by the manufacturer.

The calibration of the hot wire system was checked before and after each test point in the following manner; (1) with the probe located in the freestream velocity, the tunnel speed was set at 0, 50, 100, 150, and 200 ft/sec; (2) voltages were recorded at each of these tunnel speeds for the 3 anemometer units, 3 linearizer units, computer output, and the oscillograph trace deflections. Calibration curves were then generated from this

data, The calibration curves indicated that the combined hot wire system had a linear output over the range of 0-200 ft/sec with $\pm$ 2% accuracy and no evidence of intermittency or significant drift tendencies.

Once the response of each of the three hot wire elements was established by the calibration procedure outlined above, the output voltages from the analog computer were continuously monitored along with the output voltages from the linearizers to indicate the integrity of the system during the wind tunnel tests. In the free stream, the response of the tangential and radial components of velocity was zero and the axial and total velocity components matched the wind tunnel operating velocity consistently.

The vorticity meter was calibrated before and after each vortex survey by mounting the calibration collar on the sensor and recording the output rpm as a function of tunnel velocity at 50, 100, 150, and 200 ft/sec. The calibration curves of the vorticity meter indicated a $\pm$ 2% level of accuracy and no evidence of intermittency or drift tendencies.

III. WIND TUNNEL TESTS

The wind tunnel tests were conducted in the University of Maryland 7.75 x 11-foot Subsonic Wind Tunnel. The experimental effort consisted of two specific tasks, namely, vorticity-meter surveys and hot-wire surveys.

Vorticity-meter surveys were conducted in the first phase of the test program to obtain measurements of the average vorticity distribution of the trailing vortex and to determine the specific location of the vortex core to aid in the subsequent hot-wire surveys. Traverses were made across the tip-vortex wake in increments of 1/4-inch to pinpoint the center of the core (the general location of the tip vortex was known either from earlier tests (ref 5) or was determined by visualizing the vortex with smoke). When the location of the center of the vortex core was determined, surveys were made in increments of 0.05 to 0.10-inch through the center of the core in the spanwise direction and also in a direction normal to the chord. The vorticity meter readings at each location were averaged several times over 1-second intervals to obtain the time-averaged value of the vorticity. The calibration of the vorticity meter was checked before and after each run with the rpm calibration collar.

The hot-wire surveys were performed in a slightly different fashion than the vorticity-meter surveys since a real-time, rather a time-averaged vortex velocity profile was sought. Flow visualization tests indicated that the trailing vortex could wander intermittently and in order to obtain as close to an instantaneous velocity distribution as possible, traverses were made through the vortex normal to the chord of the airfoil at a speed of approximately 20 inches/sec. The time averaged location of the center of the vortex core was located initially by traversing the wake at fixed positions in the spanwise direction with the vortex meter, and plotting the time-averaged rotational speed of

the vorticity meter versus the position of the traverse. It was noted that the vorticity meter measurements of the trailing vortex core region were repeatable so that vortex wandering was not a significant problem.

Using the vorticity measurements as a guide to locate the general downstream position of the trailing vortex, the triaxial hot wire probe was traversed back and forth through the vortex in a direction normal to the chord at a speed of approximately twenty inches per second. To maximize the number of good vortex intersections, the position of the hot-wire probe was adjusted in the spanwise plane until the maximum peak to peak tangential velocity excursions were observed. A number of data points were repeated at this setting. From this data base, those profiles were selected which indicated the most symmetric tangential velocity distribution. Up to thirty-two individual traverses were conducted for each test case. With some test cases, particularly with vortex injection, the trailing vortex exhibited a broad, well-defined core region and the mean velocity distribution was highly regular and repeatable. Only a few traverses were required to measure the details of this flowfield. For the unmodified vortex, there was a higher tendency for the vortex to wander and the core radius was smaller, so that a larger number of traverses were required to obtain symmetric core intersections.

In addition to the surveys of the tip vortex normal to the chord, the triaxial hot-wire probe was also held stationary in the center of the vortex for each test configuration for a period of approximately five seconds, and time-averaged recordings were made of the turbulence level in the core. This data has meaning from the aspect that the hot-wire probe was always located in the general vortex core region and the turbulence level was averaged over this spatial zone. From these records it was sought to compare the time averaged turbulence levels against the real-time turbulence levels.

IV. DISCUSSION OF RESULTS

The influence of turbulent injection and a passive geometric turbulence generator on the velocity distribution of a trailing vortex has been investigated under the present research program in order to provide insight into the dynamics of trailing vortices and in order to demonstrate that the injection of core turbulence will restructure the concentrated viscous vortex core into a more diffuse profile characteristic of an "aged" vortex. The results of the investigation are presented in this section according to the following sequence. Sample hot-wire data is presented first and briefly discussed in terms of its characteristics. Next, the tabulated tangential and axial velocity profiles of the trailing vortices are considered and the dominant trends are outlined. A presentation of the turbulent velocity component of the trailing vortex follows. Drawing on the steady and unsteady velocity distributions associated with the trailing vortex, the present data base is then correlated against current empirical and analytic models. Next, the results of the vorticity meter surveys are presented and compared against the hot-wire data. Finally, on basis of the complete experimental results, the scaling and application of turbulent vortex injection to full-scale flight vehicles is considered.

Under the present research effort measurements were made of the three dimensional unsteady velocity field of a trailing vortex by a triaxial hot-wire system for a range of test conditions summarized in Table I. All of the hot-wire surveys were made by traversing across the core in a direction normal to the wing chord. The hot-wire measurements conducted on the 21-inch chord model were repeated by a vorticity meter. The vorticity meter surveys were conducted by traversing the vortex core in two directions, normal to the chord and spanwise. The typical velocity profile of the trailing vortex observed by the hot-wire system is presented in the following sections.

A. Typical hot-wire velocity measurements

The mean velocity profiles observed during the hot wire trailing vortex surveys were recorded on a light-pen oscillograph. Sample oscillograph records of hot-wire vortex surveys are presented in Figures 9 and 10 to illustrate the basic characteristics of the hot-wire vortex signature for the unmodified vortex and the vortex with injection. The hot-wire signatures consist of the three velocity components in the wind tunnel x, y, z coordinate system as well as the total velocity vector. These velocity vectors are redefined in terms of a cylindrical coordinate system with the origin located at the center of the vortex core (Fig. 7). Note that the typical hot-wire signal consists of an unsteady voltage which corresponds to the mean velocity profile of the trailing vortex in the r, θ, and z direction with an oscillatory signal superimposed on each component arising from the turbulence present. In addition, the total velocity vector is shown which is a vector sum of the three orthogonal components.

At the left hand side of Fig. 9, the hot-wire probe is traversing across the wind tunnel toward the trailing vortex. The radial, v_r, and tangential velocity, v_θ, does not vary significantly with time. The axial, v_z, and the total velocity component, v_t, is also constant with time and is equal to the free-stream velocity . As the probe approaches the core of the trailing vortex, the tangential velocity component increases, reaches a maximum value, goes through zero, establishes a minimum value, and begins to approach the zero level again. However, before ambient conditions are reached, the probe is stopped, its direction is reversed,and a second traverse is initiated back through the vortex core producing a second trace which is essentially a mirror image of the first trace. When the traverse cycle is complete, the probe has returned to its original position and all of the velocity components have reverted to their previous levels. Note that the tangential velocity component still indicates the effect of the trailing vortex so the probe has not been moved sufficiently far away so that the induced velocity field is negligible.

However, the other velocity components have returned to their normal steady state values.

The hot-wire vortex traverse sequence shown in Figure 9 is repeated in Figure 10 for the same model but under the influence of a 1/2-inch diameter sonic injection nozzle. Note that the tangential velocity distribution in the core region of the trailing vortex is considerably lower for the injected vortex (Figure 10) than for the uninjected vortex (Figure 9). Outside of the core region, the tangential velocity distribution for both sample cases is quite similar. Looking at the axial velocity component in Figure 10, it can be seen that the turbulent jet produces an excess of axial velocity in the core region of the trailing vortex which is above the ambient free stream velocity. In comparison, the unmodified vortex (Figure 9) showed an intermittent axial flow profile with evidence of both velocity excesses and deficits as a function of radial distance from the center of the core.

The traverse records presented in Figures 9 and 10 are typical of the hot-wire surveys and demonstrate the strong axial symmetry which was observed in the tangential velocity distribution of the trailing vortices. The same dominant axial symmetry can be noted in the surveys conducted with the vorticity meter discussed in section IV. E and shown in Figures 39-41.

From the sample hot-wire traverse data for the unmodified and the injected vortex, it can also be noted that the turbulent velocity levels are maximum at the center of the vortex core and decrease with radial distance, returning to the ambient level at a distance approximately 4 radii from the center. The turbulence can be observed in the oscillatory level of all three velocity components and in the oscillatory component of the total velocity vector which indicates the overall turbulence level. Caution must be exercised, however, in drawing more detailed conclusions about relative turbulence levels from the sample oscillographs shown in Figures 9 and 10 because of the higher sensitivity assigned to the radial and tangential velocity components and

because of the limited frequency range of the oscillograph system (0-400Hz). Some evidence of galvo ringing and probe vibration due to starts and stops can also be seen in the oscillatory component of the tangential velocity profile. However, these limitations did not comprise the accuracy of the measurements since the oscillograph records were used to provide an indication of the mean velocity profile while the turbulent velocity distributions were recorded independently on a magnetic tape recorder. A discussion of the turbulent velocity distribution based on the oscillatory component of the total velocity vector is presented in section IV C.

The oscillograph measurements, illustrated by the sample data sets in Figures 9 and 10, were used to establish the mean velocities of the trailing vortex by filtering out the high frequency oscillating components not associated with the fundamental vortex profile. The following section indicates the manner in which the data were reduced and the results of the analysis.

B. Velocity distribution of the trailing vortex

From hot-wire vortex surveys similar to the sample oscillograph records shown, a data base was collected on the mean velocity distribution of trailing vortices with and without the influence of vortex injection and a tip spoiler. In order to establish a consistent and accurate profile of the trailing vortex velocity distribution, the following data acquisition and reduction process was followed:

1. To assure positive vortex core intersections, fine adjustments were made on the spanwise location of the triaxial hot-wire probe relative to the generating wing until the observed tangential velocity profiles during the traverses normal to the chord consistently indicated the peak maximum and minimum values;
2. A large number of vortex intersections were recorded and from this available data set, three sample traverses were selected for each test configuration on the basis of consistency and repeatability;
3. Turbulence was eliminated from the sample traverses by drawing a smooth curve midway through the high frequency oscillatory components superimposed on the mean axial and tangential velocity profiles;
4. Under the assumption of axial symmetry the profiles were averaged about the center of the core;
5. The three sample tangential and axial velocity profiles for each test configuration were plotted on the same figure and a curve was fitted through the average of the three sets of data points.

The tangential and axial velocity distributions obtained in this manner presented both the general velocity profile and the degree of scatter which is associated with the unsteady turbulent vortex phenomena.

The tangential and axial velocity distribution of the unmodified trailing vortex for the 21-inch chord semispan model at 6.5

chord lengths downstream is given in Figure 11. The velocity distribution of the trailing vortex in Figure 11, as well as all of the subsequent figures, extends over a region ± 6 inches from the center of the vortex. Although the vortex was surveyed across the total width of the wind tunnel, it was found that essentially all of the circulation was contained in a region ± 6 inches from the center of the vortex. Since all of the changes in the vortex occurred within this narrower viscous region, the velocity distributions were also presented over this region.

The numbers at the top of Figure 11, and subsequent figures, denote the different hot-wire measurements upon which the data was based, i.e., Run 21-6 represents the 6th vortex intersection during the 21st hot-wire traverse sequence. An indication of the accuracy and repeatability of the hot-wire surveys is given by the scatter in the data points from run to run. The largest scatter in tangential velocity measurements, approximately 15%, occurs at the location of the peak tangential velocity and decreases with increasing radial distance from the centerline of the core. At a point seven core radii from the center of the vortex, the difference between three independent tangential velocity measurements is less than 2%. This type of resolution, ranging from 2 to 15%, as shown in Figure 11, is typical of the present trailing vortex surveys. Since the hot-wire system was calibrated to within 2% accuracy, it is believed that the observed scatter in the measurements represents the unsteady characteristics of the trailing vortex possibly due to vortex wandering or to changes in the vortex itself. The relative scatter and repeatability of the data points shown in Figure 11, as well as the subsequent figures, is an indication of the repeatable characteristics of the trailing vortex when sampled repeatedly at a traverse speed of approximately 20-inches/second.

The tangential velocity distribution of the unmodified trailing vortex in Figure 11 indicates a well defined peak velocity in the core followed by a decreasing velocity in the outer regions.

A weak axial velocity component can be observed in the vortex core region which fluctuated approximately $\pm$ 7% relative to the background freestream velocity.

The velocity distribution of the trailing vortex for the 21-inch chord semispan model with the 1/2-inch diameter sonic jet nozzle at 6.5 chordlengths is presented in Figure 12. Note that the peak tangential velocity has decreased to 41% of its noninjected value and the core radius has increased to 420% of its noninjected value. Moreover, a downstream axial flow component has been established in the core region with a peak velocity excess approximately 11% of the freestream velocity. This axial velocity component agrees with the axial velocity of the turbulent jet by itself without the trailing vortex. It can also be seen that the tangential velocity distribution for the unmodified vortex, Figure 11, approaches the tangential velocity profile of the vortex with turbulent injection, Figure 12, at a radial distance 3-1/2 to 4 inches from the center of the vortex core. There is evidence of a slight overshoot in circulation in the outer regions of the vortex since the tangential velocity associated with the unmodified vortex becomes lower than the tangential velocity of the vortex with mass injection for radial distances greater than 3.5 inches. This circulation overshoot phenomena appears in present data base. It can also be seen in the independent pitot static measurements conducted by Snedeker (Reference 10) of an injected trailing vortex. A circulation overshoot profile has also been theoretically postulated for an unmodified vortex on basis of turbulent mixing models (Reference 11).

The influence of a 5/8-inch diameter sonic nozzle on the trailing vortex of the 21-inch chord model is shown in Figure 13. The axial velocity excess has increased to 10% of the freestream velocity while the peak tangential velocity and the vortex core radius are approximately the same as for the 1/2-inch nozzle. For this test condition, unlike the previous injection case, there

is no evidence of circulation overshoot. Figures 12 and 13 indicate that no additional benefits can be gained by increasing the diameter of the sonic injection nozzle from 1/2 to 5/8 inches diameter in terms of reducing the peak tangential velocity of the trailing vortex.

The velocity distribution of the unmodified trailing vortex for the 8-inch chord semispan model at 6.5 chordlengths is presented in Figure 14. The tangential velocity distribution in Figure 14 is similar to the profile shown previously in Figure 11 for the 21-inch chord semispan model indicating a slightly lower peak tangential velocity and a slightly smaller core radius. There is evidence of a slight positive axial velocity component in the trailing vortex of the 8-inch chord semispan model which was not evident with the 21-inch chord semispan model. The positive axial velocity component in the wake of the 8-inch chord semispan model agrees with the theoretical vortex rollup model of developed by Batchelor (Reference 12) and expanded by Brown (Reference 13). According to this model, the axial velocity component in the vortex core region may be either greater or less than the free stream velocity depending upon the ratio of the profile drag to induced drag as given by the relationship

$$(v_{z\ max} - U_\infty)/U_\infty = [3\Gamma_0^2 U_\infty^2 s^2/16\pi^2 - 3(C_D - C_{D_i})C/8\pi s]s/r$$

For the 8-inch chord semispan model, a positive axial velocity component is predicted when the test parameters are substituted into the above relationship

The influence of sonic injection from a 5/16-inch diameter nozzle on the mean velocity distribution of the trailing vortex of the 8-inch chord model at 6.5 chord lengths downstream is shown in Figure 15. With tip vortex injection, the peak tangential velocity has decreased to 56% and the core radius has increased to 440% of the values relative to the unmodified vortex (Figure 14). A positive axial velocity has been established in the core region

with a peak velocity excess 10% of the free stream velocity for the injected vortex. A distinct circulation overshoot in the region r = 2 to r = 4 inches can be seen in comparing the tangential velocity profiles shown in Figures 14 and 15.

As shown in Figure 16, increasing the size of the sonic injection nozzle to 3/8-inch diameter from 5/16-inch produced a small additional decrease in the peak tangential velocity of the trailing vortex from 56 to 52%, and further increased the core radius from 440 to 500% of the unmodified vortex. With the 3/8-inch diameter nozzle, the peak axial velocity excess in the vortex core was also increased to 14% of the free stream velocity. Again, a distinct circulation overshoot can be seen by comparing the tangential velocity profile of the unmodified vortex in Figure 14 with the profile of the injected vortex for the 3/8-inch diameter sonic nozzle (Figure 16).

The mean velocity distribution in the wake of the 8-inch chord model with the 3/8-inch diameter sonic nozzle and no trailing vortex ($\alpha = 0^{\circ}$) is shown in Figure 17. For comparison, a self-similar solution for a round jet in a free stream (Reference 14) is also shown in Figure 17 by a dashed line. Note that the experimentally measured axial velocity profile of the turbulent jet demonstrates good agreement with an exponential profile. Comparing the axial velocity of the solitary jet, Figure 17, with the axial velocity profile of the jet-trailing vortex combination, it can be seen that the peak axial velocity excess with the jet alone and no trailing vortex is 17% of the free stream velocity, whereas the peak axial velocity excess in the core of the jet-vortex combination is slightly lower, being 14% of the free stream velocity. This suggests that some coupling may have occured between the axial jet and the swirling vortex flow at 6.5 chord lengths downstream. Further evidence of this coupling can be noted by the changes in the axial velocity distribution of the jet with and without the influence of the trailing

vortex. The axial velocity profile of the solitary jet demonstrated an exponential profile, shown in Figure 17, whereas the axial velocity distribution for the vortex-jet combination showed a pronounced linear type of axial velocity distribution. In Figure 16, as well as in all of the previous figures illustrating vortex injection (Figures 12, 13, and 15), the axial velocity decreased linearly with radial distance.

The linear axial velocity distribution which appears to be characteristic of the injected trailing vortex may have an important influence on the stability characteristics of the trailing vortex. Note that the linear axial velocity profile shown in Figure 16 establishes a constant destabilizing shear gradient in the vortex core region. On the other hand, if no coupling were to take place and the jet profile shown in Figure 17 were superimposed over the vortex profile shown in Figure 16, then there would be a weak shear gradient in the viscous core and the destabilizing influence of the jet shear would be primarily in the outer potential-flow region. In the former case, premature vortex aging may occur whereas in the latter case the jet may produce only a weak perturbation on the trailing vortex.

The hot-wire surveys shown in Figures 14 and 16 were repeated further downstream at 16.5 chord lengths to investigate the effect of downstream distance on the general characteristics of the trailing vortex. The mean velocity distribution of the trailing vortex for the 8-inch chord unmodified model at 16.5 chord lengths downstream is shown in Figure 18. Basically, very little change can be noted in the unmodified vortex at 16.5 chord lengths when compared to its characteristics at 6.5 chord lengths (Figures 18 and 14 respectively). The peak tangential velocity has decreased slightly from 49 to 48% of the free stream velocity, and the core radius has increased from 5 to 8% of the model chord. It can also be noted that the nonuniform positive axial velocity in

the vortex core region at 6.5 chord lengths has become a non-uniform axial velocity deficit at the station 16.5 chord lengths downstream. Similar variations in the axial velocity component of an unmodified trailing vortex with downstream distance have also been noted by other investigators (e.g. Reference 13).

The effect of downstream location on the velocity distributions of the trailing vortex with tip vortex injection are presented in Figure 19. The measurements taken at 16.5 chord lengths downstream are compared with the same type of measurements made at 6.5 chord lengths (Figure 16). It is noted that as the downstream distance was increased from 6.5 to 16.5 chord lengths the peak tangential velocity of the injected trailing vortex decreased from 27 to 22% of the free stream velocity and the core radius decreased slightly which may be due to a restructuring of the vortex associated with the circulation overshoot. The circulation overshoot is still present at 16.5 chord lengths downstream but is noticeably less than the circulation overshoot observed at 6.5 chord lengths. A basic restructuring of the injected vortex can be noted in the velocity profiles as evidenced by the steady axial velocity components, the reduced tangential velocities, and the return to a swirl profile with less circulation overshoot between 6.5 and 16.5 chord lengths downstream. The velocity distribution in Figure 19 indicates a 5% decrease in peak tangential which is higher than the corresponding 1% decrease in peak tangential velocity for the unmodified vortex over the same downstream interval. While this variation is not significantly higher than the scatter within the hot-wire surveys, it does suggest that a vortex-jet interaction may be occurring in the flow.

The change in the axial flow distribution from 6.5 to 16.5 chord lengths downstream also shows evidence of coupling between the swirling vortex core and the turbulent jet profile. From

Figure 19 it can be seen that the peak axial velocity in the center of the vortex is the same at 6.5 and 16.5 chord lengths downstream. Thus, the velocity excess in the center of the core has not decreased at all which is notably different from the general decay characteristics of a turbulent jet. The centerline velocity in a circular turbulent jet is inversely related to the downstream distance. This type of decay is not evident in the axial velocity profiles indicated in Figures 16 and 19.

The influence of the tip spoiler on the trailing vortex velocity profile for the 8-inch chord model at 6.5 chord lengths downstream is shown in Figure 20. The tip spoiler reduced the peak tangential velocity to 40% and increased the core size to 500% of the unmodified value at 6.5 chord lengths downstream. It is noted that the tip spoiler also established a strong axial velocity defect in the core region having a magnitude of 23% of the free stream velocity. The velocity deficit in Figure 20 associated with the tip spoiler shows a Gaussian profile characteristic of the axial velocity deficit of a turbulent wake. This is different from the axial velocity profile of the injected vortex which demonstrated a linear type of profile as a function of radial distance from the vortex center (Figures 15, 16, 19). The difference noted in the axial velocity profiles may help to explain the differences observed in the decay characteristics of the injected vortex and the vortex with the passive geometric turbulence generator. Since an axial velocity deficit, or excess, in the vortex core region generates a destabilizing shear gradient the observed axial velocity gradients provide an indication of the stability of the trailing vortex structure. It can be noted in Figure 20 that the tip spoiler generates a significant axial velocity deficit in the core of the trailing vortex which results in a destabilizing shear gradient being superimposed over the core region. Comparing the effect of the tip spoiler and the turbulent

jet on the trailing vortex at 6.5 chord lengths downstream (Figures 20 and 19), it is seen that the tip spoiler produces a more intense destabilizing shear gradient than the turbulent jet. This may be correlated with the tangential velocity profiles at 6.5 chord lengths downstream which also indicate that the tip spoiler produces a lower peak tangential velocity and a larger core radius than the turbulent jet.

Initially, at 6.5 chord lengths, the tip spoiler produces a larger change on the vortex then turbulent injection, but this is no longer true at 16.5 chord lengths downstream as shown in Figure 21. Note that the peak tangential velocity has become higher, increasing from 19 to 23% of the freestream velocity, and the core radius is smaller, decreasing from 22 to 19% of the wing chord, between 6.5 and 16.5 chord lengths downstream. It can also be seen in Figure 21 that the peak axial velocity deficit is decreasing in magnitude (23 to 15%) and is spreading out radially as a function of downstream distance. Thus, the destabilizing shear gradient of the trailing vortex under the influence of the tip spoiler has decreased from 6.5 to 16.5 chord lengths downstream. In comparison, the axial velocity distribution of the injected vortex has not changed significantly over the same downstream interval (Figure 19). It is significant to note that by 16.5 chord lengths downstream the destabilizing shear gradient associated with the tip spoiler approaches the destabilizing shear gradient of the injected vortex. Similarly, by 16.5 chord lengths downstream, the passive geometric turbulence generator and the turbulent jet both achieve approximately the same reduction in the peak vortex tangential velocity and the same increase in core radius.

Comparing the tangential velocity distribution of the trailing vortex under the influence of the passive turbulence generator (Figure 21) to the unmodified trailing vortex (Figure 18) it can

be seen that there exists a definite circulation overshoot in the region outside of the vortex core. The circulation overshoot is less evident at 16.5 than at 6.5 chord lengths downstream. At 16.5 chord lengths the circulation overshoot demonstrated by the trailing vortex with the tip spoiler and the turbulent jet is approximately the same in terms of radial extent and magnitude.

In order to determine the effect of a subsonic turbulent jet on the trailing vortex characteristics, measurements were also conducted with the 8-inch chord model and the 3/8-inch diameter convergent nozzle at intermediate pressure ratios corresponding to subsonic injection velocities. The velocity distributions of the trailing vortex for the 8-inch chord model with the 3/8-inch diameter nozzle with 0.3 and 1.1 lb. of thrust is presented in Figures 22 and 23, respectively. At the higher thrust setting, the peak tangential velocity is 57% and the core radius is 370% of the value of the unmodified vortex. With 0.3 lb. of thrust, these values become 64% and 270%, respectively. In terms of reducing the peak tangential velocity, Figures 22 and 23 show that additional reduction in peak tangential velocity consumes significantly more thrust. On the other hand, further spreading of the vortex core is possible with higher injected thrust levels. In comparison to the previous surveys with turbulent injection, Figures 22 and 23 indicate that an appreciable reduction in the peak tangential velocity and spreading in the core radius of the trailing vortex can be achieved with subsonic injection at reduced thrust levels.

To briefly summarize the data presented in this section, it is important to note the large scale changes which resulted when a turbulent jet and a turbulent wake was introduced into the core of the trailing vortex. The effect of the turbulent jet and the tip spoiler can be clearly seen in the present data base in terms

of restructuring the trailing vortex into a more diffuse profile characteristic of an "aged" vortex. Differences can also be noted in the manner in which the turbulent jet and the tip spoiler alter the characteristic profile of the trailing vortex, particularly as a function of downstream distance.

When the effects of the passive geometric turbulence generator are compared against the effects of turbulent injection on the characteristics of the trailing vortex, the differences can be summarized as follows;

1. The peak tangential velocity of the vortex increased with downstream distance for the tip spoiler but decreases as a function of downstream distance for the turbulent jet-vortex configuration.
2. The centerline axial velocity deficit associated with the tip spoiler diminishes with downstream distance whereas the centerline axial velocity excess of the vortex-jet combination remains approximately the same with downstream distance.
3. The destabilizing shear gradient associated with the axial flow decreases more rapidly with downstream distance for the tip spoiler than for the turbulent jet-vortex combination.

These differences indicate that the trailing vortex under the influence of the tip spoiler does not appear to decay with downstream distance in terms of a reduced peak tangential velocity while the unmodified vortex and the vortex with turbulent injection do, in fact, indicate such a decay. The trailing vortex with the tip spoiler tends to return to a coherent concentrated viscous core structure as indicated by the decrease in the core radius, the decrease in the axial velocity deficit, and the decrease in the destabilizing shear gradient associated with the

axial velocity deficit. The present measurements suggest that a passive geometric turbulence generator may not be an effective vortex dissipating mechanism.

Although the same decrease in core size was observed with the injected vortex as with the vortex under the influence of the tip spoiler, the turbulent jet-vortex combination showed a continuous decrease in the peak tangential velocity and maintained a steady axial velocity excess as a function of downstream distance. This suggests that the turbulent jet can be effective in terms of restructuring the trailing vortex into a more diffuse profile characteristic of an "aged" vortex and these benefits can be maintained and improved with downstream distance.

The tangential and axial velocity profiles presented in this section can also provide a valuable insight into the dynamics of jet-vortex and wake-vortex nearfield interactions. In practical terms, this experimental data base can be applied to the trailing vortex problems associated with fixed and rotary wing aircraft, as discussed later in Section IV F.

C. Turbulent velocity distribution of the trailing vortex

An indication of the unsteady velocity distribution of the trailing vortex can be seen in the sample oscillograph records shown previously in Figures 9 and 10. Unsteady velocity distributions were also obtained from magnetic tape records of the high frequency of the oscillatory component of the total velocity vector. Samples of the turbulent velocity distributions observed during hot-wire surveys across the trailing vortex core of the 8-inch chord model at 6.5 and at 16.5 chord lengths downstream are shown in Figures 24 and 25. The photographs were taken from a display of the magnetic tape records on a storage oscilloscope. A low sweep speed was selected for the oscilloscope so that the

peak-to-peak variations in unsteady velocity could be seen during typical vortex traverse sequences. The core of the trailing vortex was intersected from one side, the motion of the probe was reverse, the core of the trailing vortex was intersected from the other side, and finally the probe returned to the original start position. Thus, a double peak type of signature was generated from the two rapid traverses.

The photographs in Figures 24 and 25 illustrate the unsteady total velocity components observed by the hot-wire system during typical traverse sequences across the core of the trailing vortex at 6.5 and 16.5 chord lengths downstream. The distributions are shown for the unmodified vortex, injected vortex, and the vortex with the tip spoiler at the two downstream locations. The vertical scale in the photographs represents the total velocity component and the horizontal scale represents time. The vertical scale is the same for both sets of figures and is equal to 3 ft/sec per division. The traverse speed was also constant in these tests, but the start-stop sequence was manually controlled so that the vortex intersection pattern varied slightly from figure to figure.

As indicated in Figure 24A, the turbulence level does not vary significantly as the probe is traverse through the unmodified vortex core. The fluctuating velocity component varied at most by a factor of two, indicating that the turbulence level in the core of the trailing vortex is on the order one to two times that of the ambient turbulence level. The intermittent sharp spikes in the record are associated with random high level fluctuations in the free stream turbulence level, which appeared throughout the test for which there was no explanation. The average peak-to-peak turbulence level for the unmodified

vortex was approximately 4.8 ft/sec so that the rms level was 1.7 ft/sec, $\sqrt{\overline{q^2}'}/U_\infty \approx 1\%$. This 1% turbulence level represented the lower bound on the sensitivity of the instrumentation system and corresponds to the turbulence level of the University of Maryland Wind Tunnel at the probe location.

When the hot-wire probe was traversed in a cyclic fashion through the vortex (Figure 24 B) the turbulence level increased from the ambient level to a level five to six times the ambient turbulence level whenever the hot-wire probe was inside the vortex core and then dropped back to the ambient level again whenever the probe was outside of the core region. Thus, Figure 24 B indicates four spikes in the turbulence level which corresponds to four repeated intersections of the vortex core by the hot-wire probe. A fluctuation in the ambient profile can be noted when the probe was between traverse cycles, which was associated with the start-stop-reverse sequence of the traverse mechanism.

For the vortex modified by the tip spoiler, the turbulence level increased six to seven times above the ambient level. This is indicated by the peak amplitude of the six regular spikes in the turbulence distribution in Figure 24 C corresponding to six repeated intersections of the vortex core by the hot-wire probe. Comparing Figures 21 B and C, it can be noted that the peak turbulence level in the core of the trailing vortex was slightly higher for the tip spoiler than for the turbulent jet. This correlates with the previous velocity profiles which indicated that the tip spoiler generates a higher incremental axial flow component than the turbulent jet and a more pronounced shear gradient in the vortex core region at 6.5 chord

lengths downstream of the 8-inch chord model.

Sample turbulence records are presented for the 8-inch chord model at 16.5 chord lengths downstream in Figure 25. The records at 16.5 chord lengths indicate that the turbulence level of the unmodified vortex is on the order of one to two times the ambient turbulence level while the turbulence level of the trailing vortex with the tip spoiler and the turbulent jet is on the order of four to five times the ambient turbulence level. Comparing the sample hot-wire records at 6.5 and 16.5 chord lengths downstream, there is no significant change in the peak turbulence level of the unmodified vortex but there is a decrease in the peak turbulence level for the injected vortex and the vortex with the passive geometric turbulence generator.

The hot-wire surveys of the 21-inch chord model at 6.5 chord lengths downstream showed a similar type of turbulent velocity signal as the oscilloscope records presented in Figures 24 and 25 for the 8-inch chord model. Rather than repeat the same type of qualitative data, these results have been tabulated and are discussed later in this section.

In addition to the turbulence measurements obtained by traversing the hot-wire probe across the core of the trailing vortex, measurements were also carried out with the hot-wire probe held stationary in the center of the vortex for each of the test configurations. A typical record of the unsteady total velocity component indicated by the hot-wire probe sitting in the center of the trailing vortex core is shown in Figure 26. The oscilloscope records in Figure 26 indicate that the turbulence level in the core of the unmodified vortex 6.5 chord lengths downstream from the 21-inch chord model was on the order of one to two times the ambient turbulence level. When the sonic jet

was turned on, the turbulence level in the core of the vortex increased to three to five times above the ambient turbulence level. These turbulence levels corresponded to the peak turbulence levels observed during a continuous traverse sequence. Similar measurements were made at 6.5 and 16.5 chord lengths downstream of the 8-inch chord model. Again the sampling of the core by the stationary hot-wire probe indicated approximately the same peak turbulence levels for each of the configurations as the continuous traverse sequence. This suggests that vortex wandering did not play a significant role during the trailing vortex surveys.

From typical tape records illustrated in Figures 24-26 and from typical oscillograph data illustrated in Figures 9 and 10, a composite graph has been made of the rms turbulence level in the core of the trailing vortex. The oscillograph records provided an accurate description of the radial distribution of turbulence in the vortex core in the low frequency range (0-400 Hz). The single channel magnetic tape records indicated the amplitude of the high frequency turbulence (240-18,000 Hz) but did not have the capacity to record the position signal. In order to obtain an approximate profile of the core turbulence of the trailing vortex, these two different sources of data have been combined. The oscillograph records have been used to establish the radial distribution of turbulence in the core. The magnetic tape records have been used to determine the peak turbulence levels in the flow field. In this manner, an approximate composite model has been made of the core turbulence levels as shown in Figures 27 and 28. These composite turbulence distributions were made under the assumption that the dominant turbulence spectrum was contained over the frequency range where the two recording instruments overlapped,

240-400 Hz. Subsequent spectrum analysis of the hot-wire data indicates that this assumption is valid when only approximate comparative turbulence levels are sought.

For the 21-inch chord model, the core turbulence for the unmodified vortex was on the order of the ambient turbulence level as indicated in Figure 27. The turbulence level predicted for an unmodified trailing vortex on the basis of the variable mixing length model of Reference 23 is also shown in Figure 27. When superimposed over the background turbulence level, the theoretical model applied to McCormick's data at $z/c = 34.5$, $U_\infty = 132$ ft/sec predicts a lower turbulence level in the core of the unmodified trailing vortex and predicts a higher turbulence outside of the vortex core region than was observed experimentally. (Correlation between the present hot-wire surveys and the theoretical vortex decay model of Baldwin et al is discussed in more detail in Section IVC.) With the 1/2 and the 5/8 inch diameter sonic nozzles, the turbulence level in the vortex core increased by a factor of four to five respectively over the unmodified vortex. The injected turbulence also showed a marked drop-off with radial distance so that the turbulence was contained within four core radii from the center of the vortex.

The core turbulence for the 8-inch chord semispan model is shown in Figure 28. The turbulence level in the unmodified vortex was higher than the ambient turbulence level by as much as a factor of two, and appeared to be concentrated within a broad region extending outward approximately three core radii from the center of the vortex. This turbulence level may be related to localized boundary layer separation on the model due to its relatively high angle of attack ($\alpha = 12°$). Between 6.5 and

16.5 chord lengths downstream, no significant variation in the core turbulence level was observed for the unmodified vortex. For the 3/8-inch diameter sonic nozzle, the peak turbulence level was approximately six times the ambient turbulence level at 6.5 chord lengths downstream and approximately four times the ambient turbulence at 16.5 chord lengths downstream. The injected turbulence showed a marked drop-off with radial distance so that the turbulence was contained within three to four core radii from the center of the vortex. With the tip spoiler, the peak turbulence levels were approximately seven and five times the ambient level at 6.5 and 16.5 chord lengths downstream respectively. The turbulence generated by the tip spoiler was also contained within a region extending radially outward a distance of three or four core radii from the center of the vortex. The turbulence level with the passive geometric turbulence generator and with the turbulent vortex injection decreased between 6.5 and 16.5 chord lengths downstream by approximately 30%.

Comparing the core turbulence of the trailing vortex behind the 8-inch and the 21-inch chord models (Figures 27, 28) note that the turbulence is contained within the same approximate dimensionless radial distance for both of the models suggesting that a similarity solution may be applicable to describe the turbulent mixing process in the modified vortex. Also note that the peak turbulence levels are approximately the same at the same absolute downstream location. The location 6.5 chord lengths downstream of the 21-inch chord model corresponds to approximately 16.5 chord lengths downstream of the 8-inch chord model. It can be observed that the turbulence profiles are very close in amplitude and radial distribution for these two cases.

In addition to the measurement of the magnitude and the spatial distribution of the core turbulence, a spectral analysis has been made of the turbulence of the trailing vortex under this research program to provide an insight into the vortex decay process. From sample traverse turbulence records, such as those shown in Figures 24 and 25 indicating a continuous intersection of the vortex core region, those records were selected which indicated the peak turbulence levels in the vortex core. Approximately a 1/2 second real time record containing the characteristic turbulence distribution in the vortex core was selected for each test configuration and digitized into a record consisting of 16,384 points. The digitized records indicated the real time turbulence in the trailing vortex during a continuous traverse sequence extending over a spatial region approximately $\pm$ 5 inches from the center of the trailing vortex.

Sample digitized turbulenct velocities for the vortex with turbulent injection, and the vortex with the tip spoiler at different downstream locations are shown in Figures 29, 30, and 31. In this sequence of figures, it can be seen that the frequency content of the ambient free stream is relatively high. The unmodified vortex contains more low frequency components than the background turbulence level. Turbulent injection and the tip spoiler significantly increase the overall turbulence level in the vortex core region and add to the low frequency components in particular.

The digitized unsteady total velocity components shown by the sample data in Figures 29, 30, and 31 have been processed by a fast-Fourier transform computer program to produce a continuous frequency spectrum of the core region of the trailing vortex from 240 to 18,000 Hz with a band width of 2 Hz. In these narrow bandwidth spectrums, it was noted that the turbulence distribution

exhibited a broad-band frequency spectrum for all of the cases considered. For the sake of a more convenient representation, the results were converted into octave bands and are summarized in Figures 32-34.

The octave band frequency spectrum of the unmodified trailing vortex of the 8-inch chord model at 6.5 chord lengths downstream in Figure 32 indicates relatively little change in the turbulence level as a function of frequency. According to Figure 32, the turbulence level in the unmodified vortex core follows the turbulence level of the ambient free stream in the range 240-1,000 Hz. Between 1,000 and 8,000 Hz the turbulence level in the trailing vortex core is higher than the ambient level by as much as 6 db. It is possible that this elevation in the turbulence level above the ambient level may be a sign of natural self-induced decay modes although more data would be required to establish this point. In the range 8,000 - 18,000 Hz, the spectrum of the unmodified vortex again matches the turbulence level of the ambient freestream velocity.

The turbulent spectrum for the injected vortex in Figure 32 indicates that the sonic jet introduces a high level of turbulence into the core of the trailing vortex. At 300 Hz, there is a broadband peak in the spectrum of the injected vortex which is 15 db above the ambient level. In the frequency range 400 - 18,000 Hz the turbulence level decreased by approximately 2.5 db per octave and matched the ambient turbulence level at the high frequency end.

The turbulent spectrum of the tip spoiler in Figure 32 indicates that the tip spoiler is also introducing a significant amount of turbulence into the core of the trailing vortex. The

spectrum of the vortex with the tip spoiler shows a broadband peak centered at 400 Hz which is approximately 18 db higher than the ambient level, and approximately 3 db higher than the turbulence level of the injected vortex. In the range 500 - 18,000 Hz the spectrum of the tip spoiler indicates approximately a 3 db drop per octave and matches the ambient turbulence level at the high frequency end. According to the spectrums presented in Figure 32, the jet and the tip spoiler increased the turbulence level by 15 and 18 db, respectively, above the level of the uninjected vortex at the low frequency end, ~400 Hz and there was no increase in the turbulence level at the high frequency end. Note that if the self-induced decay mode of the unmodified trailing vortex occurs over the frequency range 10,000 to 8,000 Hz, then the sonic jet and the tip spoiler increases the turbulence level over this frequency range five times above the unmodified turbulence level. This should result in a significantly more rapid mixing of the vortex core region and lead to a faster decay. However, if the turbulent spectrum of the jet and the tip spoiler could be shifted from a predominantly low to a predominantly high frequency content, then the forced and natural frequencies of the trailing vortex core would be more closely matched and an even more rapid decay could be achieved.

The turbulence spectrum for the 8-inch chord model at 16.5 chord lengths downstream is presented in Figure 33. The turbulence distribution of the unmodified vortex in Figure 33 indicates a relatively flat spectrum over the range 240-18,000 Hz with approximately a 5 db dip in the spectrum around 8,000 Hz. This is similar to the previous spectrum at 6.5 chord lengths (Figure 32) in terms of the general profile and the overall amplitude. In fact, both profiles show the same slight dip in the spectrum at 8,000 Hz. It can be concluded that the turbulence in the core of the unmodified trailing vortex does not change appreciably from 6.5 to 16.5 chord lengths downstream

for the 8-inch chord model.

The turbulent spectrum of the trailing vortex with the tip spoiler and the sonic jet in Figure 33 is approximately 10 db higher than the unmodified vortex core in the frequency range 240-400 Hz with a 2 to 4 db decrease per octave at higher frequencies. Note that the turbulent spectrum of the injected vortex behaves somewhat differently than the spectrum of the vortex with the tip spoiler. In the range 240-3,000 Hz the turbulence level of the injected vortex is consistently 3 db lower than the turbulence level of the vortex with the tip spoiler. At approximately 4,000 Hz the two spectrums have equal amplitudes. Above 4,000 Hz, the turbulence level of the injected vortex decreases at approximately 2 db per octave while the turbulence level of the tip spoiler drops at a rate of approximately 8 db per octave. Thus, the turbulence level of the injected vortex is approximately 8 db higher at 18,000 Hz than the turbulence level of the tip spoiler. This trend may be interpreted to mean that the sonic jet is introducing more high frequency turbulence into the vortex core than the tip spoiler at 16.5 chord lengths downstream. It may also help to explain why the turbulent jet starts to show a better performance at 16.5 chord lengths downstream than the tip spoiler in terms of producing a more diffuse vortex core structure characteristic of an "aged" vortex.

Comparing the turbulent velocity spectrum of the vortex core with the tip spoiler and the vortex core with the turbulent jet at 6.5 and 16.5 chord lengths downstream (Figures 32 and 33) it can be seen that both measurements indicate the same general broadband characteristics, that is, a peak turbulence level in the low frequency range and a nearly constant decrease in the level per octave with higher frequencies. However, the entire spectrum is approximately 5 db lower at 16.5 chord lengths than at 6.5 chord lengths for the injected vortex and the vortex with the tip spoiler. This indicates that the turbulence introduced by the tip

spoiler and by the turbulent jet into the core of the trailing vortex is decreasing as a function of downstream distance as noted earlier. However, Figure 33 indicates that at 16.5 chord lengths downstream the turbulence level generated by the passive geometric turbulence generator and by the jet produces a turbulence level which is still on the order of 10 db above the turbulence level of the unmodified vortex.

The turbulent spectrum of the trailing vortex core for the 21-inch chord model at 6.5 chord lengths downstream is shown in Figure 34. The turbulence level in the core of the unmodified vortex remains approximately constant with frequency with the exception of a 5 db high broadband peak centered at approximately 400 Hz. This peak may be related to the natural decay mode of the trailing vortex which would imply that the 21-inch chord model produces a trailing vortex with a frequency approximately 1/10-th of the natural decay frequency of the trailing vortex of the 8-inch chord model. However, the peak at 400 Hz may also be related to the freestream turbulence level at this particular downstream location. In either case, more data is required to establish the significance of this low frequency broad-band peak in the spectrum.

Turbulent injection raises the turbulence level in the core of trailing vortex by approximately 15 db between the injected and the uninjected vortex at 240 Hz according to Figure 34. This elevated turbulence level decreases at approximately 4 db per octave over the range 300 - 18,000 Hz so that the injected and the uninjected turbulence levels are the same magnitude at the high frequency end.

Comparing the unmodified vortex of the 21-inch chord model with the unmodified vortex of the 8-inch chord model, it can be noted that the former spectrum peaks in the low frequency range, ~400 Hz, whereas the latter spectrum peaks at a higher frequency

range, suggesting again that the turbulent vortex decay process is linked to the scale of the generating wing. The spectrum of the injected vortex at 6.5 chord lengths downstream of the 21-inch chord model is very similar to the spectrum of the injected vortex at 6.5 chord lengths downstream of the 8-inch chord model. This supports the contention that downstream distance rather than time may be the relevant factor in the turbulent mixing process within the viscous vortex core region. For these two similar spectrums the actual vortex age varied by a factor of three.

D. Correlation with theoretical and empirical models

The present research effort measured the effect of a turbulent jet and a geometric turbulence generator on the general vortex characteristics. The observed trailing vortex parameters including the mean tangential and axial velocity components for the various test configurations are summarized in Table 2. The hot-wire data base shown in Table 2 for the unmodified vortex compares favorably with the trailing vortex measurements of other investigators in regard to the core size, peak tangential velocity and the eddy kinematic viscosity. A tabulation of the present research program along with the measurement of independent investigators is shown in Table 3. Note that in Table 3 the eddy kinematic viscosity of the trailing vortex is undefined for the tip spoiler since the peak tangential velocity increased rather than decreased as a function of downstream distance (Figure 23) so that a decaying exponential profile would be inappropriate.

The vortex injection system tested by Poppleton (Reference 24,25), also summarized in Table 3, was notably different from the present turbulent vortex injection since: (1) it consisted of a split wing with a round jet positioned between the two sections for injection as opposed to the conventional wing model tested with the tip vortex injection nozzle developed by RASA,

(2) the tests were conducted at considerably lower Reynolds number, and (3) the tests were conducted at significantly higher thrust coefficients. Although it is impossible to make a detailed comparison between Poppleton's data and the present research effort, it is useful to note the similarity between the two studies in terms of the general vortex characteristics such as core radii and peak tangential velocities. The injection system tested by Poppleton approximately doubled the core radius of the vortex and decreased the peak tangential velocity to approximately 70% of the unmodified value. The present injection tests increased the core radius by a factor of 3 to 5 and reduced the peak tangential velocity to 30 to 50% of the unmodified vortex.

A comparison of the trailing vortex tangential velocity distribution observed during the present test sequence with the analytic vortex decay model of (1) Hoffman and Joubert (Reference 26); (2) Lamb's viscous vortex (Reference 27); and (3) the variable mixing length model of Baldwin et al (Reference 23) is shown in Figures 35-37.

The characteristic tangential velocity distribution of the unmodified trailing vortex behind the 21-inch chord model (Figure 35) indicates that the hot-wire velocity profile agrees most closely with the turbulent vortex model of Hoffman and Joubert. This model is based on a logarithmic variation in circulation with radial distance. Under the influence of the turbulent jet for an injection rate of $\dot{m}$ = 0.12 lb/sec, the velocity profile of the trailing vortex remains approximately the same as the unmodified vortex and continues to show good agreement with the turbulent vortex model. However, at the higher injection rate of $\dot{m}$ = 0.18 lb/sec, the dimensionless tangential velocity profile

becomes noticeably different. The normalized tangential velocity is lower at most of the stations and the velocity distribution does not agree with the turbulent vortex model. It is more accurately modeled by the viscous vortex type of profile of Lamb. This reinforces the earlier observation that the turbulent axial component of the jet apparently couples with the rotating swirling flow of the vortex to produce a synergistic effect. Thus, a linear superposition of the axial jet flow and the rotating vortex flow could not produce the change in the characteristic vortex profile that is shown in Figure 35 between the unmodified vortex and the vortex with injection.

The dimensionless tangential velocity profile of the unmodified trailing vortex for the 8-inch chord model at 6.5 chord lengths downstream in Figure 36 agrees well with the turbulent vortex model, and again the effect of the turbulent jet is to lower the velocity distribution so that the profile is close to Lamb's similarity solution. The coupling between the jet and the vortex flow, demonstrated by the large shift in the velocity profile with and without turbulent injection, can be seen even more clearly for the 8-inch than for the 21-inch chord model. The tip spoiler in Figure 36 does not appear to produce a significant restructuring of the vortex flow field. With the tip spoiler, the dimensionless tangential velocity profile approaches the logarithmic turbulent vortex profile noted for the unmodified vortex.

At 16.5 chord lengths downstream of the 8-inch chord model, Figure 37 indicates that the dimensionless tangential velocity profile for the unmodified vortex, the injected vortex, and the vortex with the tip spoiler all tend to approach the self-similar solution of Lamb. Whereas at 6.5 chord lengths the unmodified vortex agreed with the turbulent vortex model of Hoffman and Joubert

(Figure 36) by 16.5 chord lengths the velocity distribution of the unmodified vortex approached the viscous vortex model of Lamb.

A similar type of variation with downstream distance can be noted for the tip spoiler. Initially, the profile of the trailing vortex with the geometric turbulence generator demonstrates a logarithmic type of circulation distribution (Figure 36) which is the same as the unmodified vortex. At 16.5 chord lengths, however, the profile is again in agreement with Lamb's solution (Figure 37). On the other hand, the injected vortex approaches the similarity profile of Lamb at both downstream locations, at both 6.5 and at 16.5 chord lengths downstream.

Qualitatively then, downstream distance or time, appears to generate the same effect as turbulent vortex injection. It produces a shift in the tangential velocity profile from the initial logarithmic type of circulation distribution toward the self-similar decaying vortex profile.

The dimensionless tangential velocity profiles in Figures 36 and 37 suggest that the injected vortex will decay according to the viscous vortex model of Lamb. However, the decay rate will be faster because there is significantly more turbulence in the core region, as indicated in the previous section, which will result in a higher turbulent kinematic viscosity coefficient, υ_T. While it is possible to predict a decay rate for the injected vortex on basis of the present data, it is not certain how the turbulence level will vary in the core region at extended downstream distances. If the observed core turbulence levels are maintained beyond 16.5 chord lengths downstream then

the vortex will continue to decay at the present accelerated rate. If the observed turbulence levels decrease to the ambient turbulence level at some point further downstream, then from that point on the vortex will decay like an unmodified vortex which has the same "age" as the injected vortex at that point. In either case, the significant reduction in the peak tangential velocity and the large increase in the core size observed at 6.5 and 16.5 chord lengths downstream with the injected vortex should continue as a function of downstream distance.

Efforts have been made to correlate the hot-wire measurements observed under the present research program against current theoretical vortex decay models, particularly those of Baldwin et al (Reference 23). In figures 35-37 the mean velocity profile predicted by the variable mixing length model of Baldwin et al is also shown. Note that at z/c = 0 the variable mixing length model starts with Lamb's self-similar profile and is then allowed to deform with time under the influence of turbulent mixing and diffusion. At a point z/c = 34.5 the velocity distribution has decayed more rapidly and the profile lies below Lamb's model in the far field outer vortex regions. The hot-wire measurements conducted under the present research program do not show a tendency to approach the type of profile predicted by the variable mixing length model. Instead, the data base indicates that the unmodified trailing vortex is more accurately represented initially at 6.5 chord lengths by a turbulent vortex model than by the decaying exponential model chosen by Baldwin et al. At 16.5 chord lengths, the characteristic tangential velocity curves for the unmodified vortex, the injected vortex, and the vortex with the tip spoiler all lie on or above Lamb's model. Thus, the present data base shows a slight trend in the opposite direction to

the variable mixing length profile postulated by Baldwin et al.

A comparison of the turbulence levels measured during the hot-wire trailing vortex surveys with the turbulence levels predicted by the variable mixing length model has been presented earlier in Figures 27 and 28. Recapping these results, it was shown that the theory developed by Baldwin, et al predicts no turbulence in the core region and a low turbulence level reaching a maximum value of approximately 0.5% at a distance of 5 core radii from the vortex center. On the other hand, the hot-wire measurements indicated that the freestream turbulence level was superimposed over complete vortex profile, including the viscous core region, where the theory indicated that no turbulence should exist. The theoretical model predicted a lower turbulence level in the core region, r/r_c = 0 to 1, and a higher turbulence level in the potential region, r/r_c = 3 to 8, than was observed experimentally.

Subtracting out the background free stream turbulence level in Figures 32-34, it was noted that the spectrum of the unmodified vortex peaked at approximately 400 and 4,000 Hz respectively for the 21 and the 8-inch chord models. If these peaks in the turbulence spectrum can be related to the natural turbulent decay process within the vortex core, then the corresponding Prandtl mixing length is $L = \upsilon_t/(a_1\sqrt{\overline{q^2}}) \approx 0.32$ in. In comparison, the theoretical model of Baldwin et al indicates that a mixing length of approximately 0.15 inches corresponds to the maximum value of the eddy kinematic viscosity in the turbulent trailing vortex profile at z/c = 10.1. Thus, the high frequency turbulence component observed in the hot-wire data agrees well with the most energetic mixing length postulated by the theory of Baldwin et al.

The velocity measurements conducted under this research program have also been related to the instability models developed by Lessen et al (Reference 28, 29). The theoretical model considers the interaction of rotational and axial shear on the stability of a swirling wake to non-axisymmetric disturbances. The analysis indicates that helical instabilities which rotate opposite to the wake, that is modes of negative azimuthal periodicity (-n), are the most unstable disturbances. This is illustrated in Figure 38 where the solid lines indicate the most unstable swirl parameters of the vortex to the n = -1, -2, and -3 spiral-instability modes. The swirl parameters and thrust co-efficients measured experimentally during this research program are indicated by the data points. The experimental points lie above the theoretical curves indicating that, at the measured downstream location, the tangential velocity is greater than the axial flow component and the swirl parameters are higher than the levels required theoretically to produce a spiral instability with the largest growth rate. Although initially the jet exit velocity was considerably larger than the tangential velocity and the swirl parameter was in the unstable region indicated by theory, the theory is based on a self-similar solution, so that it is not really appropriate at earlier downstream locations.

The fact that the observed swirl parameter in Figure 38 is higher than the most unstable swirl parameter predicted by theory indicates that the spiral instabilities in the vortex are not growing at the maximum rate for the n = -1, -2, and -3 wave numbers. To achieve the maximum growth rate for these spiral instability modes the tangential velocity in the vortex should be decreased and/or the axial flow component should be increased further. However, the trend in the theoretical

curves in Figure 38 suggests that the experimental trailing vortex may have achieved maximum amplification rates for progressively higher modes (n<-3) which have not been calculated theoretically. Since the hot-wire measurements have indicated a strong continuous level of turbulence in the core of the trailing vortex, it is hypothesized that the injected vortex is in the most unstable regime for high wave numbers.

Evidence that the turbulent jet produces an unstable effect on the trailing vortex can be seen in the two measurements in Figure 38 conducted on the 8-inch chord model with the 3/8-inch diameter sonic nozzle at two downstream locations. Note that at z/c = 6.5 the swirl parameter is $v_{\theta m}/(v_{zmax}-U_\infty)$ = 1.8 whereas at z/c = 16.5 the swirl parameter has decreased to 1.6. Thus, the jet is overriding the stable rotational influence of the vortex flow and the flow is approaching the unstable boundary. This may provide an explanation for the mean velocity profiles discussed earlier which show a marked decrease in peak tangential but no decrease in the axial flow component for the vortex-turbulent jet combination. It may also explain why the peak tangential velocity of the trailing vortex increases with downstream distance for the tip spoiler but decreases for the vortex injection case. In the former case there is no helical instability while in the latter case there may be such an instability present with high wave numbers.

The stability model presented in Figure 38 indicates that the stability of the trailing vortex is strongly coupled to the axial velocity excess in the core region, $v_{zmax} - U_\infty$, and suggests that higher injection velocities may destabilize the vortex more effectively. Recently, whirl-tower test have been conducted by RASA using a supersonic tip vortex injection nozzle on a UH-1D rotor system. Flow visualization data obtained under this test indicated a considerable increase in the core size and a more rapid decay of the trailing vortex between the injected and the uninjected vortex.

Thus, there exists a potential for increasing the effectiveness of the vortex injection technique by further increasing the axial flow component in the vortex core so that progressively lower wave number instability modes can be excited as indicated in Figure 38. At the same time, increasing the jet velocity will increase the higher frequency components of the turbulence spectrum which may couple more effectively with the natural decay modes of the vortex core structure as indicated by the present hot-wire surveys. Finally, it is possible that a divergent nozzle configuration will spread the vortex to a greater extent than the present linear jet and may achieve a more rapid restructuring of the vortex core region.

E. Velocity distribution of the trailing vortex based on vorticity meter surveys

In addition to the hot-wire trailing vortex surveys described previously in the report, the trailing vortex from the 21-inch chord model was also surveyed at 6.5 chord lengths downstream by a vorticity meter. Results of these surveys are presented in Figures 39, 40 and 41 for the unmodified vortex and the vortex injected with the 1/2 and the 5/8-inch diameter sonic jet. Note that there is relatively little scatter in the data points for the horizontal and vertical vorticity meter surveys indicating that no significant asymmetries exist in the vorticity distribution of the trailing vortex. This same conclusion was previously noted for the hot-wire surveys. It is also significant to note that the vorticity profile of the trailing vortex decreases sharply in magnitude and extends farther in the radial direction with increasing rates of mass injection. The measurements in Figures 39 - 41 show good agreement with the vorticity meter profiles obtained during previous research efforts (References 4 and 5).

A comparison of the trailing vortex vorticity distribution as measured by the vorticity meter and as calculated from the hot-wire surveys under the present research program is given in Figure 42 for the unmodified 21-inch chord model. The two measurement techniques show general agreement in the shape and magnitude of the vorticity distribution in the trailing vortex. The slightly lower vorticity peak and broader vorticity distribution in the core region which is observed in the vorticity meter data in comparison with the hot-wire measurements is attributed to the different traverse techniques which were used with each device. As indicated previously, the hot-wire probe was traversed rapidly across the vortex core to obtain an instantaneous real-time profile of the trailing vortex. On the other hand, the vorticity meter is essentially an rms device which does not respond to high frequency fluctuations. The vorticity meter measurements were, therefore, conducted by time averaging the vorticity in the vortex at different radial positions. Thus, the narrower and more intense vorticity distribution indicated by the hot-wire measurements near the center of the vortex may be because of the instantaneous sampling of the vortex whereas the somewhat broader and less intense profile indicated by the vorticity meter may be due to the time averaging process involved.

A comparison of the circulation and velocity profiles calculated from the hot-wire and vorticity meter measurements is further shown in Figures 43 and 44 respectively for the unmodified vortex trailed from the 21-inch chord model. The distribution of circulation for the trailing vortex as calculated from independent hot-wire and vorticity meter surveys is shown in Figure 43. Note that the hot-wire and vorticity meter measurements indicate the same total circulation and

distribution as a function of radius. Also note that the bound circulation of the trailing vortex is approximately 80% of the calculated bound circulation of the wing assuming an elliptical loading. The tangential velocity distribution as measured by the hot-wire and the vorticity meter for the unmodified 21-inch chord model is presented in Figure 44 and again the two profiles are in general agreement. The slightly lower peak tangential velocity and broader core size calculated from the vorticity meter profile in comparison to the actual hot-wire measurement is attributed to the different sampling techniques for the two devices which were noted earlier.

A comparison of the trailing vortex vorticity distribution, circulation distribution, and tangential velocity distribution is presented in Figures 45, 46, and 47 respectively, for the 21-inch chord model with the 1/2-inch diameter sonic nozzle from the hot-wire and vorticity meter measurements. For this test condition, the vorticity meter and hot-wire measurements indicate significantly different profiles of the measured or derived results. The vorticity profiles and the corresponding circulation profiles and tangential velocity distributions measured by the hot-wire system (Figures 45-47) are consistently higher than the same data measured or derived from the vorticity meter data. For example, the circulation at r = 5 inches is 85 ft^2/sec according to the hot-wire measurements and only 30 ft^2/sec as calculated on the basis of the vorticity meter surveys. In fact, the vorticity meter measurements suggests that the turbulent jet has decreased the total circulatory strength of the vortex to 30% of the unmodified value. The hot-wire measurements indicate that the turbulent jet has significantly spread the vortex core but that the total circulatory strength

at r = 5 inches is actually slightly greater with turbulent tip vortex injection than without injection. This trend can be also seen in the measurements conducted with the 21-inch chord model and the larger 5/8-inch diameter sonic nozzle. It demonstrates the circulation overshoot which was noted in the tangential velocity profiles earlier.

A comparison of the trailing vortex vorticity, circulation, and tangential velocity distribution for the 21-inch chord model with the 5/8-inch diameter sonic nozzle is given in Figures 48, 49, and 50 respectively. Again, the radial distribution of vorticity, circulation, and tangential velocity is significantly less for the vorticity meter measurements than for the same hot-wire measurements.

In summary, the hot-wire and the vorticity meter indicated the same general tangential velocity, circulation, and vorticity distribution for the unmodified vortex. With turbulent injection, the hot-wire and the vorticity meter both indicated a spreading of the vortex. Although the two instruments indicated similar trends in terms of the radial spreading of the injected vortex core, a considerably lower level of total circulation was measured by vorticity meter than by the triaxial hot-wire system. It is believed that the hot-wire measurements represent an accurate profile of the trailing vortex but the vorticity meter data is incorrect for the surveys of the injected vortex due to the limitations of the vorticity meter.

The standard calibration technique for the vorticity meter consists of establishing the coefficient of friction of the air bearing of the paddle wheel sensor by mounting a fixed collar on the device and measuring the paddle wheel rpm over a range of free stream velocities. Thus, the efficiency of the vorticity meter is established as a function of different axial velocities according to the relation

$$\eta = \frac{1}{1+k/v_x}$$

where η is the ratio of the rotational velocity of the vanes to that of the fluid, v_x is the axial velocity at the probe location, and k is the calibration constant taken to be equal to 27.8. For the present test sequence, the efficiency factor of the vorticity meter ranged from $\eta = 0.85 - 0.90$ and included a minor correction resulting from the axial component of the jet at the probe location.

Note that the vorticity meter is not explicitly calibrated to account for changes in sensitivity due to the effects of; (1) the magnitude of the vorticity or to; (2) the gradient of the vorticity. However, comparing the vorticity distribution inferred from the hot-wire measurements against the vorticity distribution obtained from the vorticity meter surveys (Figures 42, 45, and 48) it can be noted that the hot-wire measures vorticity at extended ratial distances from the center of the trailing vortex (i.e. at r = 5 inches) whereas the vorticity meter indicates that no vorticity is present in these regions (no vorticity for r > 3 inches). The vorticity meter is apparently less sensitive than the triaxial hot-wire system in weak vorticity fields. There is no calibration available to account for this nonlinearity.

The present data base also indicates that the gradient of vorticity may have an effect on the accuracy of the vorticity meter. To relate the vorticity measurements which would be seen by the paddle wheel vorticity meter to the actual vortex field, L. V. Schmidt (Reference 30) has worked out an analytic correction factor for a trailing vortex with a nonuniform vorticity distribution in the core region. To first order, the vorticity meter will indicate a lower vorticity reading for a nonuniform vorticity field than the actual vorticity profile by a factor $a/z(\partial\xi(r)/\partial r)$ where $\partial\xi/\partial r)$ is the gradient of the vorticity distribution, a is the radius of the vorticity meter vane, and r is the radial position from the center of the vortex field. Note that for a constant vorticity field $\partial\xi(r)/\partial r = 0$

so that no correction factor is required. On the other hand, this correction would lower the vorticity meter curve for the unmodified vortex shown in Figure 42 closer to the hot-wire profile but would not account for the difference between the hot-wire and vorticity meter profiles shown in Figures 45 and 48.

The measurements under the present research program demonstrate that the vorticity meter agrees quantitively with the hot-wire surveys for the unmodified vortex but shows progressively lower readings when a turbulent jet is used to restructure the coherent vortex core. The data indicates that significant differences may exist between the two measuring techniques which are believed to be related to the magnitude and the gradient of the sampled vorticity field. On basis of the available data, it is not possible to separate out these two effects but it is felt that the vorticity gradient plays a dominant role.

These results suggest that care must be used in interpreting the results of the vorticity meter surveys. Although the trends observed by vorticity meter surveys may be essentially correct, the absolute magnitude associated with the measurements are open to question. The hot-wire measurements presented in this report are believed to represent a reliable and consistent data base for evaluating the effect of turbulent injection on trailing vortex parameters.

F. Scaling and application of vortex injection system to flight vehicles

A measure of the vortex wake hazard is the peak tangential velocity in the wake of an aircraft produced by vortices shed from the tip of a lifting surface, form the flaps, and from streamlined appendages at angle of attack. At some distance downstream, these independent vortices may combine to form coherent trailing vortices which can be a hazard to following aircraft due to their high induced velocity fields. The hot-wire trailing vortex surveys discussed in the previous sections indicate that turbulent injection may be a practical technique for eliminating the trailing vortex hazard behind full-scale fixed-wing vehicles. The hot-wire measurements indicate the following trends:

1. Initial "aging" of the vortex due to initial spreading of the core and reduction in the peak tangential velocity.
2. More rapid "aging" of the vortex with downstream distance due to the enhanced mixing and elevated turbulence level in the core of the vortex.

These phenomena are illustrated in Figure 51 where the present measurements are compared against experimental flight test measurements using the theoretical vortex decay model of Lamb as a guide.

The vortex induced wake hazard is shown in Figure 51 in terms of the peak swirl velocity, $v_{\theta max}/U_\infty$, versus the downstream distance from the generating aircraft, z/c. Hot-wire surveys obtained during the present research effort are represented by the closed symbols at z/c = 6.5 and 16.5 and flight-test measurements of the vortex wake behind a jumbo jet (Reference 19)

are shown by the open symbols ranging from z/c = 500 to 2500. Comparing the two sets of experimental results, it can be noted that while wind tunnel techniques successfully simulate the near field wake, the actual vortex wake hazard persists for significantly farther downstream distances.

The dashed and solid lines in Figure 51 correspond to the theoretical and empirical vortex decay models. The dashed line at the top of the figure, labeled $\nu_t/\Gamma_o \sim 12 \times 10^{-6}$, represents the predicted decay rate of the unmodified vortex behind the wind tunnel model according to Lamb's viscous vortex model. An eddy kinematic viscosity of $\nu_t \sim 6 \times 10^{-4}$ ft^2/sec has been calculated for this configuration on basis of the hot-wire measurements at z/c = 6.5 and 16.5. Similarly, the dashed line toward the bottom of the figure, labeled $\nu_t/\Gamma_o \sim 6 \times 10^{-4}$, represents the predicted decay rate of the vortex behind the wind tunnel model with sonic injection. For the injected vortex, the hot-wire measurements at z/c = 6.5 and 16.5 indicated a kinematic viscosity of $\nu_t \sim 3 \times 10^{-2}$ ft^2/sec which is a value 50 times higher than that of the unmodified vortex. Thus, turbulent injection appears to not only reduce the peak tangential velocity of the vortex initially, at z/c = 6.5, but also promotes a much more rapid decay of the vortex at extended downstream locations. This can be seen by comparing the two decay curves for the unmodified and the injected vortex.

The solid line in Figure 51 represents an empirical curve fit to the jumbo jet vortex wake flight-test measurements . Note that the flight-test data does not match the trend predicted by the self-similar solution of Lamb. It shows a less rapid

decay initially and a more rapid decay at extended downstream distances than indicated by theory. However, the viscous decay model of Lamb has been the basis for a majority of the vortex wake predictions and it is useful to compare the present data within the framework of this currently accepted technique.

Commercial aircraft are presently separated 5 to 10 miles to avoid the vortex wake hazard. In terms of the empirical decay rate shown in Figure 51, a five mile separation distance corresponds to $z/c \sim 1000$ and $v_{\theta max}/U_\infty \sim 0.12$. With turbulent injection, the same effect ($v_{\theta max}/U_\infty \sim 0.12$) can be achieved at roughly 1/10 the downstream distance ($z/c \sim 100$) based on extrapolating the present injected vortex measurements via Lamb's model. This identifies the tip vortex injection technique as an excellent candidate for vortex wake hazard control. It also implies that measurements must be taken farther downstream to assess changes in the wake hazard induced by the trailing vortex than has been achieved to date by investigators utilizing wind tunnel techniques.

Near field measurements of the rolling moment induced on a following model due to vortex wake may be misleading due to the effects of stall as illustrated in Figure 52. The interaction of the trailing vortex from the 21-inch chord semispan model with a two-dimensional airfoil has been calculated in Figure 52 in terms of the spanwise lift coefficient, $C_\ell = \frac{dC_\ell}{d\alpha}\,\alpha \approx 5.5\, w(x)/U_\infty$ versus lateral distance from the vortex center, x. The angle of attack distribution induced by the trailing vortex, $w(x)/U_\infty = v_\theta(r)/U_\infty$, has been taken from the hot-wire surveys. According to Figure 52, the spanwise loading on the interacting model is significantly higher in the inborad region for the uninjected vortex case than for its injected counterpart. However, when a realistic stall boundary is taken

into account, $C_{\ell_{max}} \approx 1.0$, both cases produce approximately the same spanwise loading distribution. While turbulent injection significantly reduces the vortex induced upwash field in the inboard region, the actural spanwise loading does not change significantly because the airfoil is already stalled. Outside of the viscous core region, the induced flow field is the same for both the unmodified and the injected vortex so that, again, the spanwise loading is the same. From Figure 52 it can be concluded that turbulent injection will not reduce significantly the rolling moment on an airfoil located at 6.5 chord lengths downstream in the vortex wake of the 21-inch chord semispan model. This has been verified experimentally in a RASA study conducted under NASA sponsorship (Reference 31) where the trailing vortex of the 21-inch chord semispan model was surveyed by measuring the rolling moment coefficient exerted on a following 12-inch span model located at various downstream locations up to 38 chord lengths downstream. Even at 38 chord lengths downstream, turbulent injection did not appreciably lower the induced rolling moment on the following model. This result substantiates the vortex decay trends shown in Figure 51 which indicate that the injected vortex at z/c = 38 produces a peak tangential velocity equivalent to flight test measurements made at z/c = 650. It is noted that the magnitude of the rolling moments at z/c of 650 were still unacceptable (Reference 19) because of the size of the core vortex was still less than the probe aircraft. At approximately z/c ≈ 1500 the induced rolling moment was within the limits of the control power of the probing aircraft and it is estimated that at this location the radius of the vortex core is larger than the semispan of the following aircraft. Based on the wind tunnel measurements made at 6.5 and 16.5 chord lengths downstream of the injected vortex and on the assumption that the vortex will decay as a viscous vortex which utilizes the measured viscosity, it has been shown (Figure 51) that the vortex core size

will be enlarged at a much faster rate than the uninjected vortex and a rolling moment within the capabilities of the following aircraft will be obtained at a z/c of 1/3 to 1/10 of that of the uninjected vortex.

Scaling of the present experimental measurements indicates that relatively modest levels of injected thrust are required to achieve a significant reduction in the vortex wake separation criteria.

The effect of turbulent injection on the peak tangential velocity and core radius of the trailing vortex is shown as a function of the dimensionless thrust parameter in Figures 53 and 54. The dimensionless thrust parameter is $T/\rho\Gamma_o^2$ where T is the thrust relative to the free stream ($T = \rho A(U_j - U_\infty)^2$), and $\rho\Gamma_o^2$ is the measure of the induced drag of the wing. While there are not enough data points available in Figures 53 and 54 nor sufficient correlation in the data points to indicate that $T/\rho\Gamma_o^2$ is the true scaling parameter for turbulent vortex injection, data obtained by other investigators (Reference 32) has also shown good correlation with this type of thrust parameter. Additional tests would be required to establish the thrust scaling shown in Figures 53 and 54, but until this data is made available, it is useful to interpret the present results in terms of the parameter $T/\rho\Gamma_o^2$.

The experimental results in Figures 53 and 54 indicate that most of the reduction in tangential velocity and most of the increase in core size occurs for low thrust values, $T/\rho\Gamma_o^2 \approx 0.02$. For higher thrust parameters, the curves approach as asymptote and only minor additional benefits are gained. The present data base also indicates that the 21 and the 8-inch chord models fall on separate curves in terms of the injected thrust versus the peak tangential velocity and core radii. Note that for a given dimensionless thrust level, the trailing vortex of the 21-inch

chord model achieves approximately a 20% lower tangential velocity ratio than the trailing vortex of the 8-inch chord model. This may be related to the scaling of the two models.

Recall that for the 8-inch chord model at 6.5 chord lengths downstream the turbulence spectrum of the unmodified vortex was greater than the background wind tunnel turbulence spectrum in the high frequency range, $\sim$ 4000 Hz (Figure 32). In this frequency rang injection raised the turbulence spectrum on the order of 5 db above the spectrum of the unmodified vortex. On the other hand, for the 21-inch chord model the spectrum of the unmodified vortex was above the ambient turbulence spectrum in the low frequency range, $\sim$ 400 Hz (Figure 34). This corresponded roughly to the peak turbulence spectrum of the injected jet and here turbulent injection raised the turbulence level in the vortex core substantially more, by approximately 10 db above the turbulence level of the unmodified vortex. Thus, turbulent injection may be more effective for the 21-inch chord model than for the 8-inch chord model because in the former case the peak turbulence spectrum of the jet is in the same frequency range as the natural decay process of the unmodified vortex. This trend suggests that a close coupling between the turbulence spectrum of the axial jet and the swirling vortex can significantly increase the effectiveness of turbulent injection in terms of producing a more diffuse viscous profile characteristic of an "aged" vortex. It also suggests that the decay curve for the injected vortex in Figure 51 may be significantly enhanced by "tuning" the turbulence spectrum of the vortex to the natural decay modes.

The data in Figures 53 and 54 indicates that a dimensionless thrust parameter of $T/\rho\Gamma_o^2 \simeq 0.02$ is required to cut the peak tangential velocity of the vortex in half and to increase the core radius of the trailing vortex by a factor of approximately 3 over its unmodified value. Applying this value to a

current jumbo jet transport in the landing configuration, the bound circulation of the wing is $\Gamma_o \simeq 5000$ so that approximately 1700 lbs of thrust would be required to restructure each tip vortex, or 3400 lbs of thrust for the complete vortex pair. This latter figure represents about 2% of the total installed thrust of a jumbo jet. Thus, the present model tests suggest that by ducting approximately 4% of the thrust of each outboard engine into a wing tip injection nozzle, the peak tangential velocity of the trailing vortex could be cut in half and the core radius could be increased by a factor of 3 of the unmodified vortex at a location 6.5 chord lengths downstream from the vehicle.

Extrapolating this change in the vortex characteristics to larger downstream distances via the viscous decay model of Lamb (Figure 51), it is estimated that injection of the trailing vortex with 2% of the total installed thrust may reduce the vortex wake separation criteria by as much as a factor of ten.

As noted before, the trailing vortex sheets can originate from the tip, flap, or body so that the exact injection system is indicated by the aerodynamics of the flight vehicle. Present tests have been conducted on a clean airfoil configuration so that only injection of the forming tip vortex was necessary. For transport aircraft in the landing mode, the flap vortex can overshadow the effects of the tip vortex (Reference 33) so that a practical injection system would have to include nozzles directed at the forming flap vortex. On basis of past experience with vortex flows, it is believed this modification can be successfully carried out with the vortex injection technique.

In summary, the existing tip vortex injection technique is applicable to the tip as well as to the flap vortex. Moreover, the present model tests indicate that for a few percent thrust

reduction the injection technique may reduce the vortex wake hazard separation criteria by an order of magnitude. The technique appears to meet the important qualifications for controlling the vortex wake hazard associated with fixed-wing aircraft.

In addition to fixed-wing vehicles, turbulent vortex injection demonstrates a significant potential for application to rotating lifting devices such as helicopter rotors. Turbulent vortex injection can effectively reduce the impulsive loading and the acoustic signature stemming from blade-vortex interaction process by reducing the peak tangential velocity and by increasing the core radius of the trailing vortex. The impulsive loading on a UH-1 helicopter rotor due to tip-vortex interaction has been calculated with and without the strong induced effect of the tip vortex by a RASA blade loading program (Reference 34) as shown in Figure 55. The effect of the tip vortex has been isolated in these numerical calculations by running two separate cases: (1) a calculation with the normal deformed wake model and (2) a calculation with the deformed wake model with the induced effects of the concentrated vortex eliminated. According to the results presented in Figure 55, when the tip vortex strength is zero, the harmonics of the induced velocity and the harmonics of the section lift are noticeable reduced. This can produce a significant reduction in the dynamic response and can lower the stress levels associated with these modes since the natural coupled modes of the helicopter blades are close to the harmonics of the loading.

A reduction in the unsteady loading presented in Figure 55 in turn results in a significant reduction in the acoustic signature of the helicopter rotor. The spectrum of the total

acoustic signature of the JH-1 helicopter rotor system has been calculated from the loading distribution shown previously with and without the influence of the tip vortex and is presented in Figure 56. Comparing the two spectrums in Figure 56 it can be seen that there is a significant change in the acoustic output with the elimination of the blade-vortex interaction, particularly in the frequency range 5 to 400 Hz. It is the frequencies in this range that propogate for long distances and are significant in terms of detectability. Thus, the 10 to 15 db reduction in the sound pressure level shown in Figure 56 by the elimination of the tip vortex can be very significant from operational consideration.

The sensitivity of the acoustic blade-slap signature to the peak tangential velocity of the trailing vortex is further shown in Figures 57 and 58. The pressure time history of the predicted rotational noise for a UH-1D rotor system is presented in Figure 57 for Γ_o = 550 ft^2/sec. Note the high frequency spikes associated with blade-vortex interactions. The pressure time history of the predicted rotational noise for a UH-1D rotor system is repeated in Figure 58 with the circulatory strength reduced to Γ_o = 220 ft^2/sec. With the induced effects of the concentrated vortex reduced by 50%, the blade-slap signature is eliminated, as illustrated by the absence of high frequency components in Figure 58. A reduction in peak tangential velocity and an increase in core size leads to a similar result as a reduction in the induced effects of the tip vortex in that both techniques will reduce blade loads and will alleviate the blade-slap phenomenon. This is illustrated in Figure 59 where the range of trailing vortex core radii observed under the present research effort is superimposed over acoustic measurements conducted on model rotors (Reference 35). Note that a tripling of the core radius by turbulent injection will reduce the overall

sound pressure level by approximately 10 to 15 db for a rotor system undergoing blade vortex interaction. This agrees well with the previous calculations shown in Figures 56 and 58, based on reducing the induced effects of the trailing vortex.

In terms of a full-scale application to either fixed or rotating wing aircraft, the vortex injection system does not compromise the aerodynamic characteristics of the lifting surface since the lift and drag characteristics of the wing remain essentially unchanged (Table 2) and the injected axial flow is recovered in the form of thrust. This substantiates earlier research efforts (Reference 2-6) which also indicated that vortex injection does not produce unfavorable lift or drag penalties on wings. By comparison, the tip spoiler in the present tests showed a 2% loss in lift and a 20% increase in drag with respect to the unmodified airfoil (Table 2). The performance penalty associated with a fixed geometric turbulence generator makes it unattractive in terms of a full-scale application.

In summary, the vortex injection system demonstrates a strong potential for reducing the vortex-wake hazard and the blade-vortex interaction problem present with full-scale aircraft and helicopters. The scaling indicates that a restructuring of the tip vortex can be achieved at modest thrust levels and without degrading the lift and drag characteristics of the vehicle.

V. CONCLUSIONS

Measurements conducted under the research program indicate that a turbulent jet and a passive geometric turbulence generator can significantly reduce the peak tangential velocities and increase the core radii of trailing vortices by introducing high levels of turbulence and strong axial velocity components into the viscous core region. The following conclusions can be drawn from the comparison of the characteristics of the injected trailing vortex, the trailing vortex under the influence of a tip spoiler, and the unmodified trailing vortex.

EXPERIMENTAL RESULTS

A. Unmodified trailing vortex

1. A slight decrease in the peak tangential velocity of the trailing vortex and an increase in core size was measured between 6.5 and 16.5 chord lengths downstream of the 8-inch chord model.

2. The rms turbulence level of the trailing vortex core was 1 to 3 times the background 1% turbulence level of the wind tunnel.

3. The peak turbulence level occurred in the viscous vortex core region and decreased to the ambient level within 3 core radii from the center of the vortex.

4. No significant change in the peak rms turbulence level was noted between 6.5 and 16.5 chord lengths downstream for the 8-inch chord model.

5. Spectrum analysis of the real-time turbulent velocity component of the trailing vortex indicated a broad band turbulence profile with no discrete high energy components.

6. The broad band spectrum of the trailing vortex of the 8-inch chord model was maximum above the background turbulence spectrum in the frequency range near 4,000 Hz.

7. The broad band spectrum of the trailing vortex of the 21-inch chord model was maximum above the background turbulence spectrum in the frequency range near 400 Hz.

8. The hot-wire surveys were in substantial agreement with the vorticity-meter surveys meter surveys in terms of the vorticity distribution.

B. Trailing vortex with turbulence mass injection

1. The peak tangential velocity decreased 40 to 60% and the core size increased by a factor of 2 to 5 in comparison to the unmodified vortex at the same downstream location.

2. A positive axial velocity component was established in the center of the trailing vortex with a peak velocity ranging from 3 to 20% of the free-stream velocity.

3. No significant decrease in the axial velocity component was observed for the trailing vortex between 6.5 and 16.5 chordlengths downstream of the 8-inch chord model.

4. Interactions between the swirling vortex flow and the injected axial flow were observed in the tangential and axial velocity profiles of the trailing vortex.

5. A circulation overshoot was observed when the tangential velocity profile of the injected vortex was compared with the tangential velocity profile of the unmodified vortex.

6. The rms turbulence level in the vortex core increased by a factor of 3 to 5 with turbulent injection in comparison to the unmodified vortex.

7. The peak turbulence level occurred at the center of the vortex and decreased to the ambient level within 4 core radii from the center.

8. The turbulence level in the center of the vortex for the 8-inch chord model was maintained between 6.5 and 16.5 chord lengths downstream.

9. Spectrum analysis of the real-time turbulent velocity component of the trailing vortex indicated a broad band turbulence profile with no discrete high energy components.

10. Turbulent mass injection raised the spectrum of the turbulent vortex core primarily in the low frequency range, 300 - 400 Hz.

11. The characteristic eddy size in the trailing vortex appeared to be associated with the same frequency, 400 Hz, as those generated by the turbulent jet for the 21-inch chord model.

12. The characteristic eddy size in the trailing vortex appeared to be associated with higher frequencies, 4,000 Hz, than those generated by the turbulent jet for the 8-inch chord model.

13. Vorticity meter surveys indicated significantly lower vorticity readings than the corresponding hot-wire measurements.

C. Trailing vortex with the geometric turbulence generator

1. The tip spoiler achieved a slightly larger reduction in the peak tangential velocity at 6.5 chord lengths downstream and approximately the same reduction in the peak tangential velocity at 16.5 chord lengths downstream as the turbulent jet.

2. The trailing vortex appeared to reform, rather than decay as a function of downstream distance as evidenced by the increase in the peak tangential velocity and by the decrease in core size between 6.5 and 16.5 chord lengths downstream.

3. A negative axial velocity component was established in the center of the trailing vortex which decreased in magnitude as a function of downstream distance from approximately 23% to 15% of the free-stream velocity between 6.5 and 16.5 chord lengths downstream.

CORRELATION OF EXPERIMENTAL RESULTS WITH THEORETICAL AND EMPIRICAL MODELS

1. The self-similar profile of Lamb was found to be a poor approximation of the trailing vortex in the near field. The unmodified vortex and the vortex with the tip spoiler showed good agreement with Lamb's profile at 16.5 chord lengths downstream, but at 6.5 chord lengths downstream, the profiles demonstrated better agreement with the turbulent vortex model of Hoffman and Joubert.

2. The tangential velocity profile of the injected vortex agreed with the self-similar viscous vortex

profile of Lamb at both 6.5 and 16.5 chord lengths downstream.

3. The wake measurements showed that the turbulent kinematic viscosity coefficient was approximately 50 times higher for the injected vortex than for the unmodified vortex.

4. On basis of the turbulent kinematic viscosity coefficients, the injected vortex at 6.5 chord lengths downstream was equivalent in age to an unmodified vortex at approximately 1,200 chord lengths downstream.

5. The turbulence measurements in the core of the unmodified trailing vortex indicated a higher turbulence level in the viscous core region and a lower turbulence level in the outer potential flow region than predicted by the variable mixing length model of Baldwin et al.

6. Correlation of the present data base with the instability model of Lessen et al indicated that a greater reduction in the tangential velocity profile of the vortex may be possible by increasing the axial component of the jet.

SCALING AND APPLICATION OF VORTEX INJECTION TO FULL-SCALE FLIGHT VEHICLES

1. Turbulent mass injection shows potential for reducing the present separation distance between fixed-wing aircraft dictated by the vortex wake hazard criteria by an order of magnitude and will require approximately 2% of the total installed thrust.

2. In the near wake of fixed-wing aircraft the influence of stall and the dominance of the potential outer flow field suppresses the beneficial effects of turbulent mass injection.

3. The 50% reduction in the peak tangential velocity of the trailing vortex achieved by turbulent mass injection can effectively alleviate the impulsive loading and blade slap problem associated with helicopters.

4. There appeared to be an optimum thrust coefficient, $T/\rho\Gamma_o^2 \simeq 0.02$, beyond which additional thrust did not bring about an equally significant reduction in the tangential velocity.

5. At the optimum thrust coefficient, $T/\rho\Gamma_o^2 \simeq 0.02$, a more significant reduction in the peak tangential velocity was achieved for the 21-inch than for the 8-inch chord model. This difference was attributed to the different broadband frequency characteristics of the trailing vortex with and without mass injection for the two different size models.

6. The mass injection system did not degrade the net performance characteristics of the lifting surface since the injected momentum was recovered in the form of thrust. The tip spoiler showed a 2% loss in lift and a 20% increase in drag with respect to the unmodified airfoil.

VI. RECOMMENDATIONS

The present detailed measurements of the vortex decay process combined with current turbulent decay and instability models have indicated that the decay of the trailing vortex could be further enhanced if the frequency of the natural decay modes of the vortex could be "tuned" to the frequency of the turbulent jet. While the existing vortex injection system can achieve a large scale restructuring and control of the concentrated vortex wake with the capability for improving aerodynamic performance, alleviating the vortex wake hazard, induced loads, and impulsive acoustic signatures, this could be achieved much more dramatically and more efficiently if the natural instability modes could be tailored to the turbulence spectrum of the swirling flow. On basis of the present research effort it is recommended that the following programs be undertaken;

1. Investigate the benefits in terms of enhanced vortex control and decay which can be achieved when the turbulence spectrum and the natural stability modes of the system are matched. This could be accomplished by conducting an experimental survey of the jet-vortex flow for the pertinent parameters suggested by the existing vortex instability theory and the limited available measurements.

2. Improve the total lift and drag characteristics of high performance aircraft through the use of line vortices by conducting a theoretical and experimental program to determine what types of incremental loadings can be achieved by a distribution of line vortices adjacent to a highly loaded lifting surface in terms of the total lift and drag of the system.

VII. REFERENCES

1. Rinehart, S.A., "Study of Modification of Rotor Tip Vortex by Aerodynamic Means", ONR Contract N00014-69-C-0169, Rochester Applied Science Associates, Inc., RASA Report No. 70-02, AD 704804, 1970.

2. Rinehart, S.A., Balcerak, J.C., White, R.P., Jr., "An Experimental Study of Tip Vortex Modification by Mass Flow Injection", ONR Contract N00014-69-C-0169, Rochester Applied Science Associates, Inc., RASA Report No. 71-01, AD 726736, 1971.

3. White, R.P., Jr. and Balcerak, J.C., "An Investigation of the Mixing of Linear and Swirling Flows", ONR Contract No. N00014-69-C-0226, Rochester Applied Science Associates, Inc., RASA Report No. 72-04, 1972.

4. White, R.P., Jr. and Balcerak, J.C., "Investigation of the Dissipation of the Tip Vortex of a Rotor Blade by Mass Injection", USAAMRDL Contract No. DAAJ02-71-C-0036, Rochester Applied Science Associates, Inc., RASA Report No. 72-03, USAAMRDL Technical Report No. 72-43 1972.

5. Balcerak, J.C and Feller, R.F., "Vortex Modification by Mass Injection and by Tip Geometry", USAAMRDL Contract No. DAAJ02-72-C-0097, Rochester Applied Science Associates, Inc., RASA Report No. 73-01, USAAMRDL Technical Report No. 73-45, 1973.

6. Balcerak, J.C. and Zalay, A.D., "Investigation of the Effects of Mass Injection to Restructure a Trailing Tip Vortex at Transonic Speeds", ONR Contract No. N00014-71-C-0226, Rochester Applied Science Associates, Inc., RASA Report No. 73-03, 1973.

7. Hopkins, E.J. and Sorensen, N.E., "A Device for Vortex-Core Measurements", Journal of the Aeronautical Sciences, Vol. 23, No. 4, April 1956.

8. McCormick, B. W., Tangler, J. L., and Sherrieb, H. E., "Structure of Trailing Vortices", J Aircraft, Vol. 5, No. 3, p. 260, (May-June 1968).

9. Corsiglia, V. R., Jacobson, R.A., and Chigier, N. "An Experimental Investigation of Trailing Vortices Behind a Wing With a Vortex Dissipater" paper presented at Symposium on Aircraft Wake Turbulence held in Seattle, Washington, September 1970.

10. Snedeker, R.S., "The Effect of Air Injection at the Torque Produced by a Trailing Vortex", AFOSR-TR-1030.

11. Donaldson, C.P., and Sullivan, R.D., "Decay of an Isolated Vortex" paper presented at Symposium on Aircraft Wake Turbulence held in Seattle, Washington September 1970.

12. Batchelor, G. K., "Axial Flow in Trailing Line Vortices", JFM, Vol. 20, Part 4, p. 645, December 1964.

13. Brown, C.E., "Aerodynamics of Wake Vortices", AIAA Journal Vol. 11 No. 4, p. 531, April 1973.

14. Squire, H.B. and Trouncer, B. A., "Round Jets in a General Stream", ARC, R&M, p. 74, January 1944.

15. Rose, R. and Dee, F. W., "Aircraft Vortex Wakes and Their Effects on Aircraft", RAE TN 2934, ARC 25419, December 1963.

16. Dosanjh, D. S., Gasparek, E. P. and Eskinazi, S., "Decay of a Discous Trailing Vortex", Aeronautical Quarterly, p. 167-188, May 1962.

17. Newman, B. G., "Flow in a Viscous Trailing Vortex", Aeronautical Quarterly, p. 149-162, May 1959.

18. Rorke, J.B. and Moffit, R.C., "Wind Tunnel Simulation of Full-Scale Vortices", NASA CR-2180, March 1973.

19. Verstynen, H.A., Jr. and Dunham, R.E., Jr., "A Flight Investigation of the Trailing Vortices Generated by a Jumbo Jet Transport", NASA TN-D 7172, April 1973.

20. Chigier, N.A. and Corsiglia, V.R., "Wind Tunnel Test Data for Wing Trailing Vortex Flow Survey", NASA TM X-62, 148, May 1972.

21. Saffman, P.G. and Govindaraju, S.P., "Flow in a Turbulent Trailing Vortex", Physics of Fluids, Vol. 14, No. 10, p. 2074-2080, October 1971.

22. Saffman, P.G., "Structure of Turbulent Line Vortices", Physics of Fluids, Vol. 16, No. 8, p. 1181-1188, August 1973.

23. Baldwin, B.S., Sheaffer, Y.S. and Chigier, N.A., "Prediction of Far Flow Field in Trailing Vortices", AIAA Paper No. 72-989, presented at AIAA 2nd Atmospheric Flight Mechanics Conference, Palo Alto, Calif., September 11-13, 1972. (Also presented in AIAA Journal, Vol. 11, No. 12, p. 1601, December 1973.)

24. Poppleton, E.D., "A Preliminary Experimental Investigation of the Structure of a Turbulent Trailing Vortex", McGill University Mechanical Engineering Research Lab Report TN 71-1, May 1971.

25. Poppleton, E.D., "Effect of Air Injection into the Core of a Trailing Vortex", J Aircraft, Vol. 8, No. 8, p. 672-673, August 1971.

26. Hoffman, E.R. and Joubert, P.M., "Turbulent Line Vortices", Journal Fluid Mech., Vol. 16, Part 3, p. 395-411, July 1963.

27. Lamb, H., "Hydrodynamics", 6th Edition, p. 591, (Dover, New York, 1945.)

28. Lessen, M, Singh, P.J, and Paillet, F., "The Stability of a Trailing Line Vortex Part I Inviscid Theory", to be published in the Journal of Fluid Mechanics, 1974.

29. Lessen, M. and Paillet, F., "The Stability of a Trailing Vortex Part II Viscid Theory", submitted for publication to the Journal of Fluid Mechanics.

30. Professor Louis V. Schm Department of Aerospace Engineering, Naval Postgraduate School, Monterey, Calif., private communication, December 1973. (To be published.)

31. Balcerak, J.C., "Whirl Tower Tests of a UH-1D Rotor System with Mass Injection of the Tip Vortex", NASA Contract No. NAS1-11409, Report to be published 1974.

32. Kantha, H. L. Lewellen, W.S., and Durgin, F. H., "Qualitative Responses of a Vortex Core to Tip Blowing and Intersecting Airfoils" ASRL-TR 153-4, August 1971.

33. Donaldson, C., Snedeker, R.S., and Sullivan, R., "A Method of Calculating Aircraft Wake Velocity Profiles and Comparison with Full-Scale Experimental Measurements" AIAA Paper No. 74-39.

34. White, R.P., Jr., "The Reduction of Helicopter Vibration and Noise Problems by the Elimination of the Blade Tip Vortex", The Shock and Vibration Bulletin 43, June 1973.

35. Widnall, S., Sing, Chu and Lee, A., "Theoretical and Experimental Studies of Helicopter Noise Due to Blade-Vortex Interaction", AHS Symposium, Durham, N.C., September 30, 1971.

Table 1. Summary of Wind Tunnel Trailing Vortex Test Conditions

21" Chord Model:

NACA 0012 profile, AR = 5.6 (full span)
U_∞ = 150 ft/sec, $\alpha_R = 8.5^\circ$

Distance Downstream (z/c)	Nozzle Configuration	Comment
6.5	none	basic wing
6.5	1/2" Diam.	wing with sonic mass injection
6.5	5/8" Diam.	wing with sonic mass injection

8" Chord Model

NACA 0015 profile, AR = 7.3 (full span)
U_∞ = 175 ft/sec, $\alpha = 12^\circ$

Distance Downstream (z/c)	Nozzle Configuration	Comment
16.5	none	basic wing
16.5	3/8" Diam.	wing with sonic mass injection
16.5	spoiler	wing with passive turbulence generator
6.5	none	basic wing
6.5	3/8" Diam.	wing with sonic mass injection
6.5	spoiler	wing with passive turbulence generator
6.5	5/16" Diam.	wing with sonic mass injection
6.5	3/8" Diam.	wing with sonic mass injection alone

Table 2. Summary of General Trailing Vortex Parameters Measured by Hot-Wire Surveys

21 inch chord semispan model AR(full span) = 5.6, NACA 0012 profile, $\alpha_R = 8.5^\circ$, U_∞ = 150 ft/sec, L = 131 lb, D = 10.7 lb, C_L = 0.57, C_D = 0.045,

z/c = 6.5

MODEL MODIFICATION	$V_{\theta m}$ ($\frac{ft}{sec}$)	V_{zm} ($\frac{ft}{sec}$)	r_c (in)	r_c/c	$V_{\theta m}/U_\infty$	V_{zm}/U_∞	$V_{\theta m}/V_{zm}$
unmodified wing	100	0	0.6	0.03	0.67	0	∞
1/2-inch diameter nozzle, sonic injection, m=0.12 lb/sec, T=3.5 lb	41	17	2.5	0.12	0.27	0.11	2.5
5/8-inch diameter nozzle, sonic injection, m=0.18 lb/sec, T=5.4 lb	41	28	2.5	0.12	0.27	0.19	1.4

Table 2. cont'd.

8-inch chord semispan model, AR(full span) = 7.3, NACA 0015 profile, $\alpha=12^{o}$
U_∞ = 175 ft/sec, L = 51 lb, D = 3.5 lb, C_L = 0.87, C_D = 0.060,

z/c = 6.5

MODEL MODIFICATION	$V_{\theta m}$ ($\frac{ft}{sec}$)	V_{zm} ($\frac{ft}{sec}$)	r_c (in)	r_c/c	V_{θ_m}/U_∞	V_{zm}/U_∞	V_{θ_m}/V_{zm}
unmodified wing	85	0	0.4	0.05	0.49	0	∞
3/8-inch diameter nozzle, sonic injection, $\dot{m}$=0.07 lb/sec, T=1.8 lb	44	25	2.0	0.25	0.25	0.14	1.8
5/16-inch diameter nozzle, sonic injection, $\dot{m}$=0.06 lb/sec, T=1.1 lb	48	18	1.75	0.22	0.27	0.10	2.7
3/8-inch diameter nozzle, subsonic injection $\dot{m}$ =0.05 lb/sec, T=1.1 lb	48	21	1.5	0.19	0.27	0.12	2.3
3/8-inch diameter nozzle, subsonic injection, $\dot{m}$ = 0.03 lb/sec, T=0.3 lb	54	5	1.1	0.14	0.31	0.03	10
tip spoiler T = - 0.7 lb	34	-40	2.0	0.25	0.19	-0.23	-0.8

z/c = 16.5

unmodified wing	84	0	0.6	0.08	0.48	0	∞
3/8-inch diameter nozzle, sonic injection, $\dot{m}$ = 0.07 lb/sec, T = 1.8 lb	38	25	1.75	0.22	0.22	0.14	1.6
tip spoiler T = - 0.7 lb	41	-26	1.75	0.22	0.22	-0.15	-1.5

Investigator	Ref.	Comment	Measuring Technique	$\frac{\Gamma_o}{\nu}$	$\frac{r_c}{c}$	$\frac{v_{\theta m}}{U_\infty}$	$\frac{I_c}{\Gamma_o}$	$\frac{v_t}{\Gamma_o}$
ROSE & DEE	15	Flight Test	Flow Vane	$\sim 10^7$	0.2	0.1	0.4	2×10^{-4}
DOSANJH ET AL	16	Wind Tunnel Test	Pressure Probe	2×10^3	0.1	0.2	0.6	5×10^{-3}
NEWMAN	17	Wind Tunnel Test	Pitot Tube	2×10^4	0.01	0.2	0.6	2×10^{-3}
McCORMICK ET AL	8	Flight Test	Vorticity Meter	$\sim 10^6$	0.4	0.4	0.6	5×10^{-5}
RORKE & MOFFITT	18	Wind Tunnel Test	Triaxial Hot-Wire, (Slow Traverse)	4×10^5	0.07	0.5	0.7	7×10^{-5}
VERSTYNEN & DUNHAM	19	Flight Test	Flow Vane	3×10^7	0.09	0.2	0.2	3×10^{-4}
CHIGIER & CORSIGLIA	20	Wind Tunnel Test	Triaxial Hot-Wire, (Stationary)	2×10^5	0.1	0.1	0.8	3×10^{-3}
SAFFMAN	21 22	Theoretical Model	-----	∞				8×10^{-3}
BALDWIN ET AL	23	Theoretical Model Applied to McCormick's Data	-----	$\sim 10^6$	0.08	0.3	0.9	2×10^{-4}
POPPLETON	24 25	Wind Tunnel Test, Split Wing	Single Element Hot Wire, (Stationary)	5×10^4	0.3	0.09	0.8	5×10^{-3}
		Split Wing with Vortex Injection	"	5×10^4	0.6	0.07	0.9	3×10^{-2}
PRESENT TESTS (8-Inch Chord Model z/c =16.5)		Wind Tunnel Test, Unmodified Wing	Triaxial Hot-Wire, (Fast Traverse)	3×10^5	0.08	0.5	0.5	1×10^{-5}
		Wing with Mass injection	"	3×10^5	0.2	0.2	0.6	6×10^{-4}
		Wing with Tip Spoiler	"	3×10^5	0.2	0.2	0.7	∞

Table 3. Survey of Published Trailing Vortex Characteristics

Fig. 1. 21-inch chord semispan model as installed in the University of Maryland Wind Tunnel with closeup photograph of injection nozzle

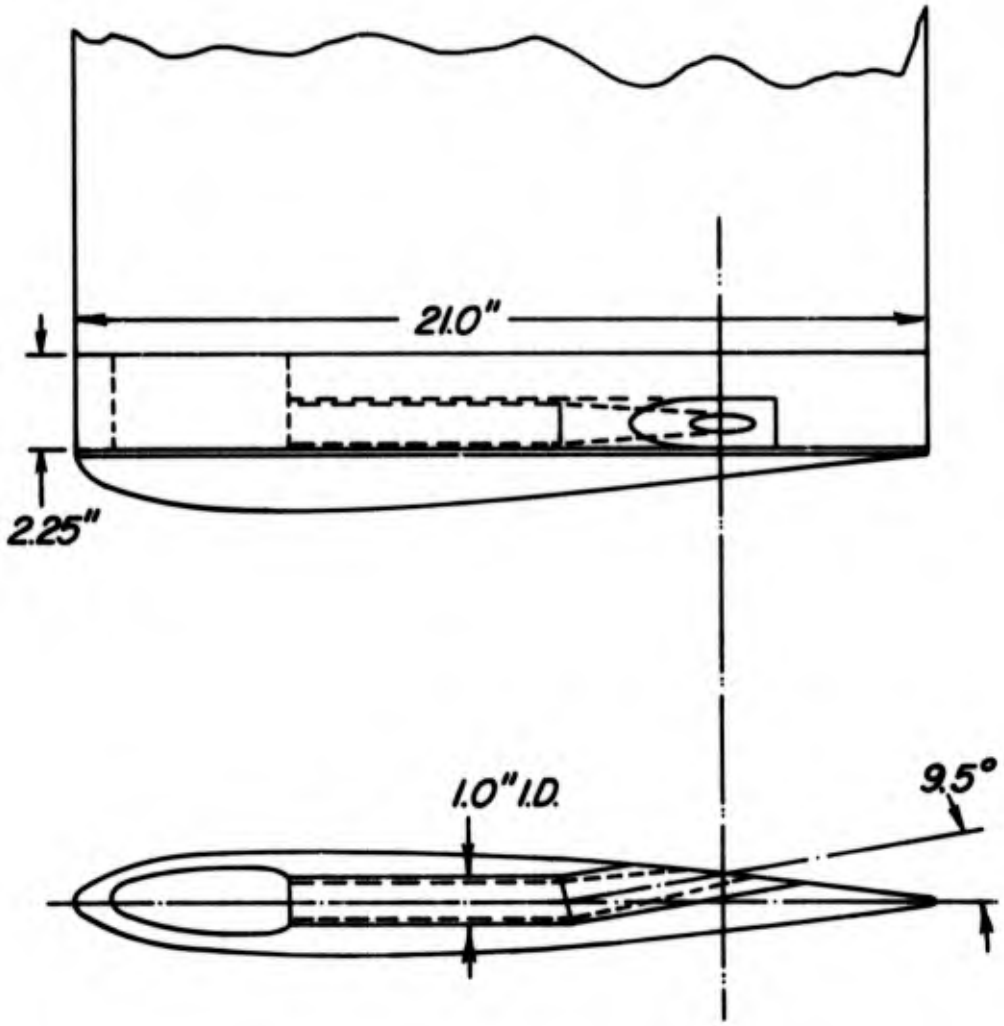

Figure 2. Sketch of the sonic tip vortex injection nozzle for the 21-inch chord semispan model

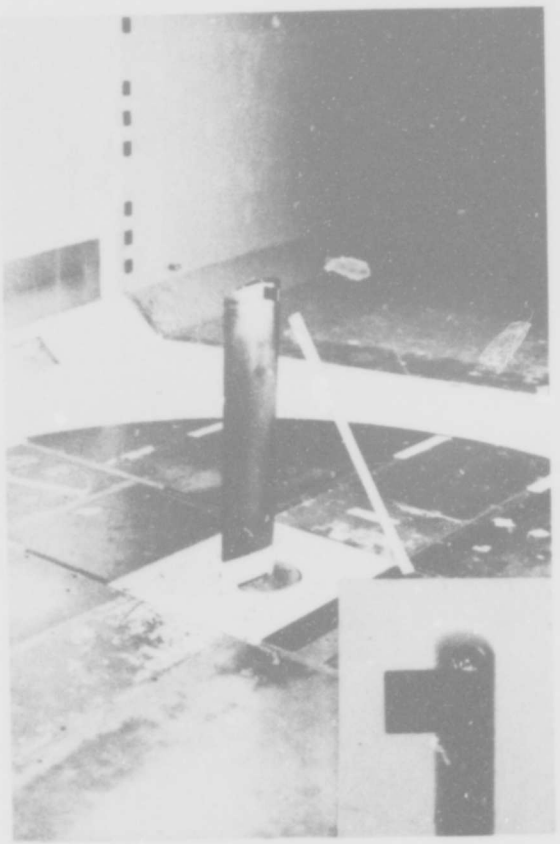

Fig. 3. 8-inch chord semispan model as installed in the University of Maryland Wind Tunnel with tip spoiler configuration

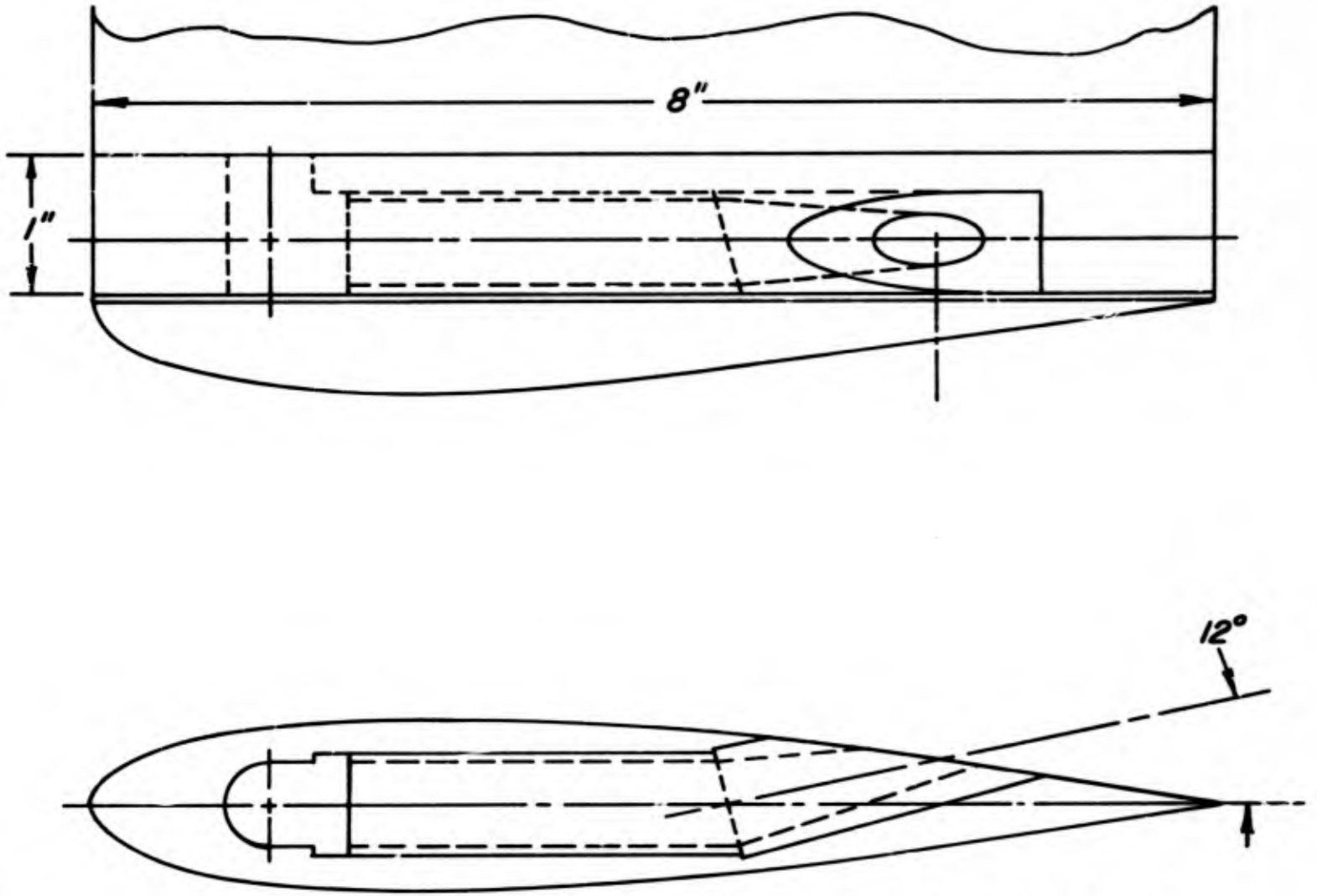

Figure 4. Sketch of the sonic tip vortex injection nozzle for the 8-inch chord semispan model

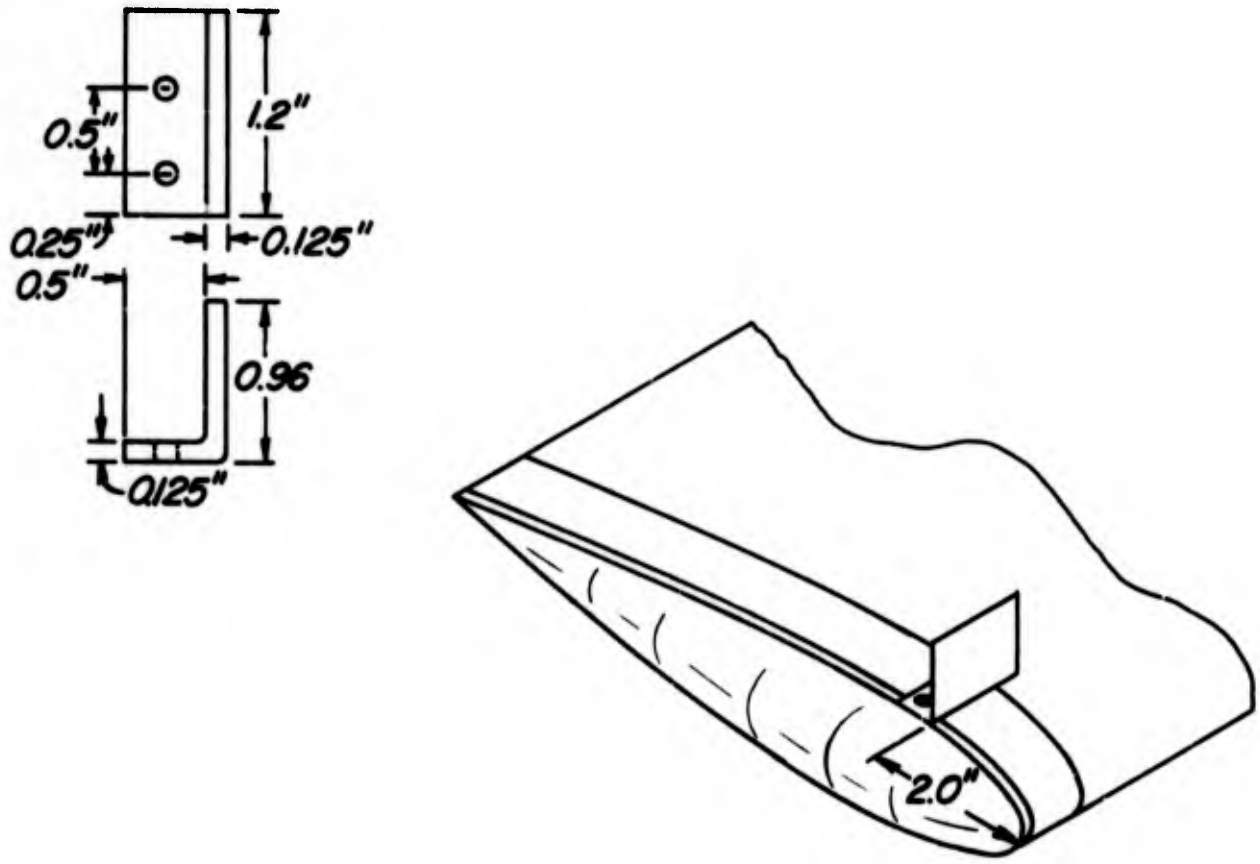

Figure 5. Sketch of the tip spoiler for the 8-inch chord semispan model

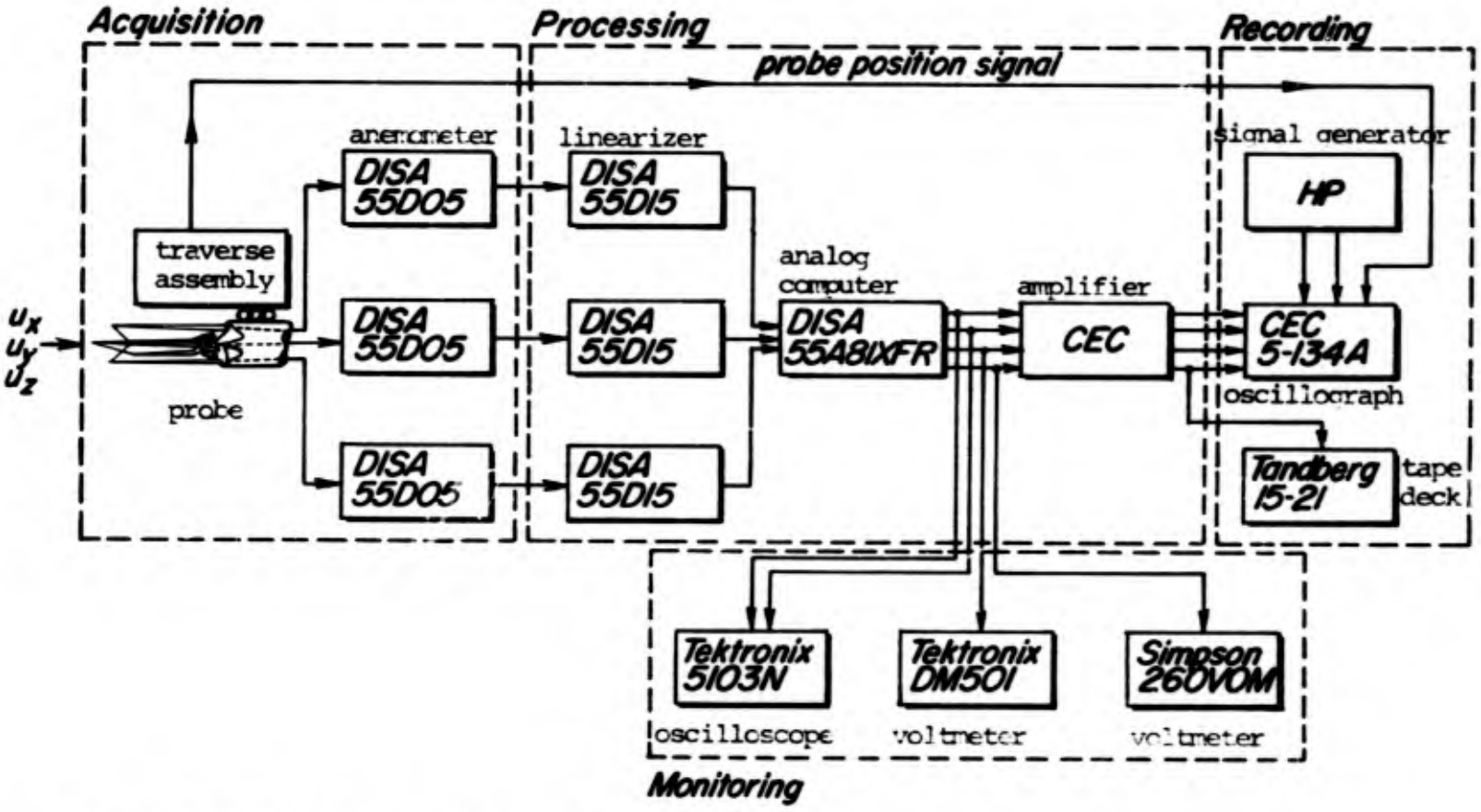

Figure 6. Block diagram of triaxial hot-wire system

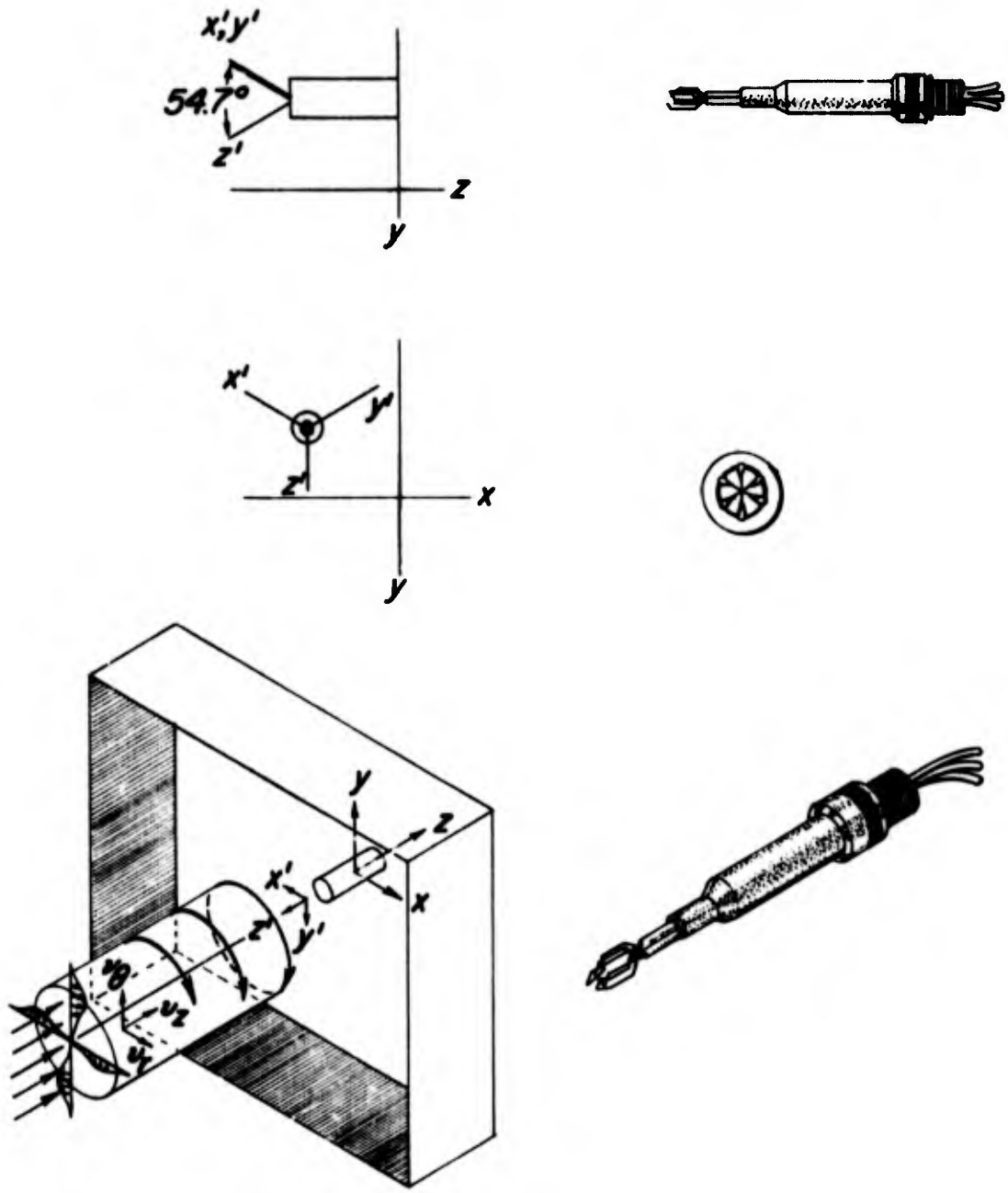

Figure 7. Sketch of triaxial hot-wire probe coordinate system

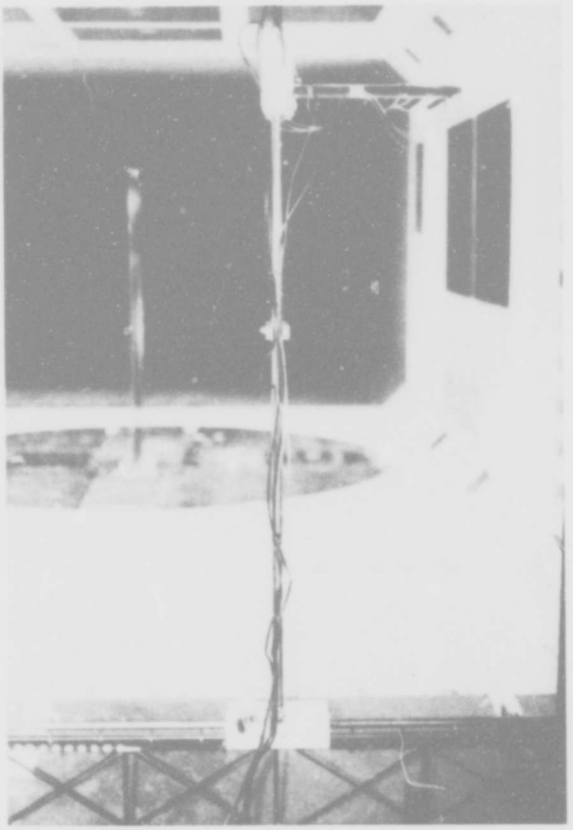

Fig. 8. Variable speed traverse mechanism installed in wind tunnel - upstream view

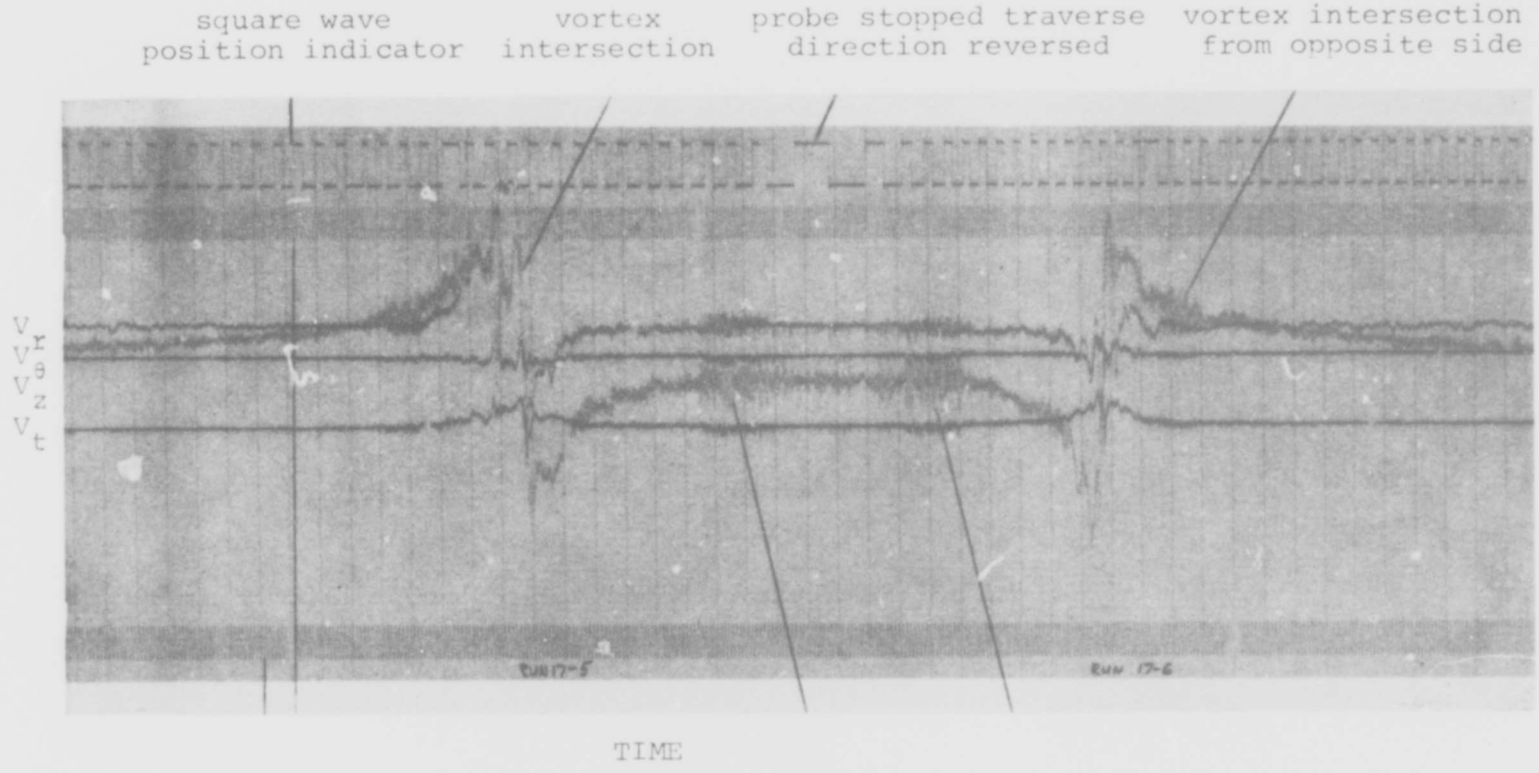

Figure 9. Sample oscillograph record of hot-wire vortex traverse for the unmodified 21-inch chord semispan model z/c = 6.5, U_∞ = 150 ft/sec, $\alpha_R = 8.5^\circ$

v_r radial velocity of trailing vortex

v_θ tangential velocity of trailing vortex

v_z axial velocity of trailing vortex

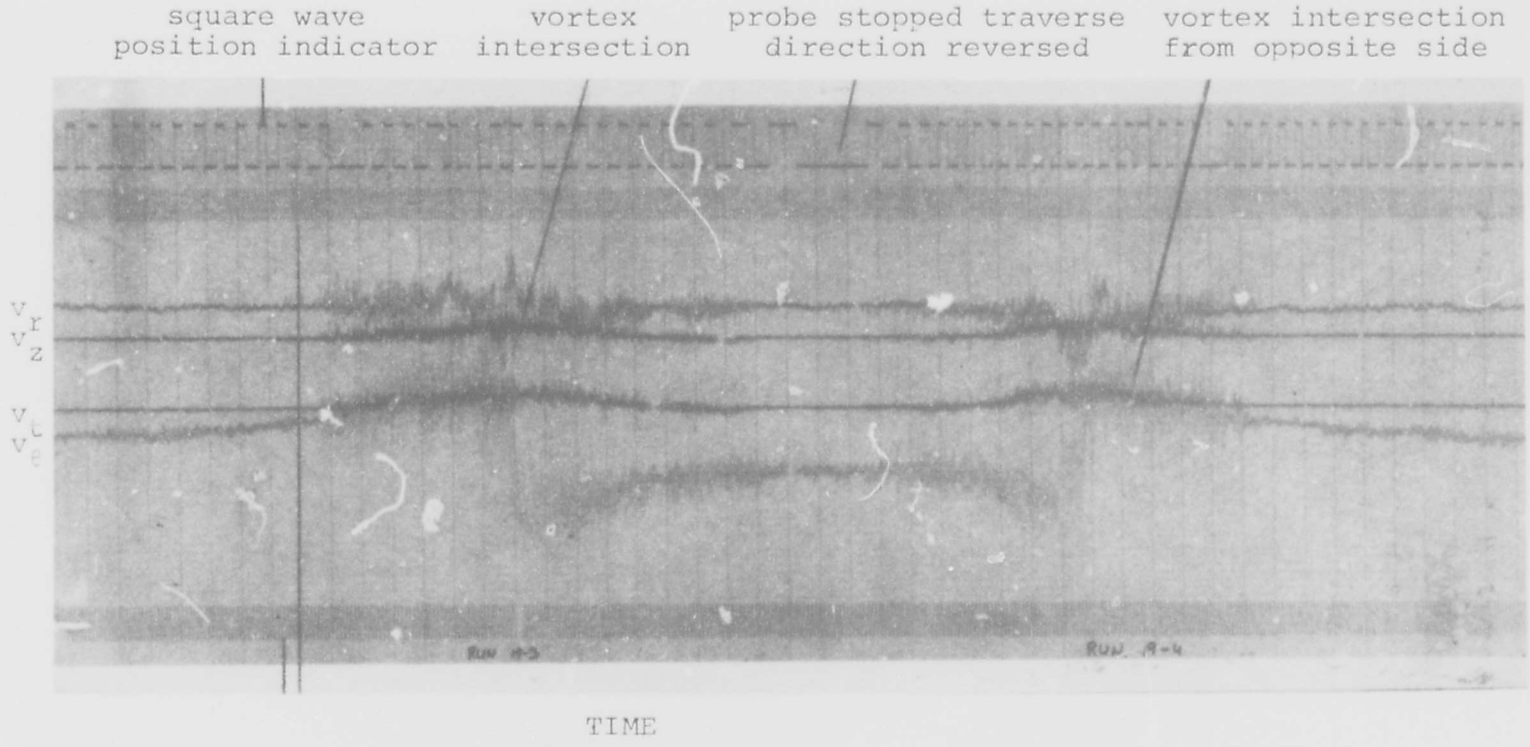

Figure 10. Sample oscillograph record of hot-wire vortex traverse for the 21-inch chord semispan model with the 1/2-inch diameter sonic jet, $\dot{m}$ = 0.12 lb/sec, z/c = 6.5, U_∞ = 150 ft/sec, $\alpha_R = 8.5^\circ$

v_r = radial velocity of trailing vortex

v_θ = tangential velocity of trailing vortex

v_z = axial velocity of trailing vortex

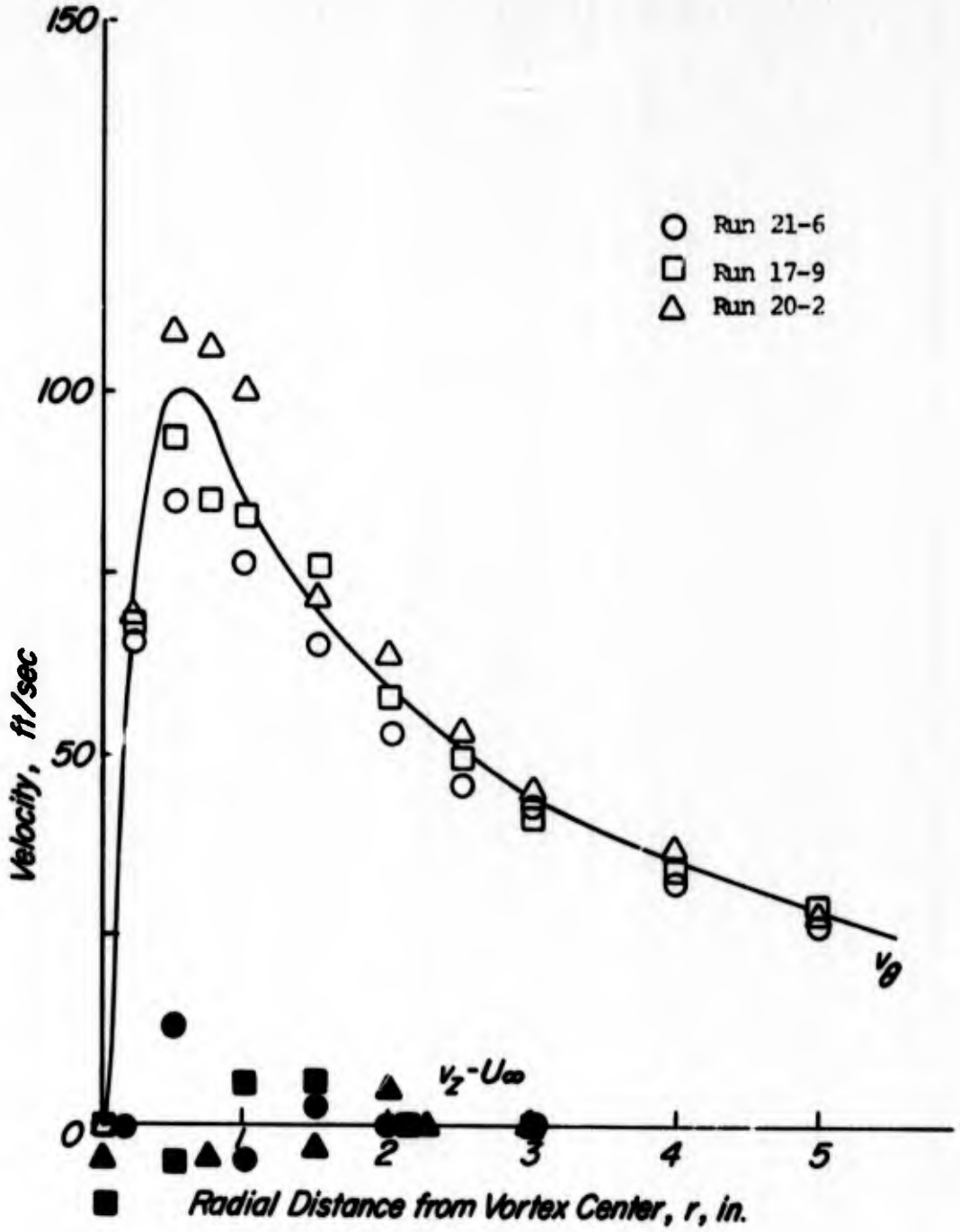

Figure 11. Mean velocity distribution of the trailing vortex for the 21-inch chord unmodified model, z/c = 6.5, U_∞ = 150 ft/sec, $\alpha_R = 8.5^\circ$

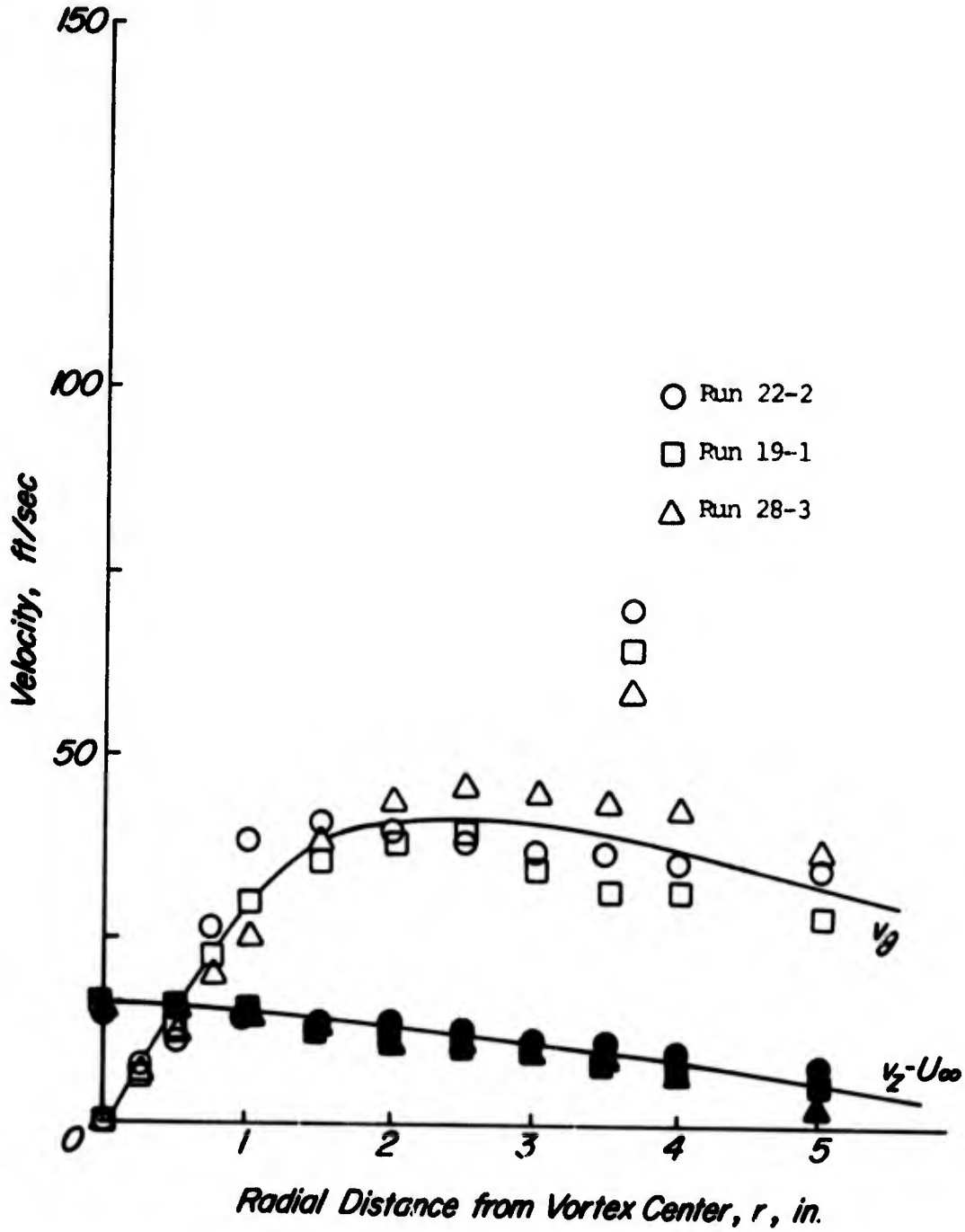

Figure 12. Mean velocity distribution of the trailing vortex for the 21-inch chord model with the 1/2-inch diameter sonic nozzle the $\dot{m}$ = 0.12 lb/sec, z/c = 6.5, U_∞ = 150 ft/sec, α_R = 8.5°

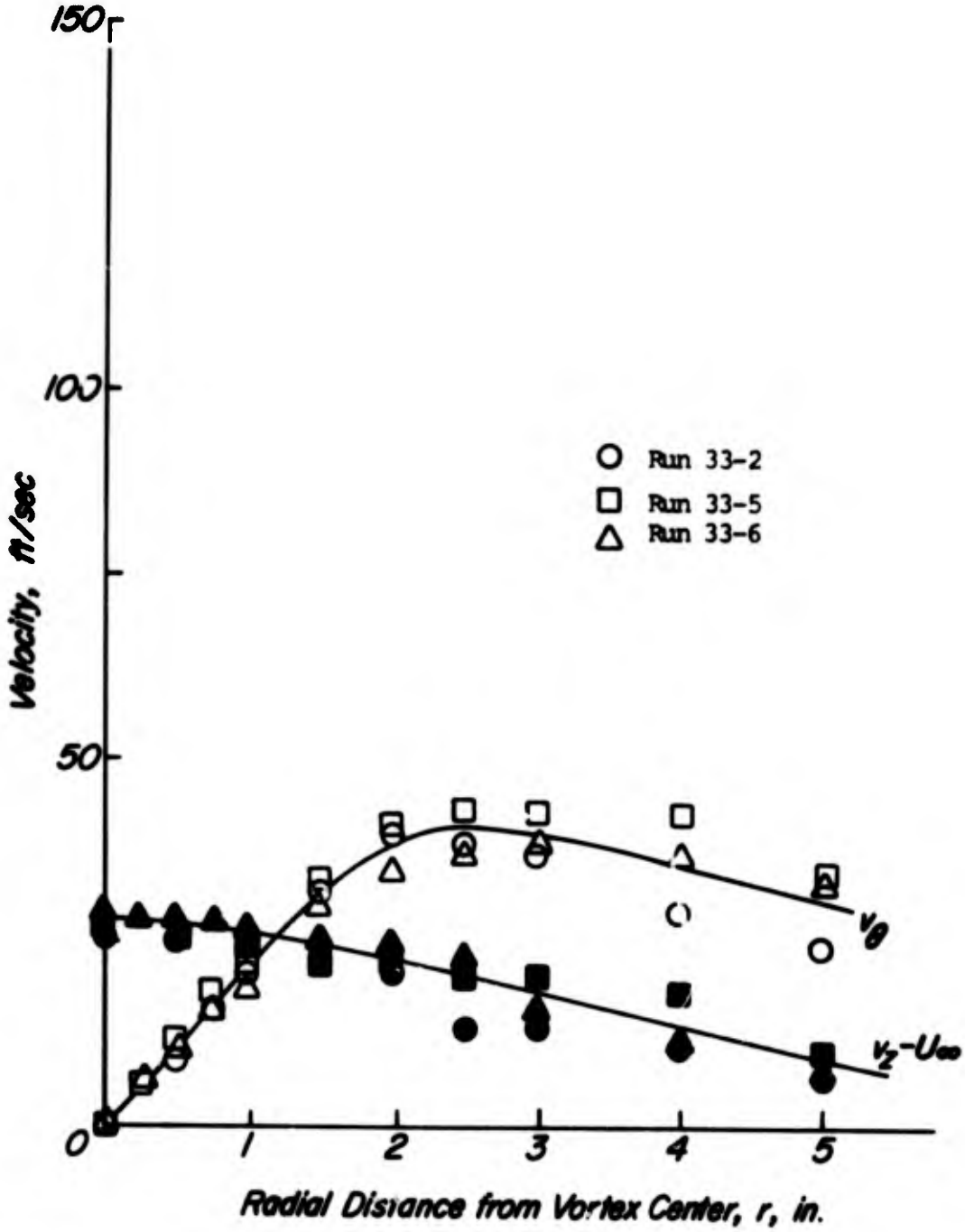

Figure 13 . Mean velocity distribution of the trailing vortex for the 21-inch chord model with the 5/8-inch diameter sonic nozzle, $\dot{m}$ = 0.18 lb/sec, z/c = 6.5, U_∞ = 150 ft/sec, $\alpha_R = 8.5^\circ$

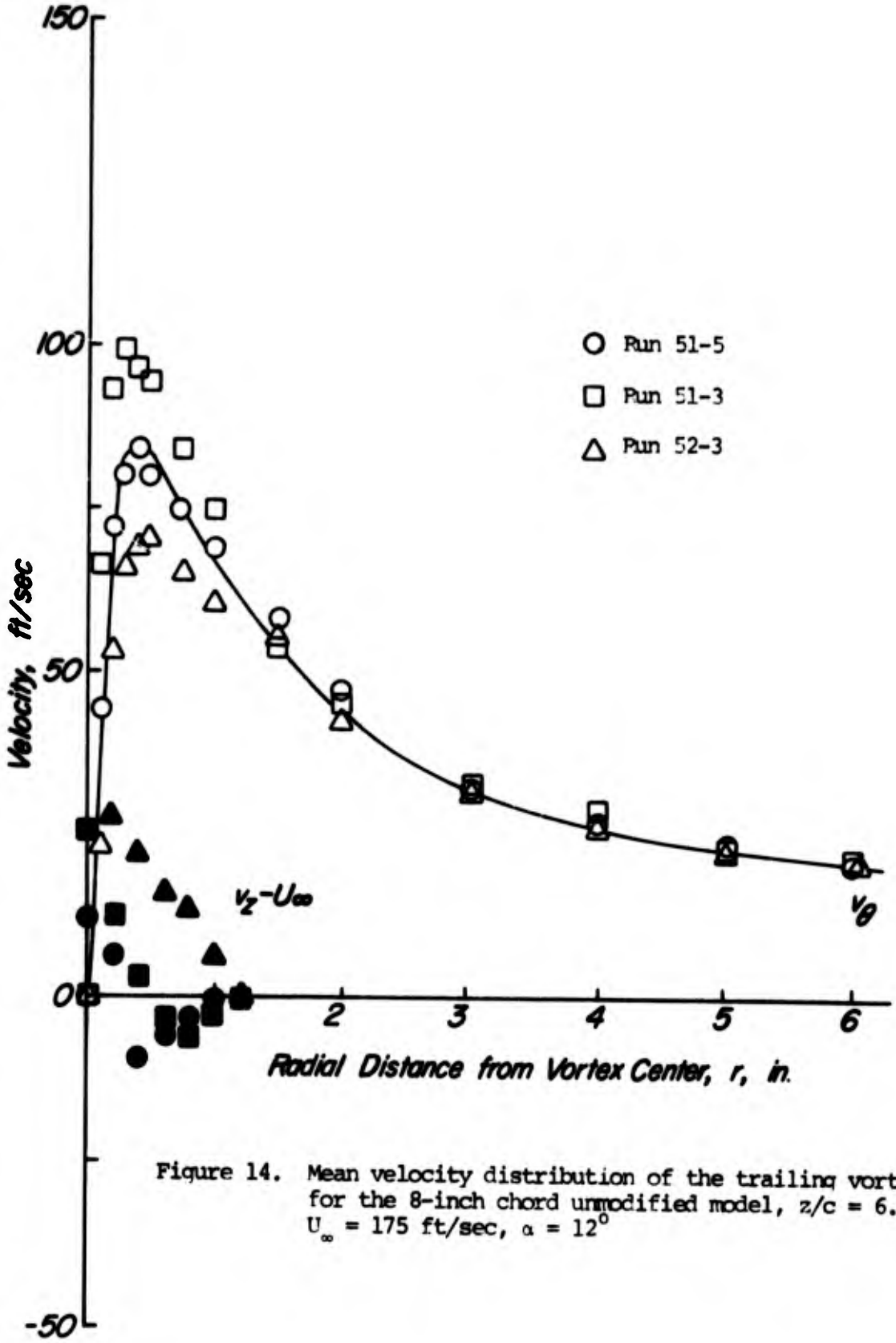

Figure 14. Mean velocity distribution of the trailing vortex for the 8-inch chord unmodified model, z/c = 6.5, U_∞ = 175 ft/sec, $\alpha = 12^\circ$

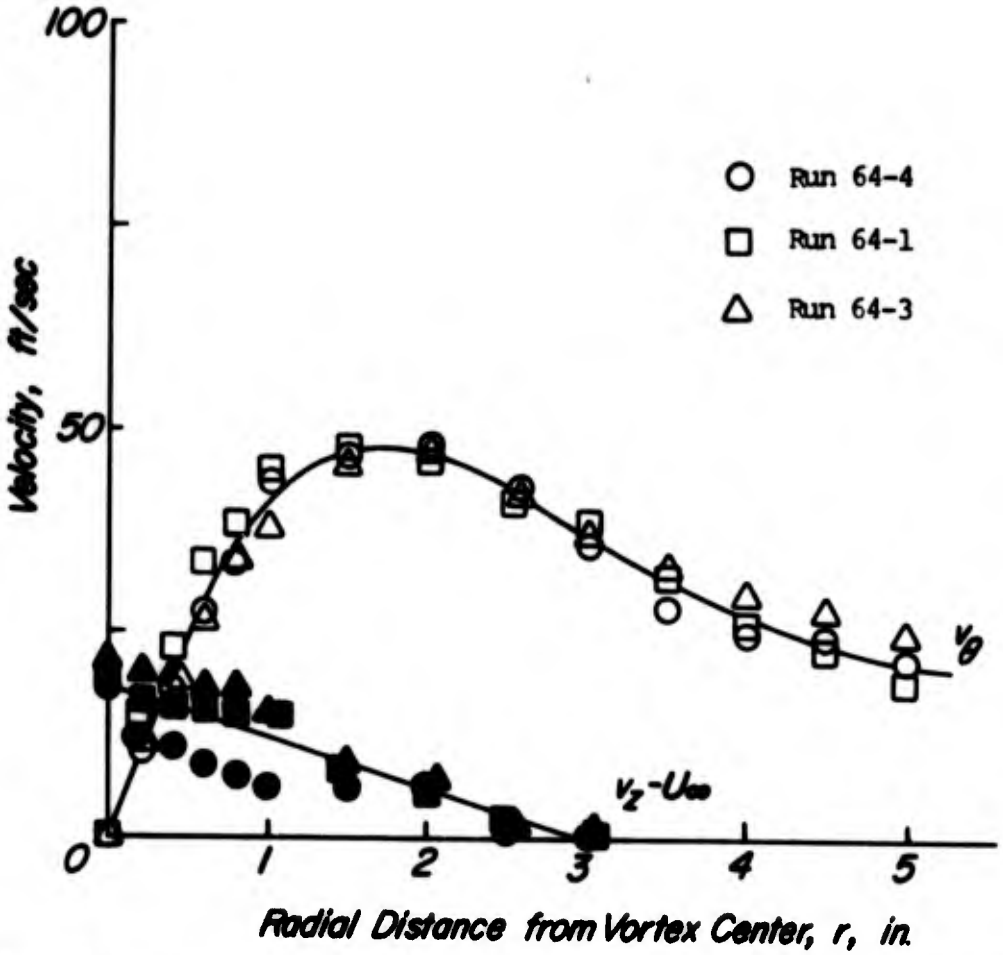

Figure 15. Mean velocity distribution of the trailing vortex for the 8-inch chord model with the 5/16-inch diameter sonic nozzle, $\dot{m}$ = 0.06 lb/sec, z/c = 6.5, U_∞ = 175 ft/sec, $\alpha = 12^\circ$

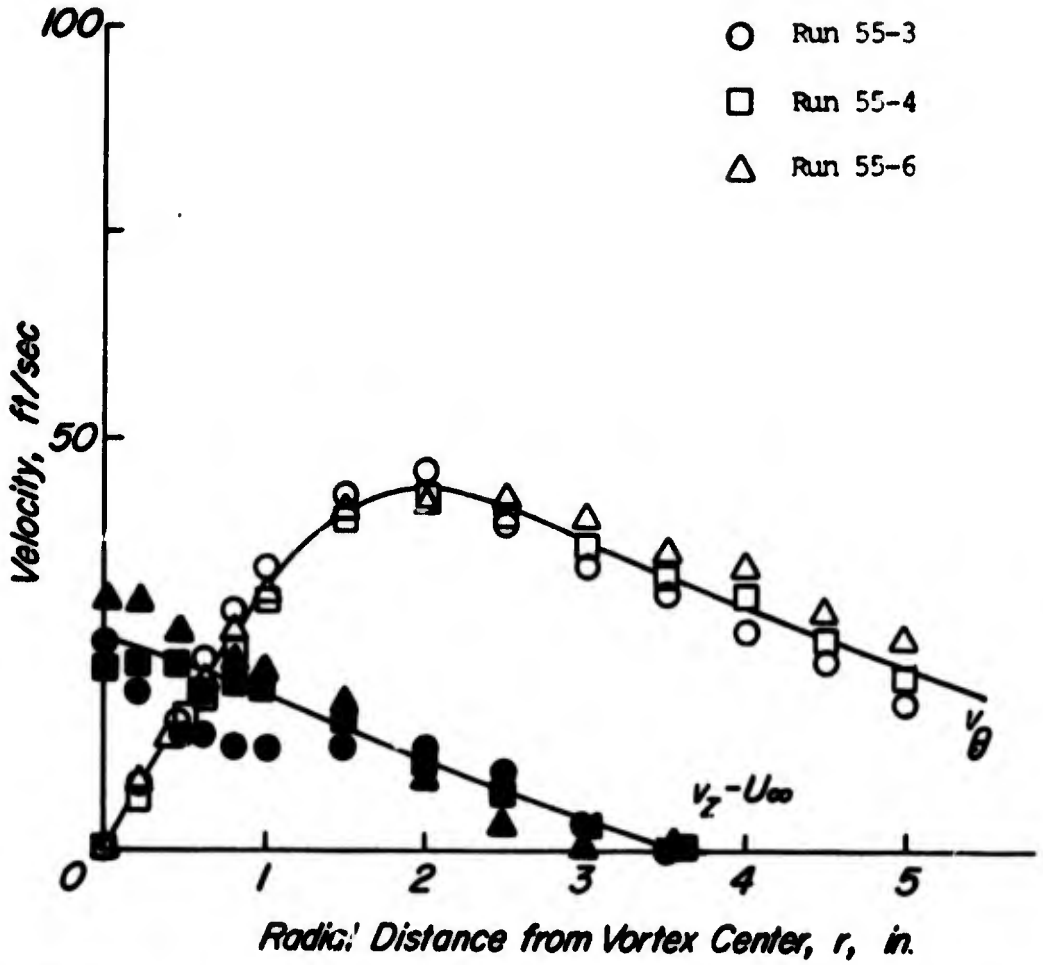

Figure 16. Mean velocity distribution of the trailing vortex for the 8-inch chord model with the 3/8-inch diameter sonic nozzle, $\dot{m}$ = 0.07 lb/sec, z/c = 6.5, U_∞ = 175 ft/sec, α = 12°

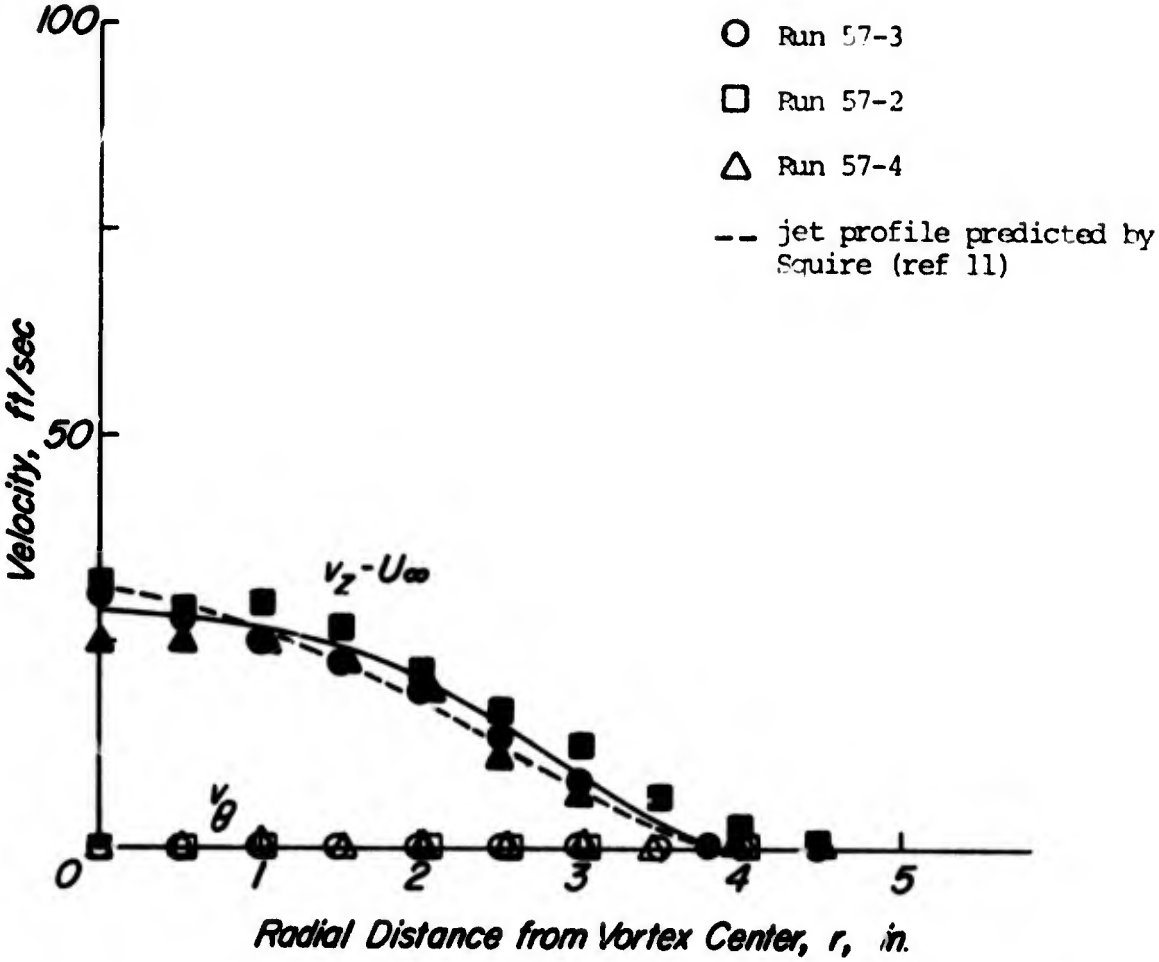

Figure 17. Mean velocity distribution in the wake of the 8-inch chord model with the 3/8-inch diameter nozzle, $\dot{m}$ = 0.07 lb/sec, z/c = 6.5, U_∞ = 175 ft/sec, $\alpha = 0^0$

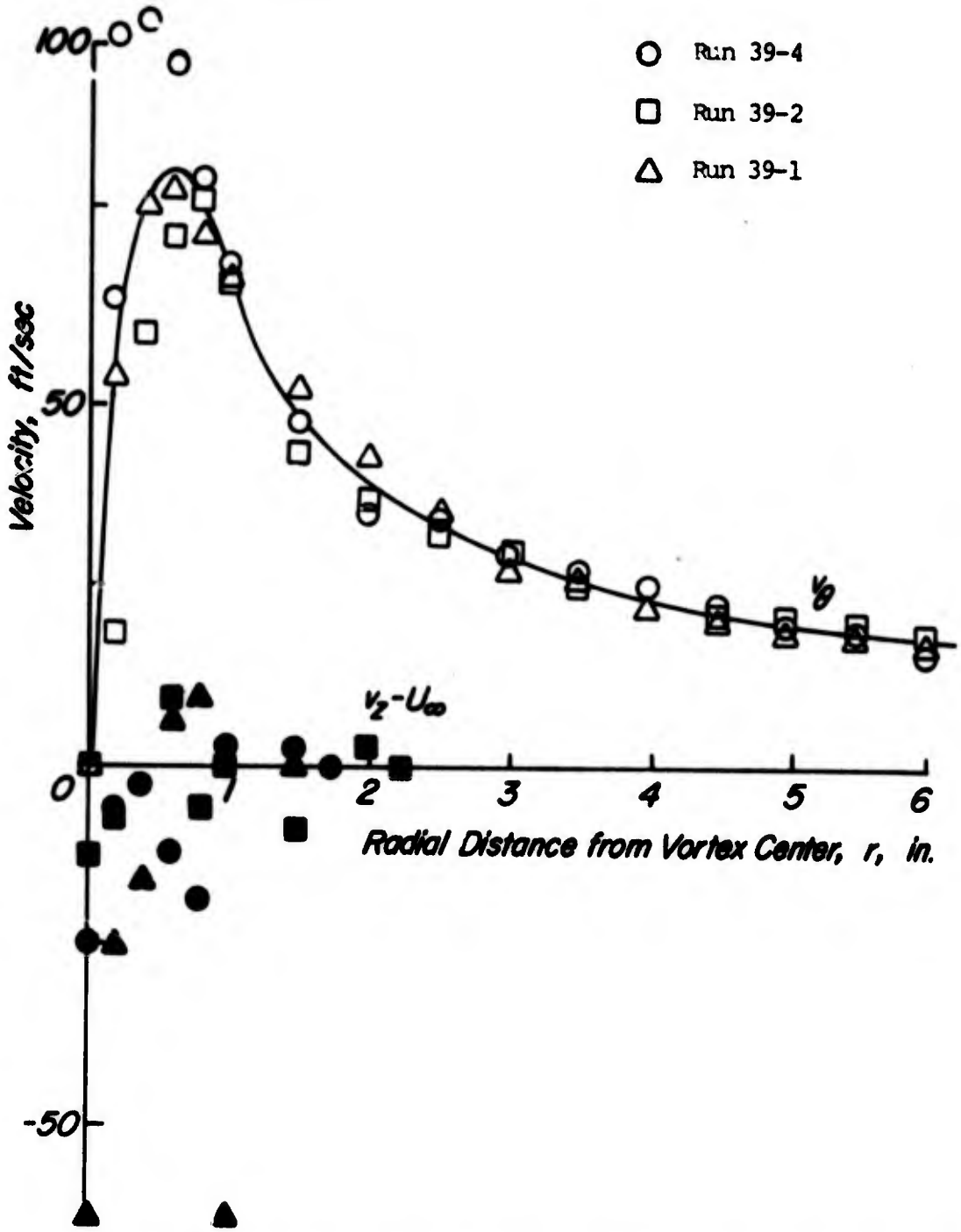

Figure 18. Mean velocity distribution of the trailing vortex for the 8-inch chord unmodified model, z/c = 16.5, U_∞ = 175 ft/sec, $\alpha = 12^\circ$

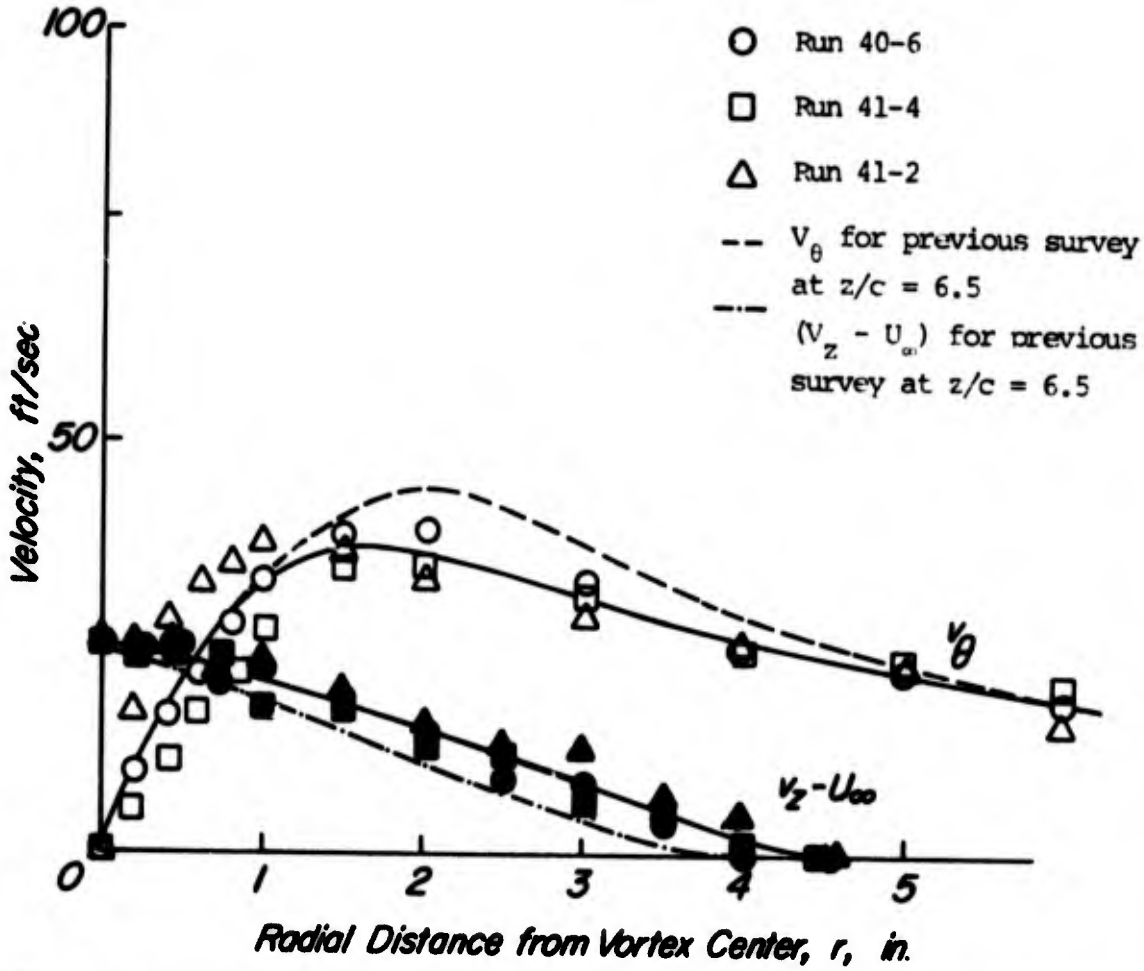

Figure 19. Mean velocity distribution of the trailing vortex for the 8-inch chord model with the 3/8-inch diameter sonic nozzle, m = 0.07 lb/sec, z/c = 16.5, U_∞ = 175 ft/sec, α = 12°

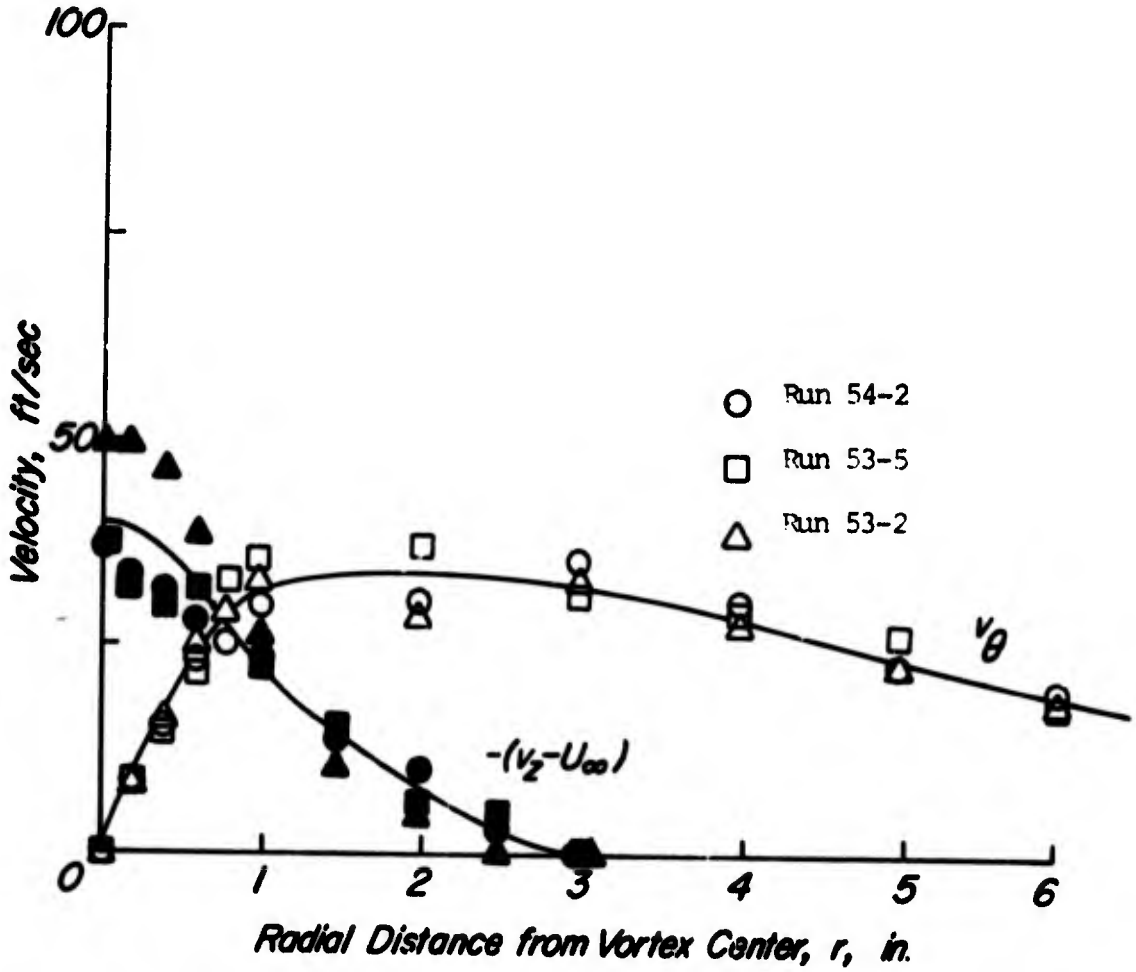

Figure 20. Mean velocity distribution of the trailing vortex for the 8-inch chord model with the tip spoiler, z/c = 6.5, U_∞ = 175 ft/sec, $\alpha = 12^\circ$

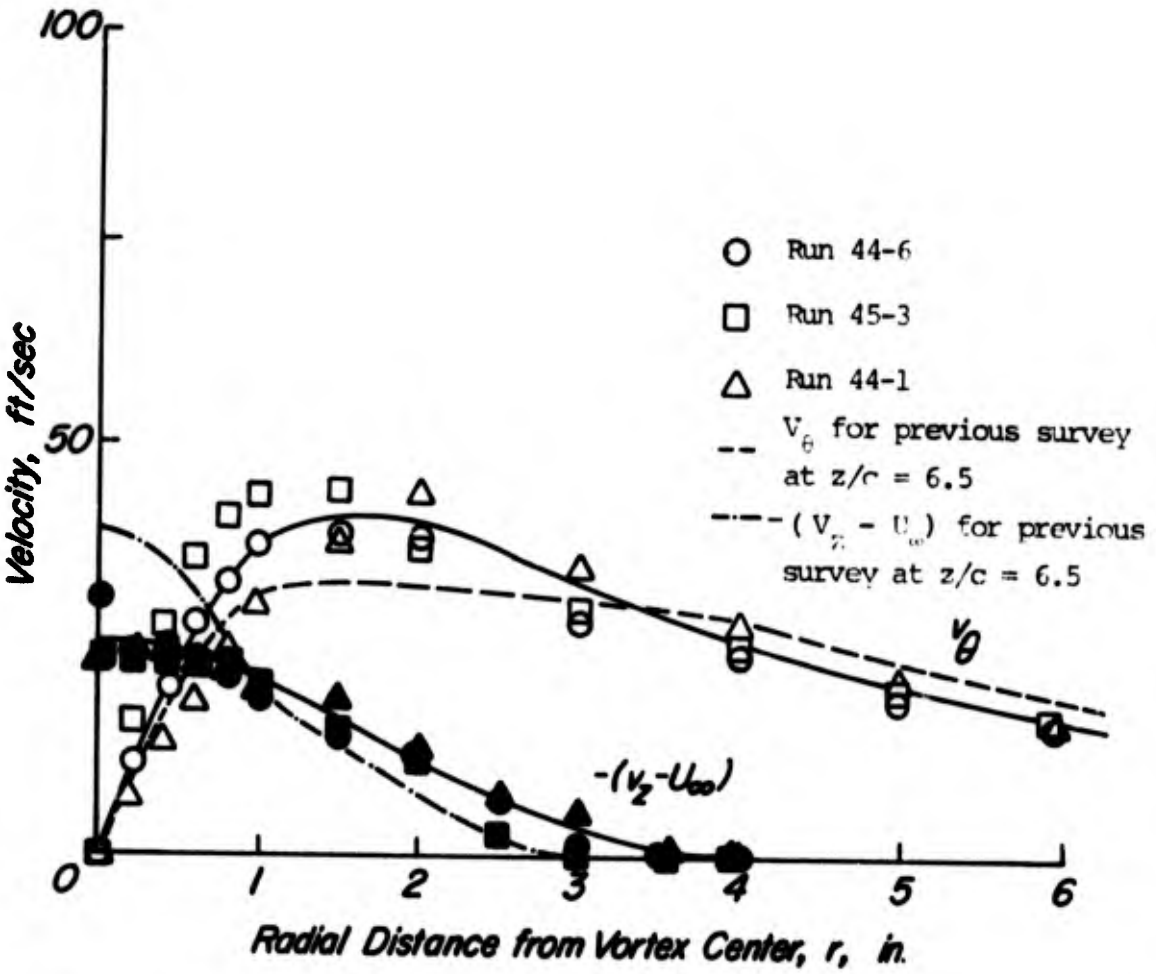

Figure 21. Mean velocity distribution of the trailing vortex for the 8-inch chord model with the tip spoiler, z/c = 16.5, U_∞ = 175 ft/sec, $\alpha = 12^\circ$

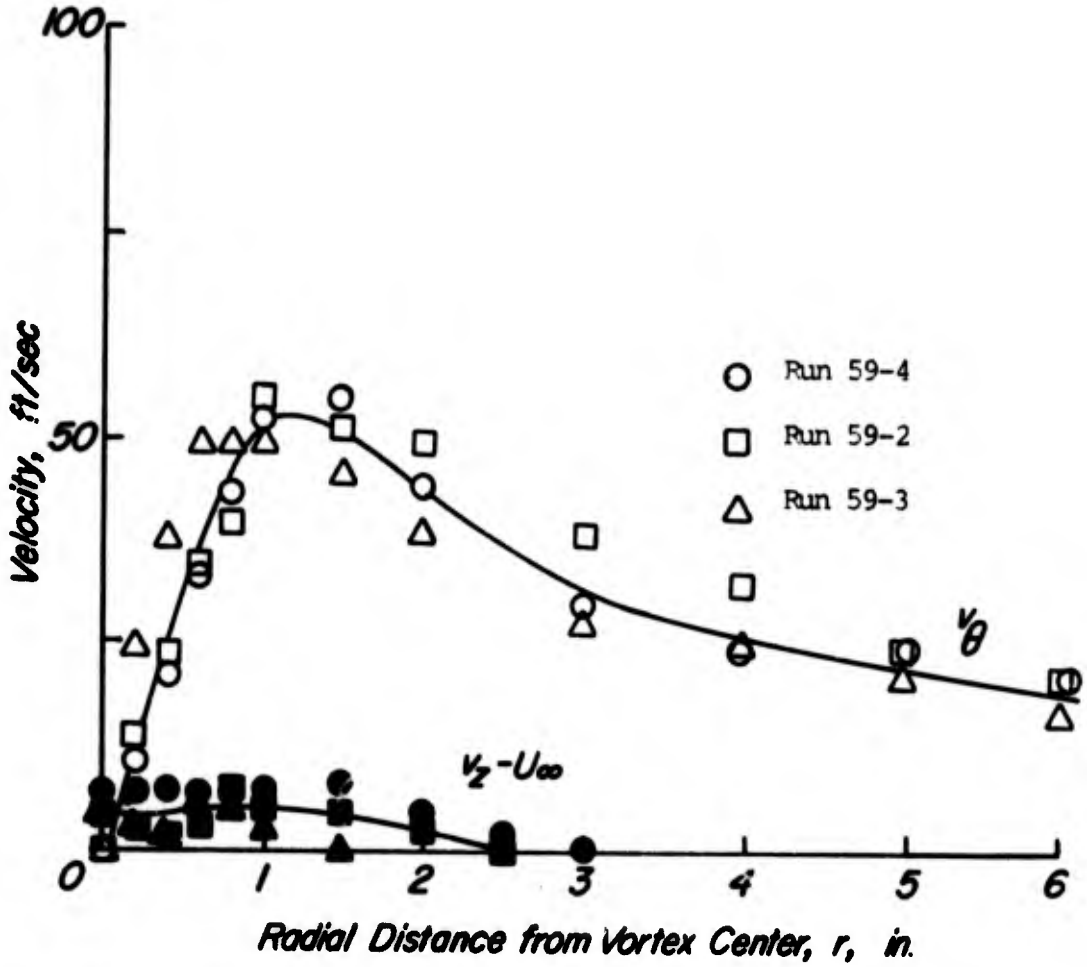

Figure 22. Mean velocity distribution of the trailing vortex for the 8-inch chord model with the 3/8-inch diameter nozzle with subsonic injection, T = 0.3 lb, z/c = 6.5, U_∞ = 175 ft/sec, $\alpha = 12^\circ$

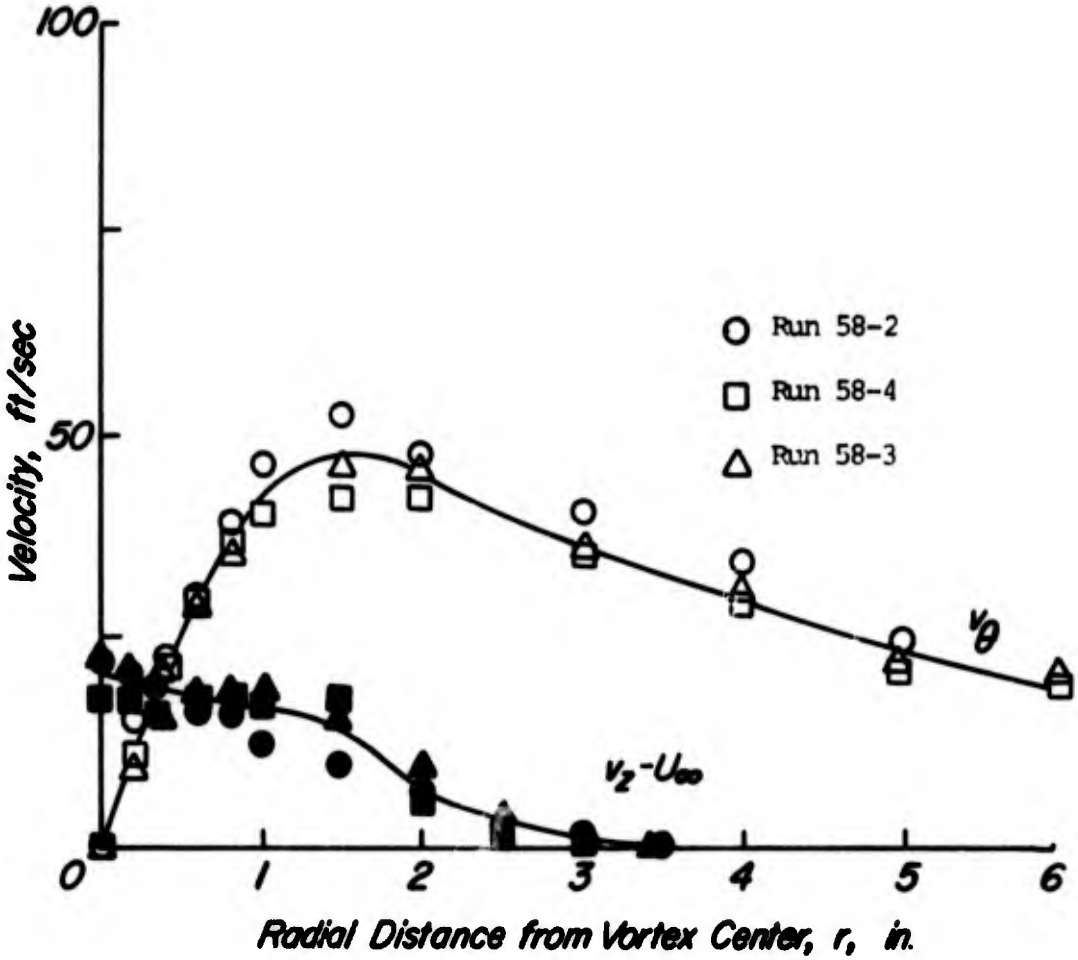

Figure 23. Mean velocity distribution of the trailing vortex for the 8-inch chord model with the 3/8-inch diameter nozzle with subsonic injection, T = 1.1 lb, z/c = 6.5, U_∞ = 175/sec, $\alpha = 12^0$

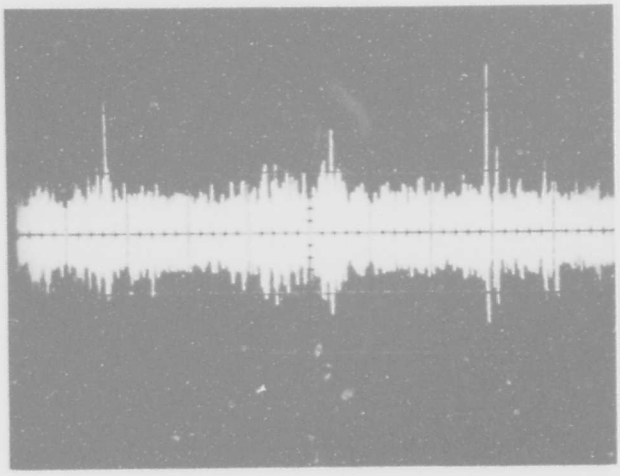

A. Unmodified model

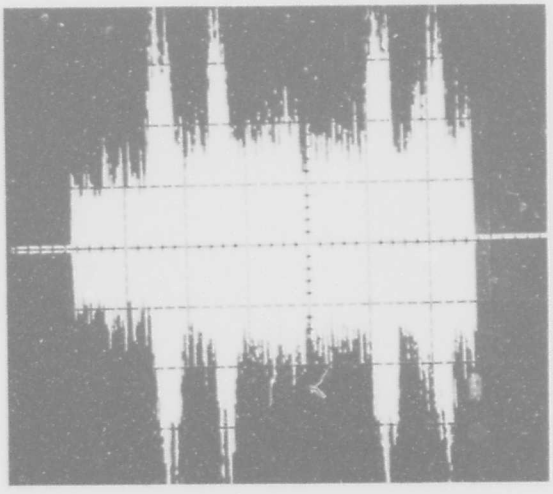

B. Model with blowing (3/8-inch diameter nozzle with sonic injection, $\dot{m}$ = 0.07 lb/sec)

Figure 24. Unsteady total velocity component observed during hot-wire traverse across the core of the trailing vortex for the 8-inch chord model at z/c = 6.5, $\alpha = 12^{o}$, U_{∞} = 175 ft/sec, (vertical scale 3 ft/sec per division)

Figure 24. (cont'd.)

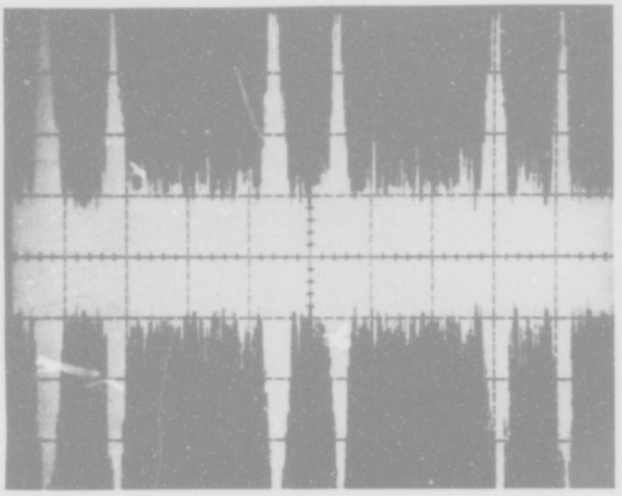

C. Model with tip spoiler

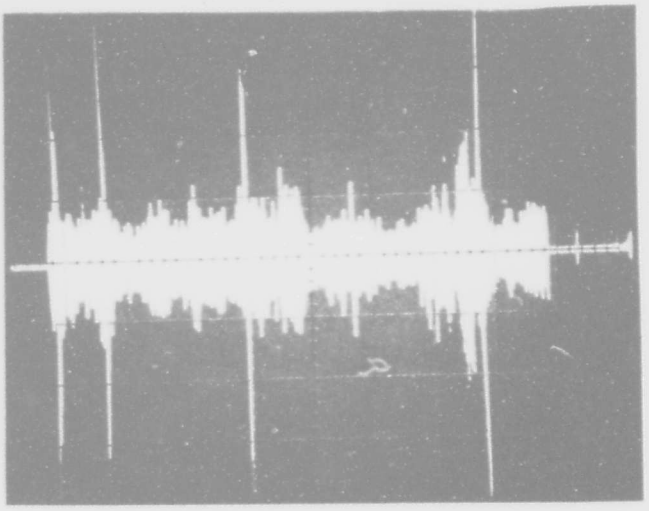

A. Unmodified model

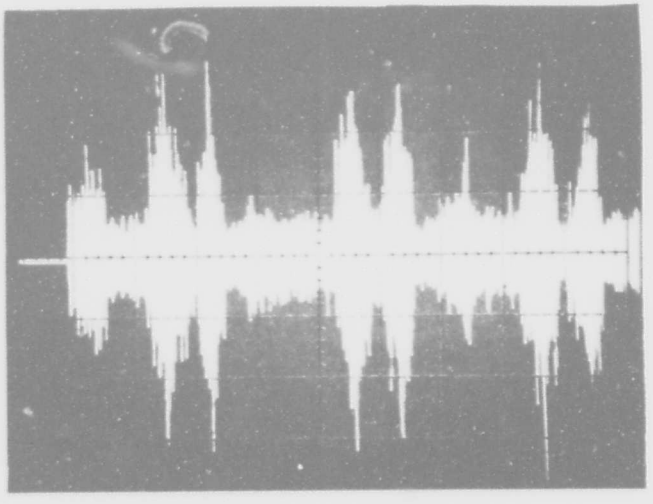

B. Model with blowing (3/8-inch diameter nozzle with sonic injection $\dot{m}$ = 0.07 lb/sec)

Fig. 25. Unsteady total velocity component observed during hot-wire traverses across the core of the trailing vortex for the 8-inch chord model at z/c = 16.5, U_∞ = 175 ft/sec, $\alpha = 12^\circ$

(vertical scale 3 ft/sec per division)

Figure 25. (cont'd.)

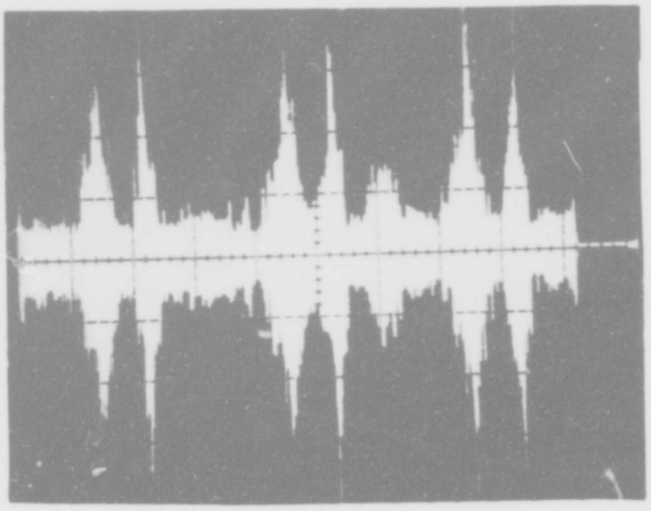

C. Model with tip spoiler

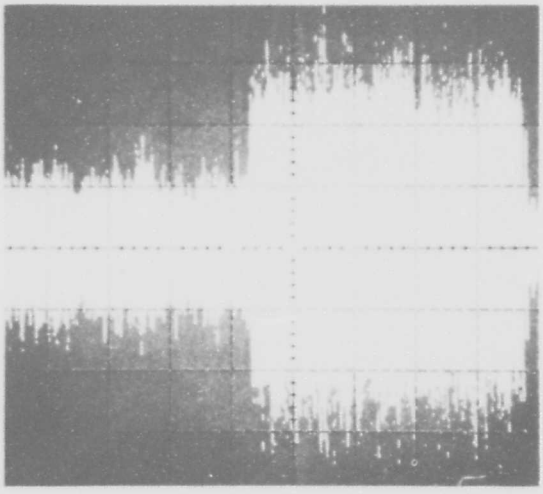

A. Left hand side; unmodified model, right hand side; model with 1/2-inch diameter sonic nozzle ($\dot{m}$ = 0.12 lb/sec)

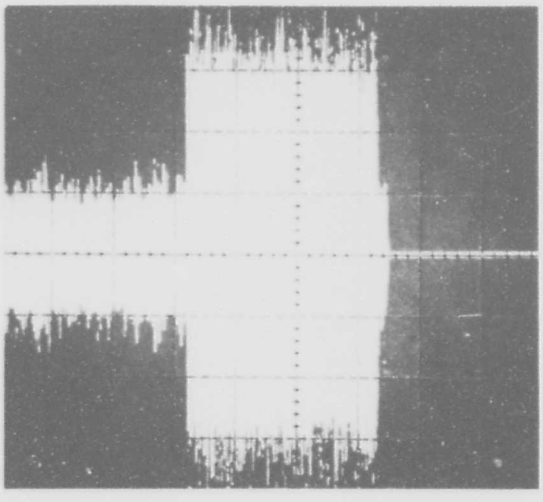

B. Left hand side; unmodified model, right hand side; model with 5/8-inch diameter sonic nozzle ($\dot{m}$ = 0.18 lb/sec)

Fig. 26. Unsteady total velocity component observed with stationary hot-wire probe positioned in the center of the trailing vortex core for the 21-inch chord model z/c = 6.5, U_∞ = 150 ft/sec, $\alpha_R = 8.5^\circ$ (vertical scale 2.6 ft/sec per division)

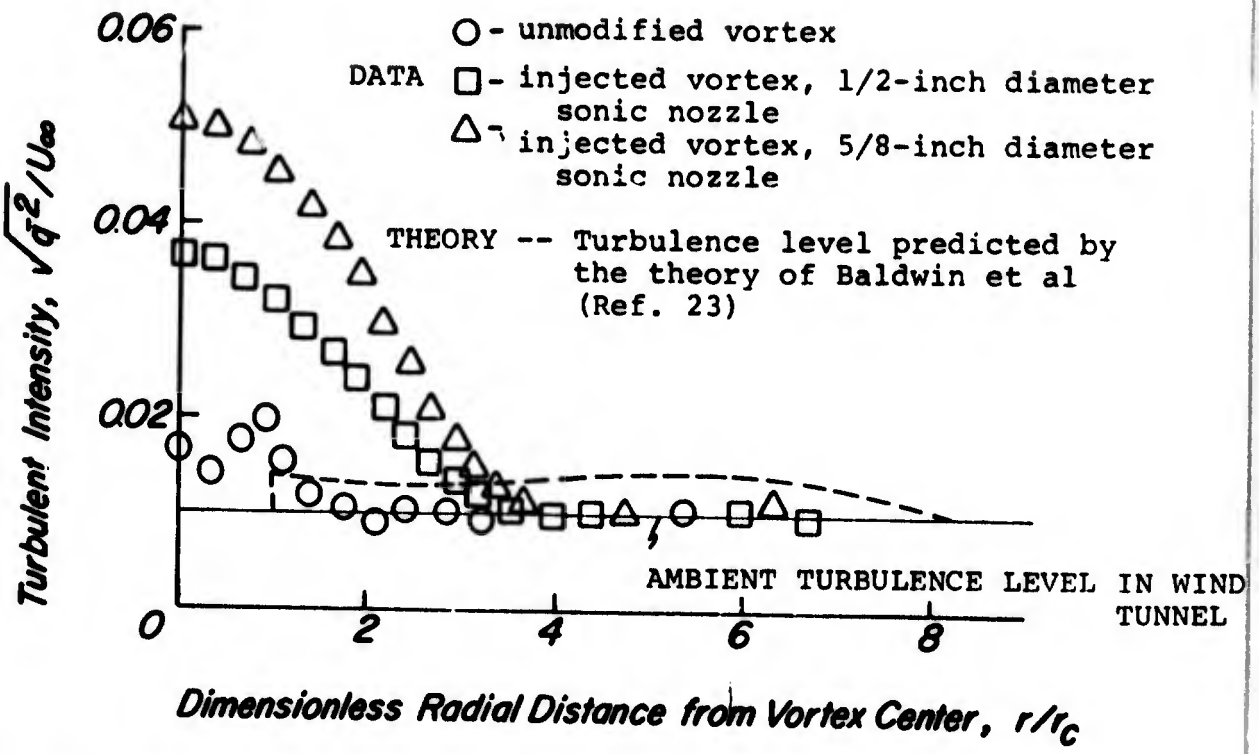

Fig. 27. Distribution of turbulence in the core of the trailing vortex for the 21-inch chord semispan model, z/c = 6.5, U_∞ = 175 ft/sec, α_R = 8.5°

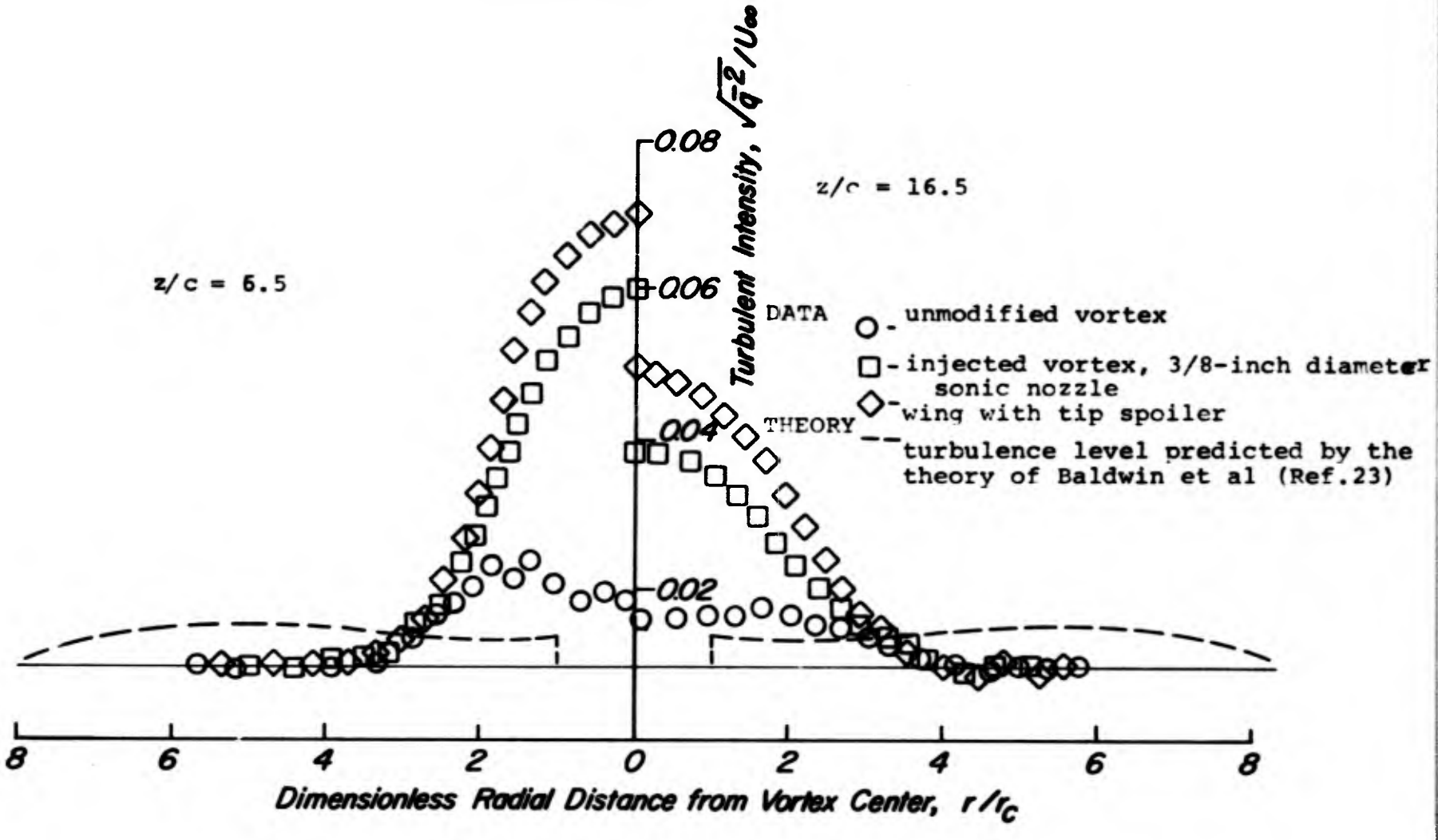

Fig. 28. Distribution of turbulence in the core of trailing vortex for the 8-inch chord semispan model, U_∞ = 175 ft/sec, α = 12°

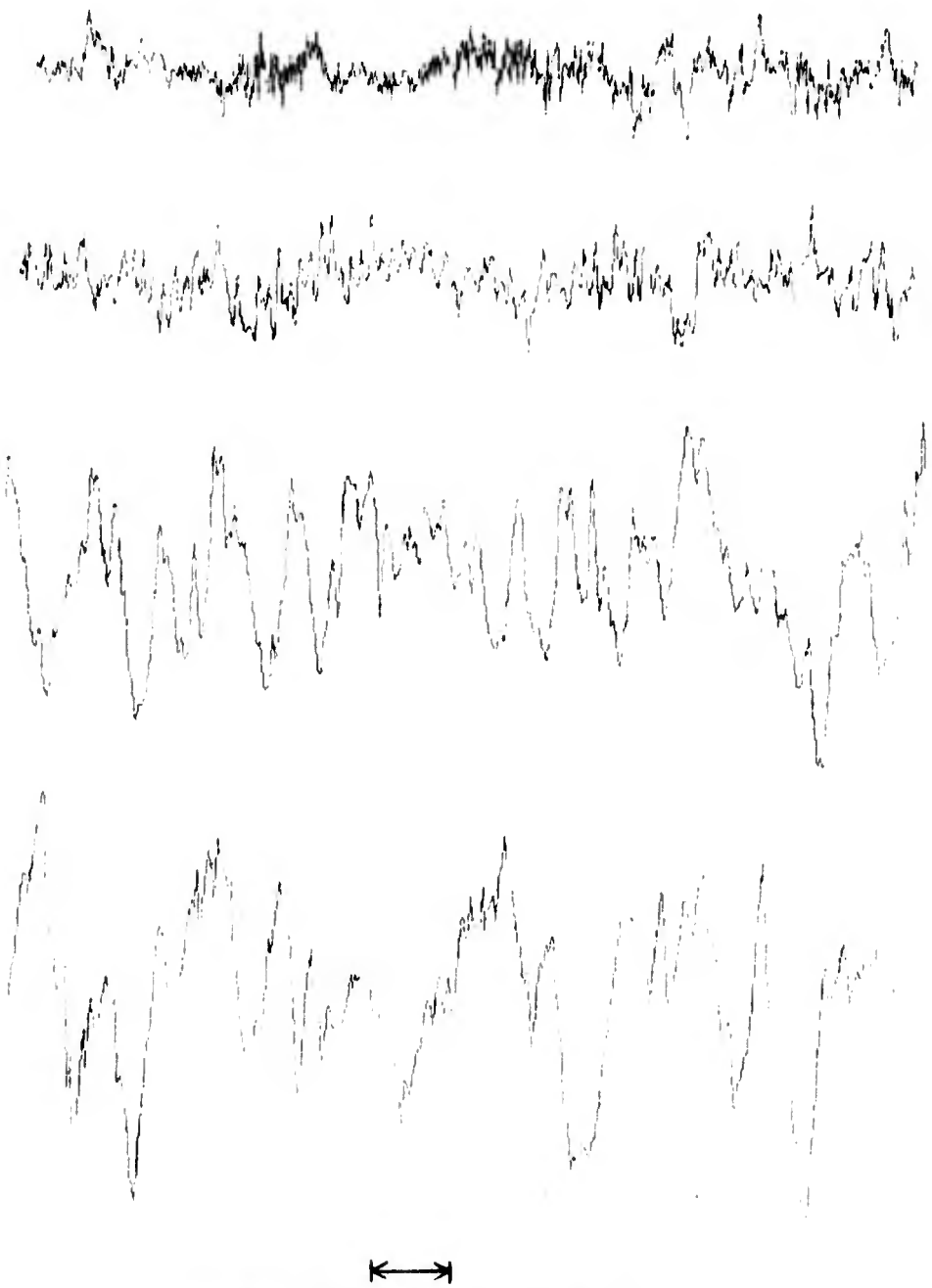

TIME SCALE 0.001 SECONDS

Fig. 29. Sample of the digitized total velocity component of the trailing vortex for the 8-inch chord model, $z/c = 6.5$, $U_\infty = 175$ ft/sec, $\alpha = 12^\circ$, top to bottom; ambient free steam velocity, unmodified vortex, vortex with 3/8-inch diameter sonic nozzle, and vortex with tip spoiler. Vertical scale is the same for each of the figures.

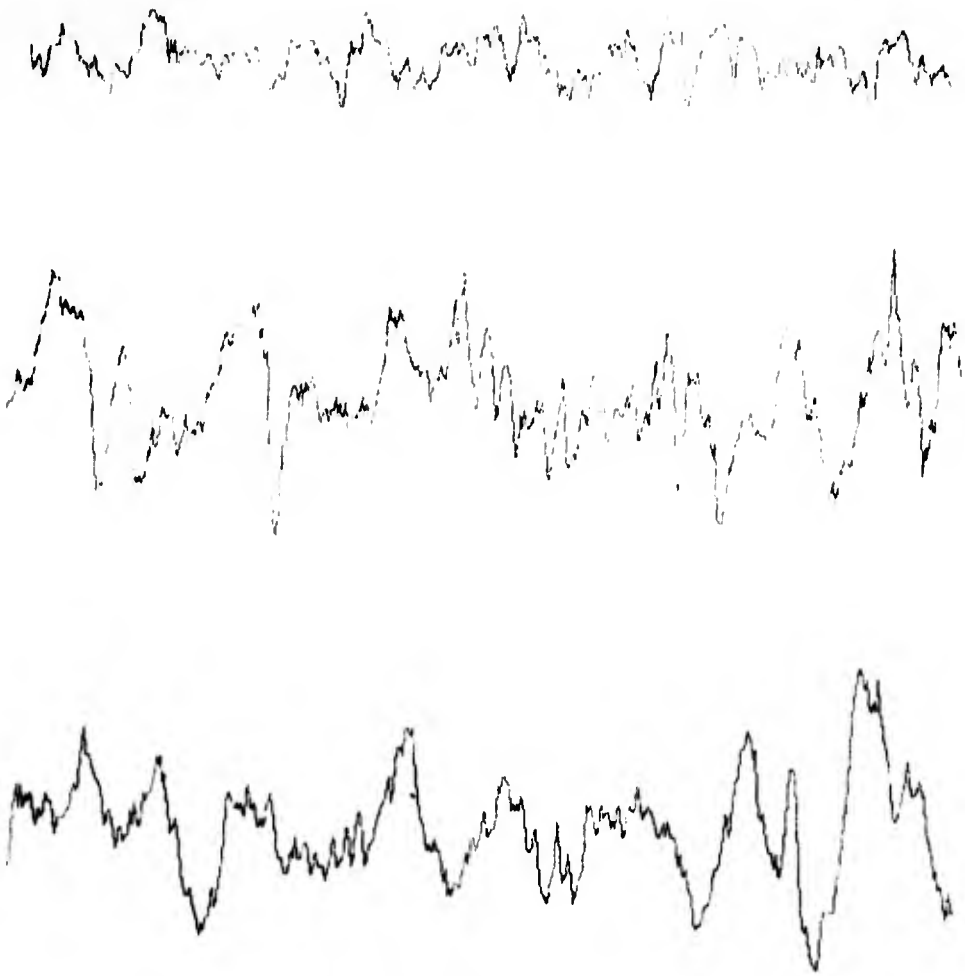

TIME SCALE 0.001 SECONDS

Fig. 30. Sample of the digitized total velocity component of the trailing vortex for the 8-inch chord model, $z/c = 16.5$, $U_\infty = 175$ ft/sec, $\alpha = 12^\circ$, top to bottom; unmodified vortex, vortex with the 3/8-inch diameter sonic nozzle, and vortex with tip spoiler. Vertical scale is the same for each of the figures.

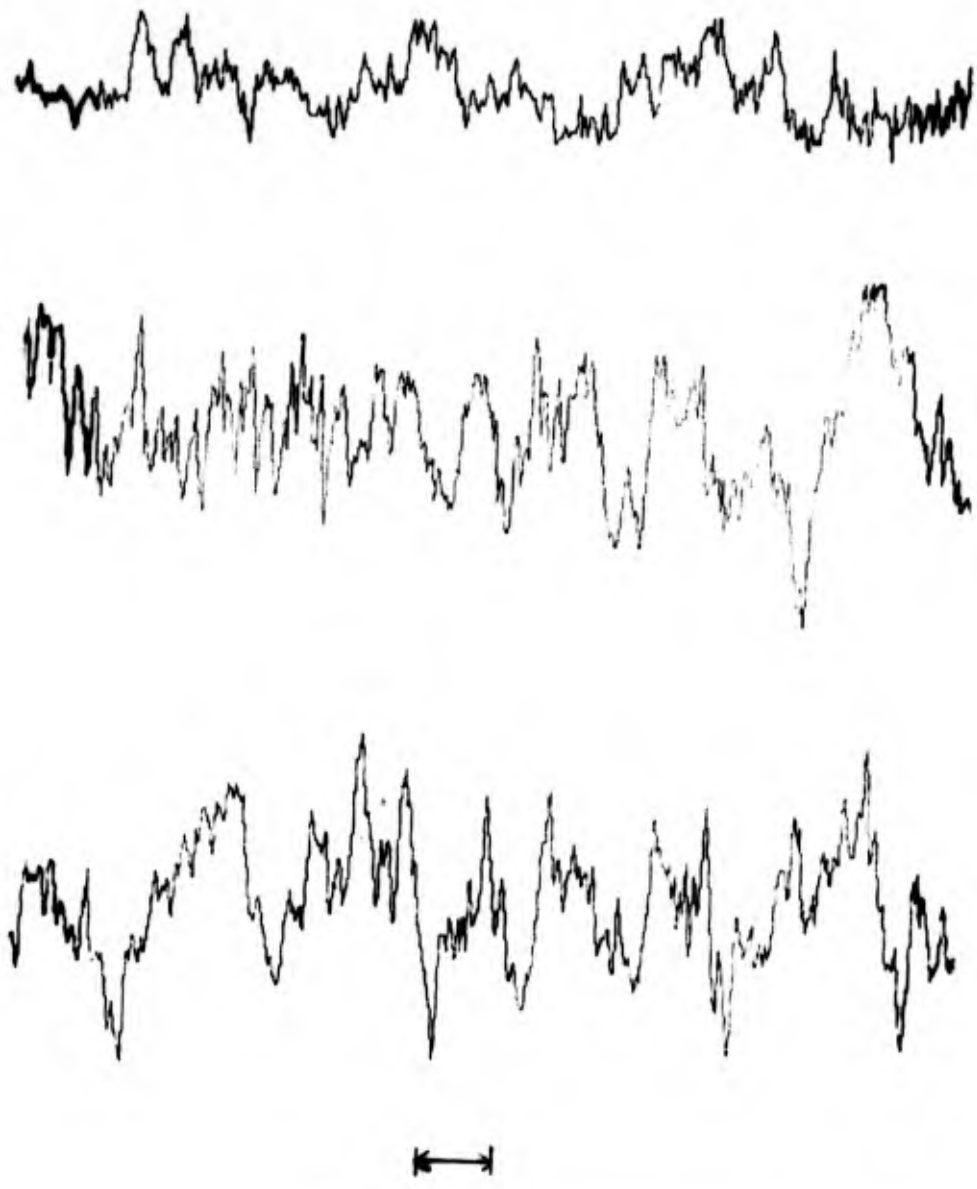

Fig. 31. Sample of the digitized total velocity component of the trailing vortex for the 21-inch chord model, $z/c = 6.5$, $U_\infty = 150$ ft/sec, $\alpha = 8.5^\circ$ top to bottom; unmodified vortex and vortex with the 1/2 and the 5/8-inch diameter sonic nozzles. Vertical scale is the same for each of the figures.

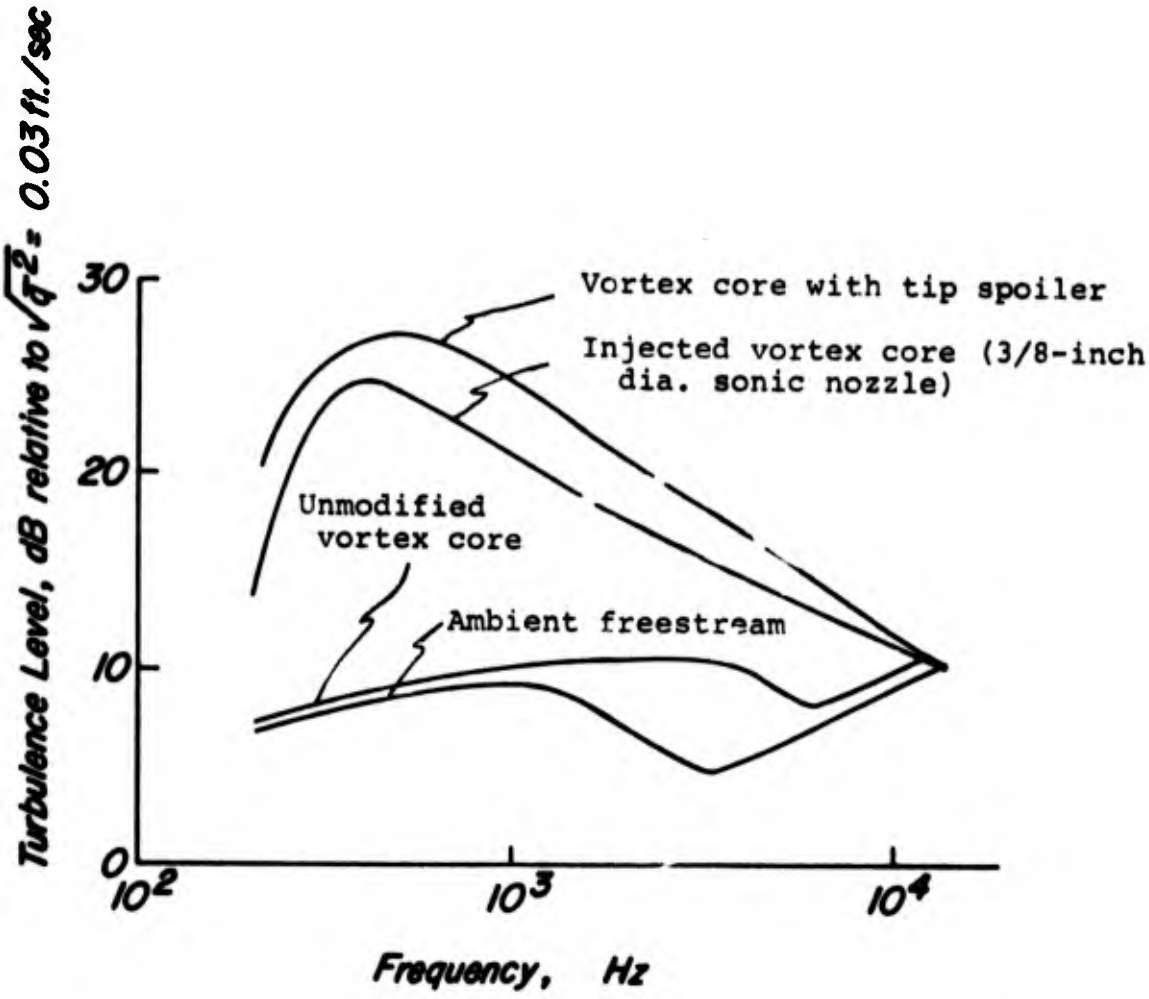

Fig. 32. Turbulent velocity spectrum of the trailing vortex core for the 8-inch chord model, z/c = 6.5, U_∞ = 175 ft/sec, α = 12°

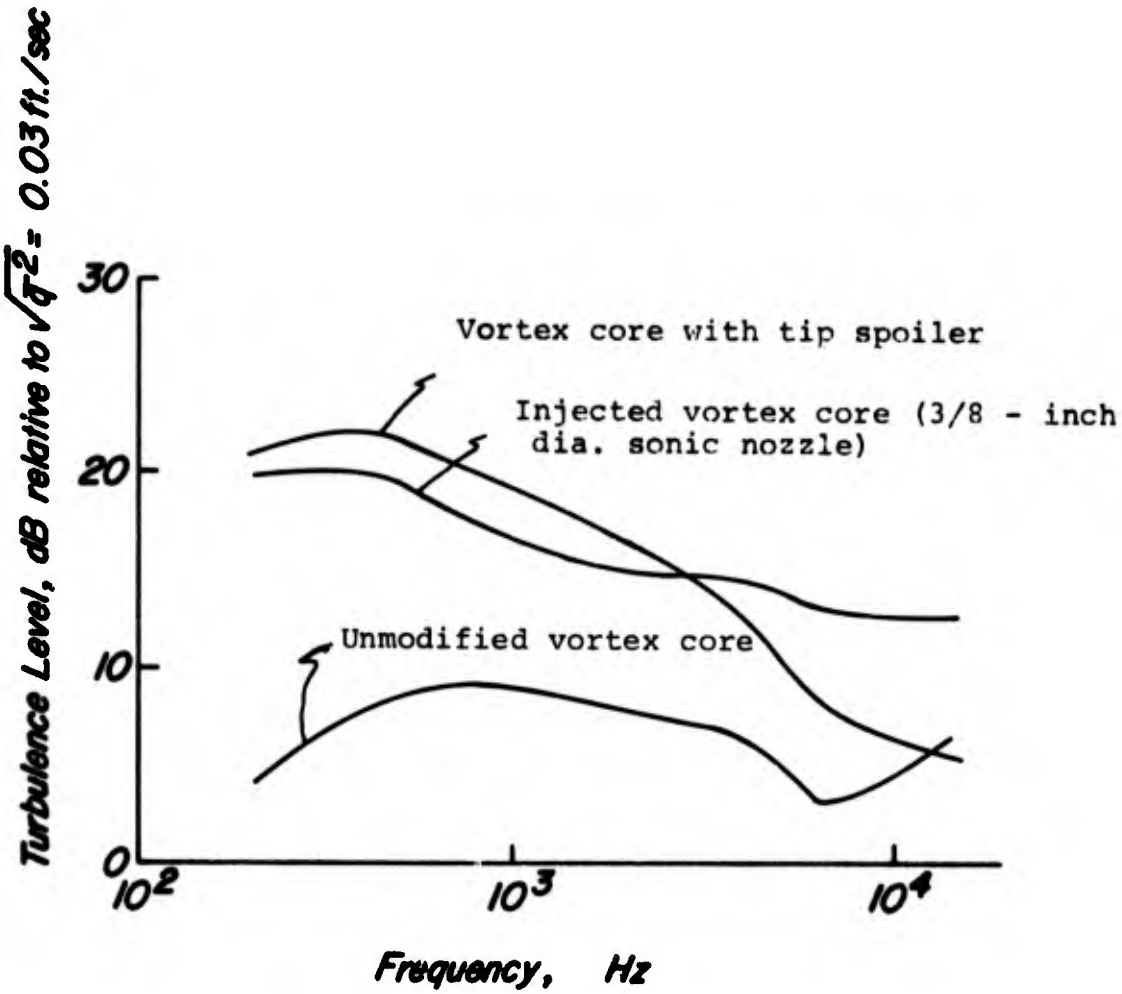

Fig. 33. Turbulent velocity spectrum of the trailing vortex core for the 8-inch chord model, z/c = 16.5 U_∞ = 175 ft/sec, $\alpha = 12^0$

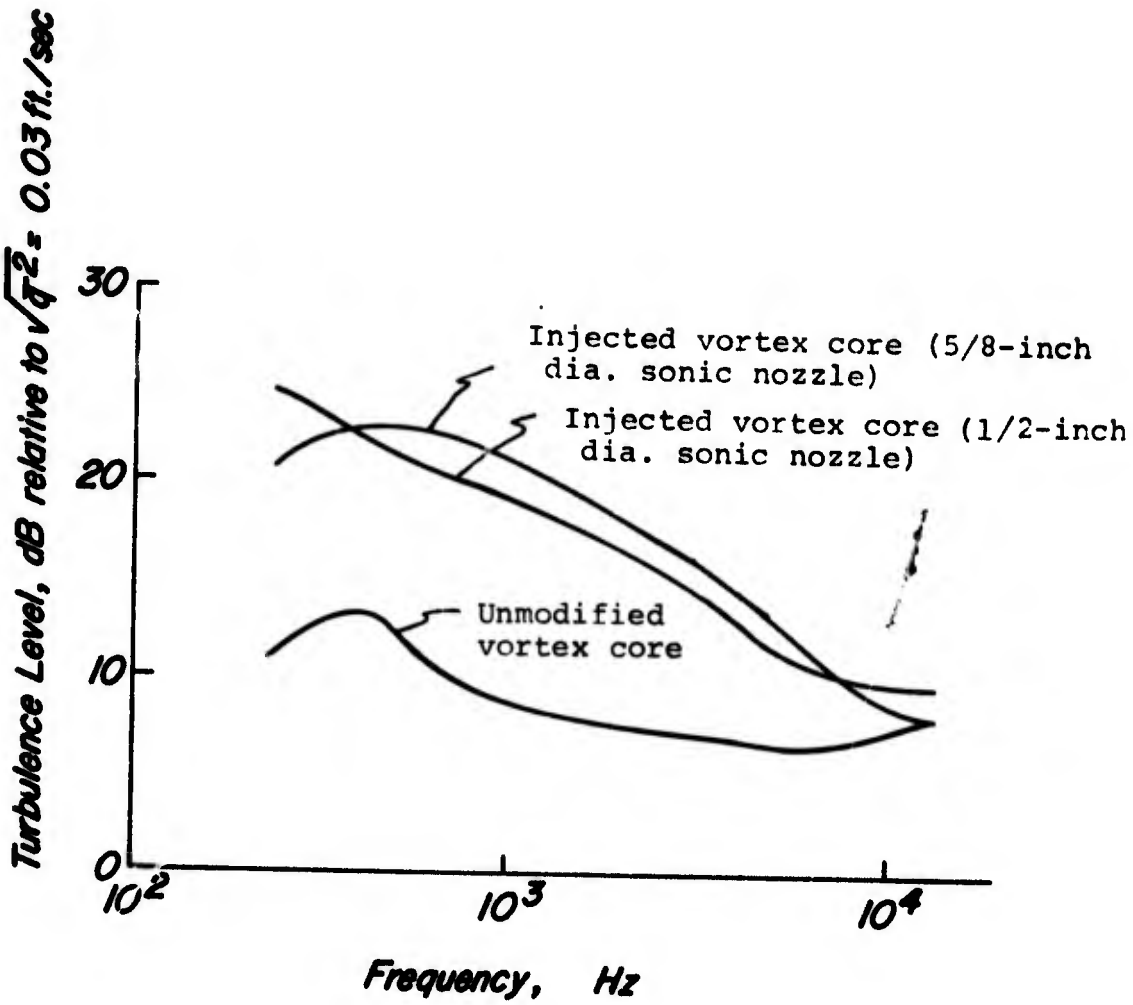

Fig. 34. Turbulent velocity spectrum of the trailing vortex core for the 21-inch chord model, z/c = 6.5 U_∞ = 150 ft/sec, α_R = 8.5

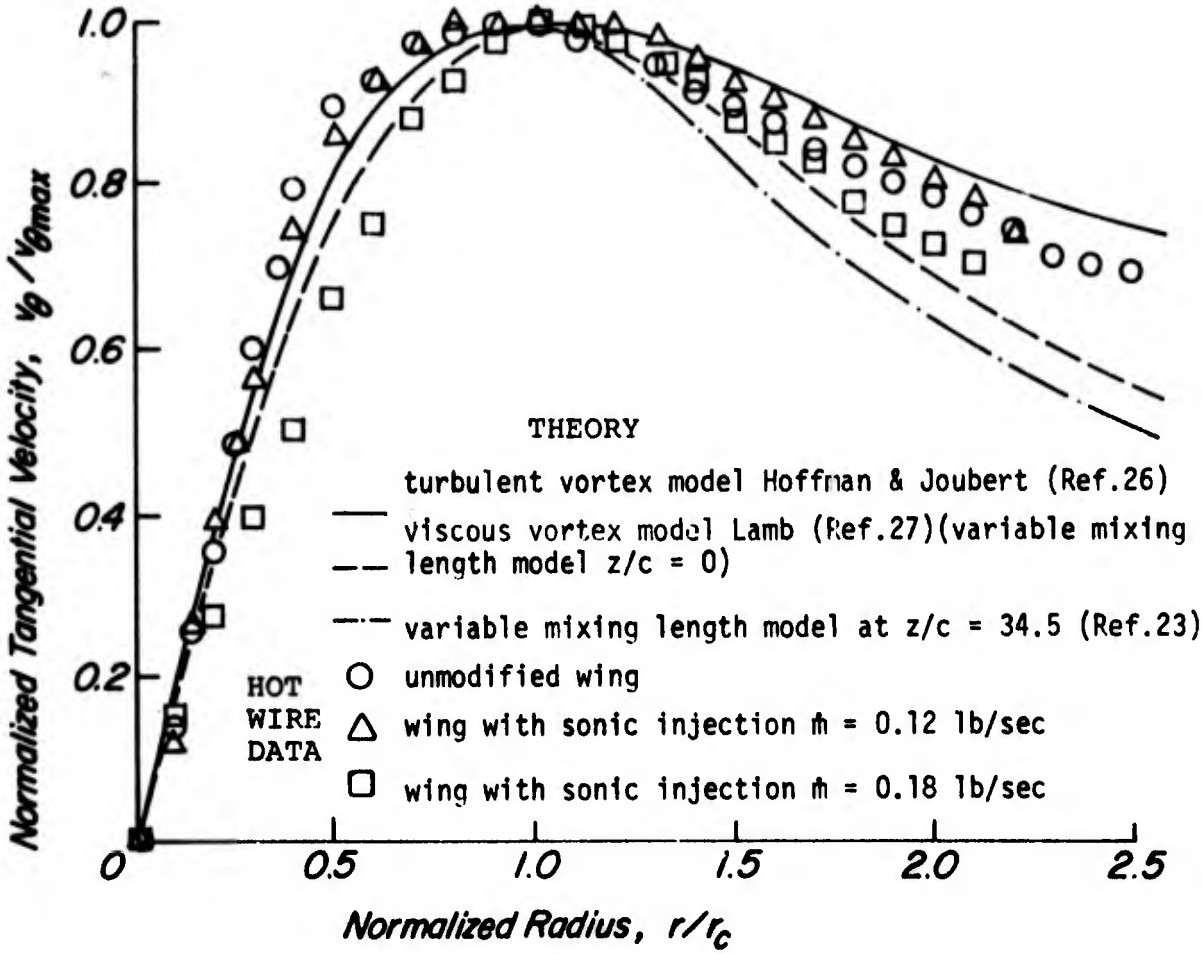

Fig. 35. Dimensionless tangential velocity profile of the trailing vortex for the 21-inch chord model with and without sonic injection at z/c = 6.5, U_∞ = 150 ft/sec, α_R = 8.5

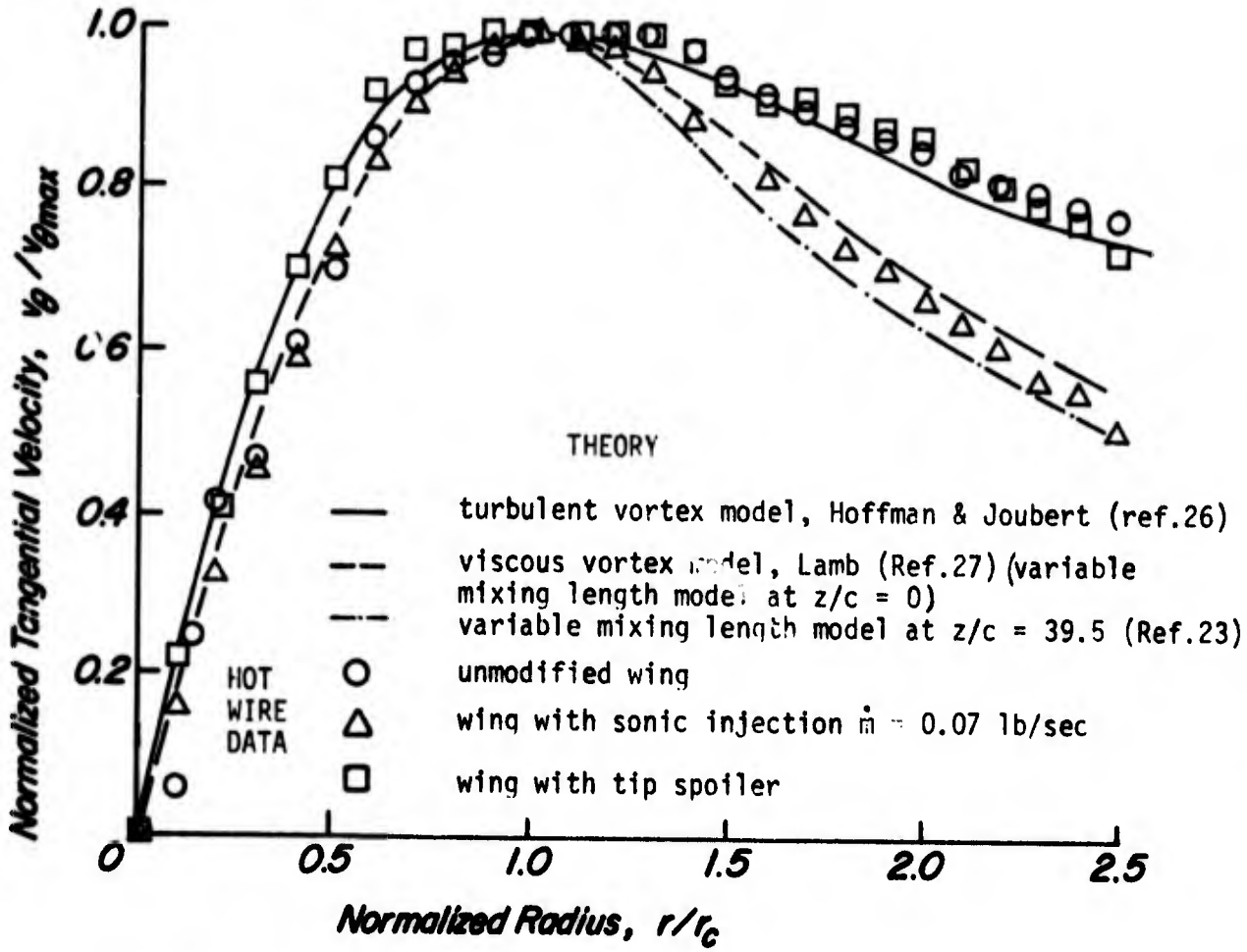

Fig. 36. Dimensionless tangential velocity profile of the trailing vortex for the 8-inch chord model with and without sonic injection and tip spoiler at z/c = 6.5, U_∞ = 175 ft/sec, $\alpha = 12^\circ$

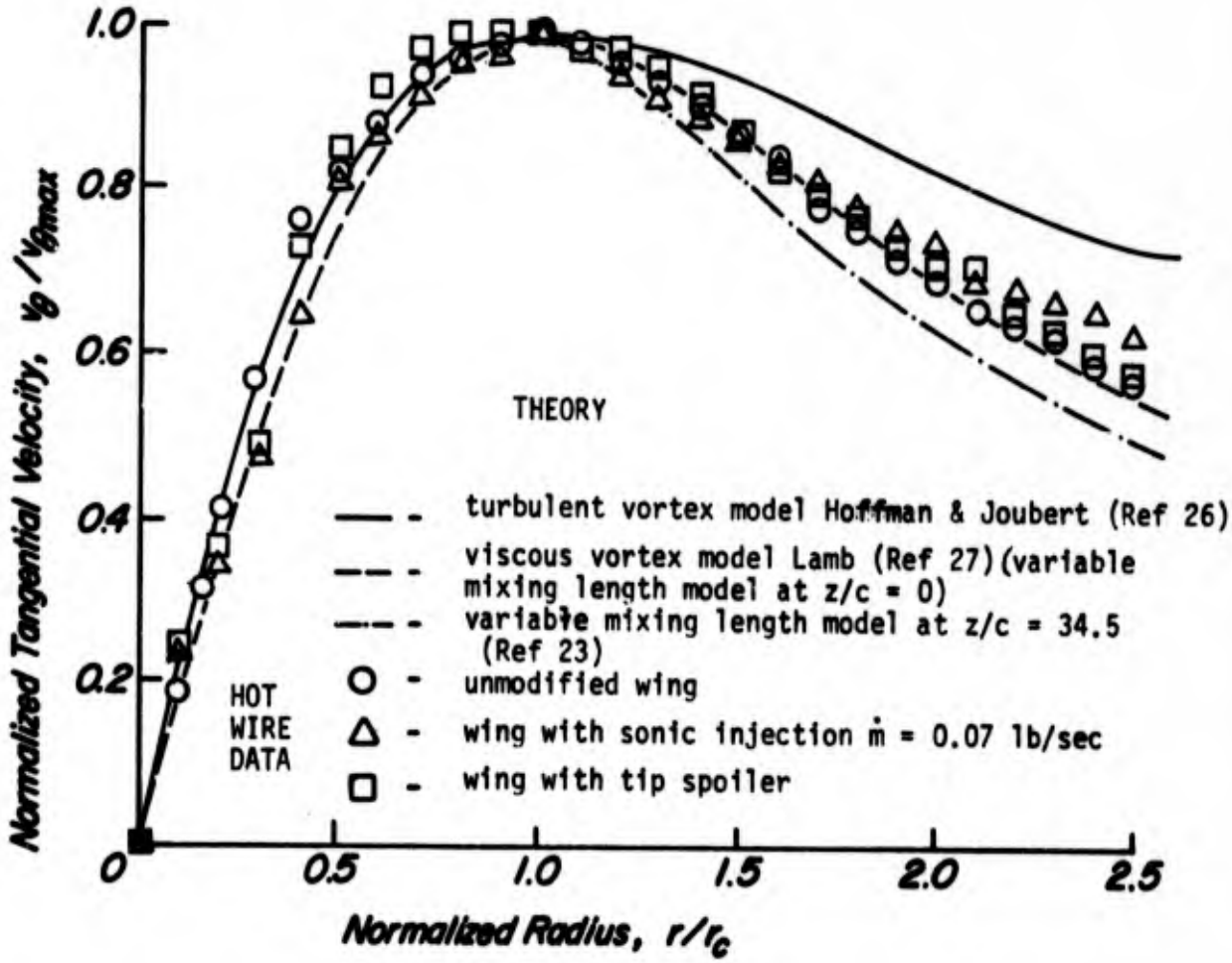

Fig. 37. Dimensionless tangential velocity profile of the trailing vortex for the 8-inch chord model with and without sonic injection and tip spoiler at z/c = 16.5, U_∞ = 175 ft/sec, $\alpha = 12^\circ$

EXPERIMENTAL DATA

z/c = 6.5

21-inch chord model, 1/2-inch diameter zonic nozzle
21-inch chord model, 5/8-inch diameter sonic nozzle
8-inch chord model, 3/8-inch diameter sonic nozzle
8-inch chord model, 5/16-inch diameter sonic nozzle
8-inch chord model, 3/8-inch diameter nozzle, subsonic injection T = 1.1 lb

z/c = 16.5

8-inch chord model, 3/8-inch diameter sonic nozzle

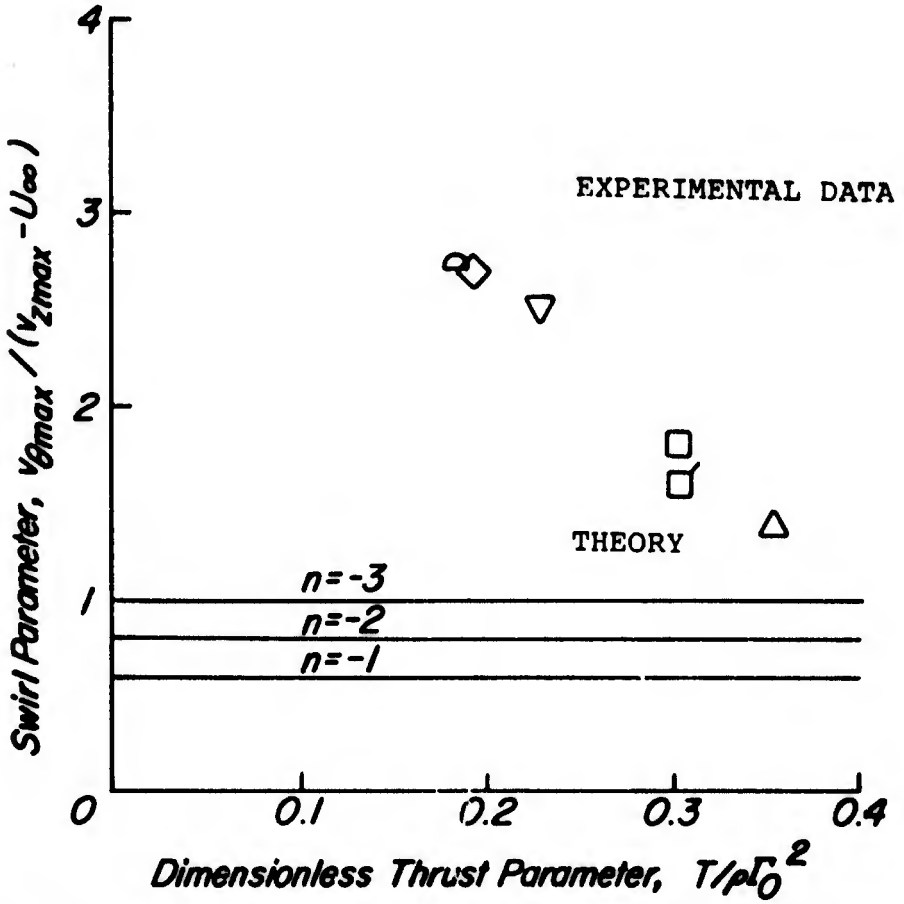

Fig. 38. Comparison of observed trailing vortex swirl parameters with viscous jet-vortex stability theory of Lessen et al (References 28, 29)

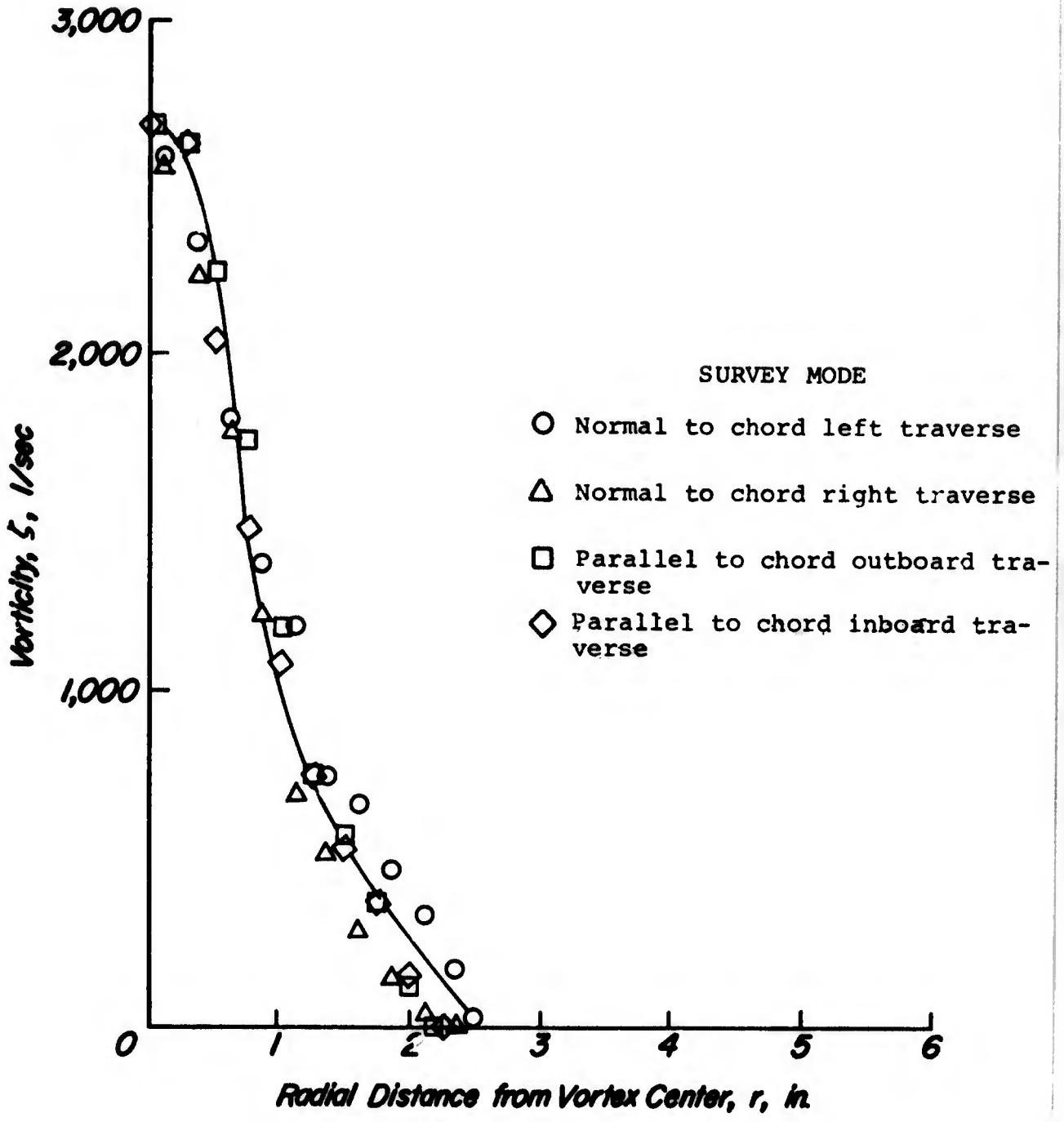

Fig. 39. Survey of trailing vortex by vorticity meter for unmodified 21-inch chord model z/c = 6.5, U_∞ = 150 ft/sec, $\alpha_R = 8.5^\circ$

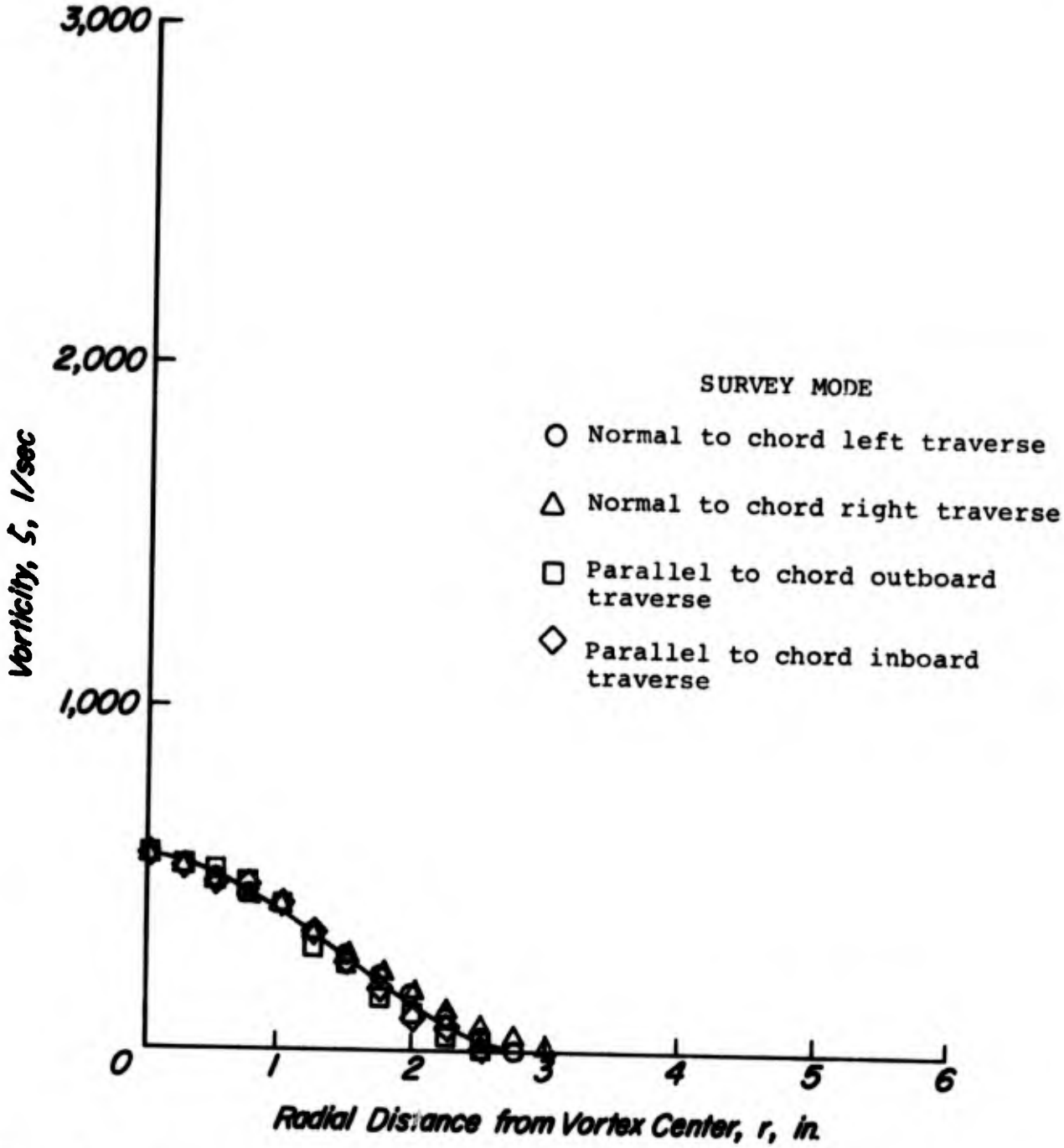

Fig. 40. Survey of trailing vortex by vorticity meter for the 21-inch chord model with the 1/2-inch diameter sonic nozzle, $\dot{m}$ = 0.12 lb/sec, z/c = 6.5, U_∞ = 150 ft/sec, $\alpha_R = 8.5^o$

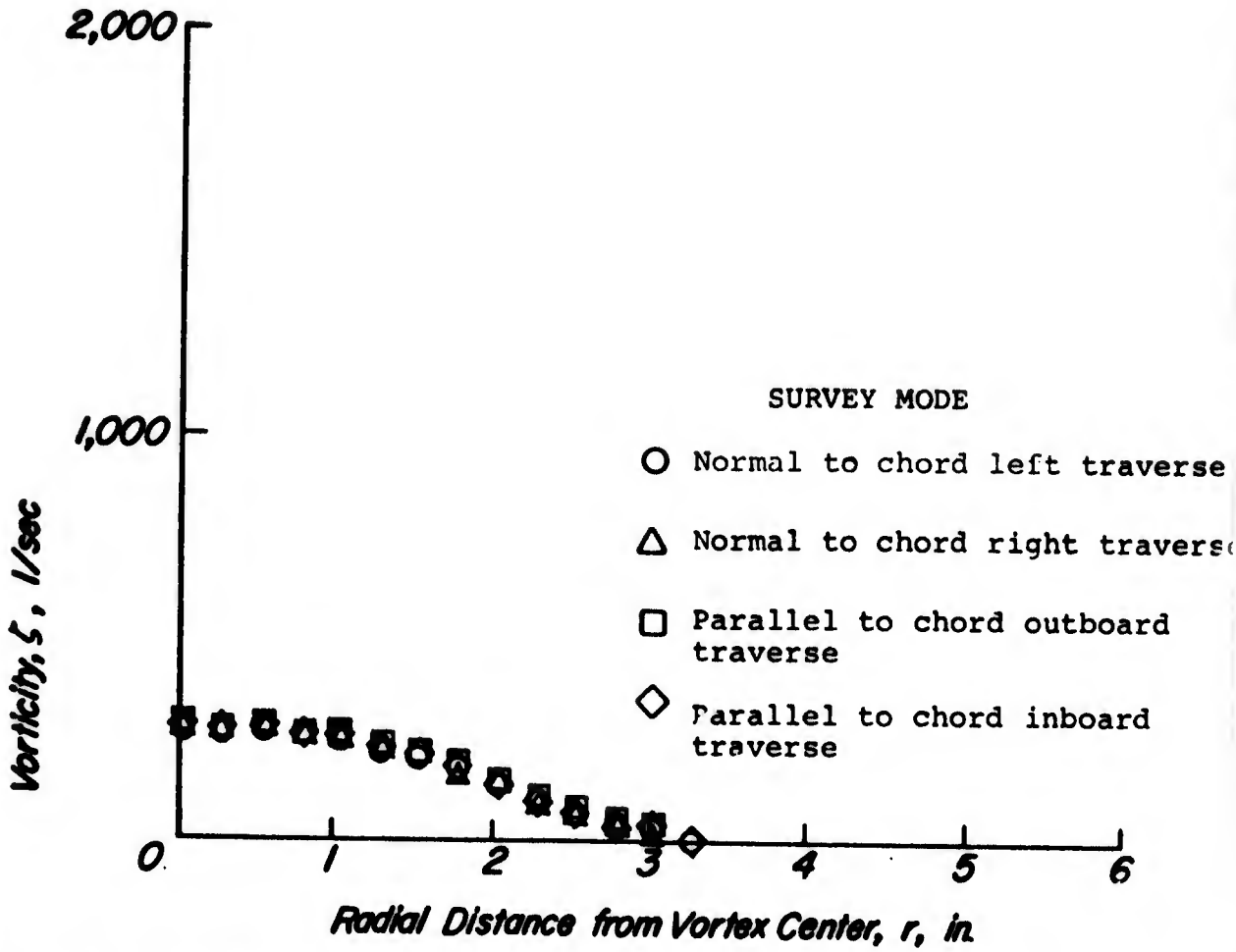

Fig. 41. Survey of trailing vortex by vorticity meter for the 21-inch chord model with the 5/8-inch diameter sonic nozzle, $\dot{m}$ = 0.18 lb/sec, z/c = 6.5, U_∞ = 150 ft/sec, α_R = 8.5°

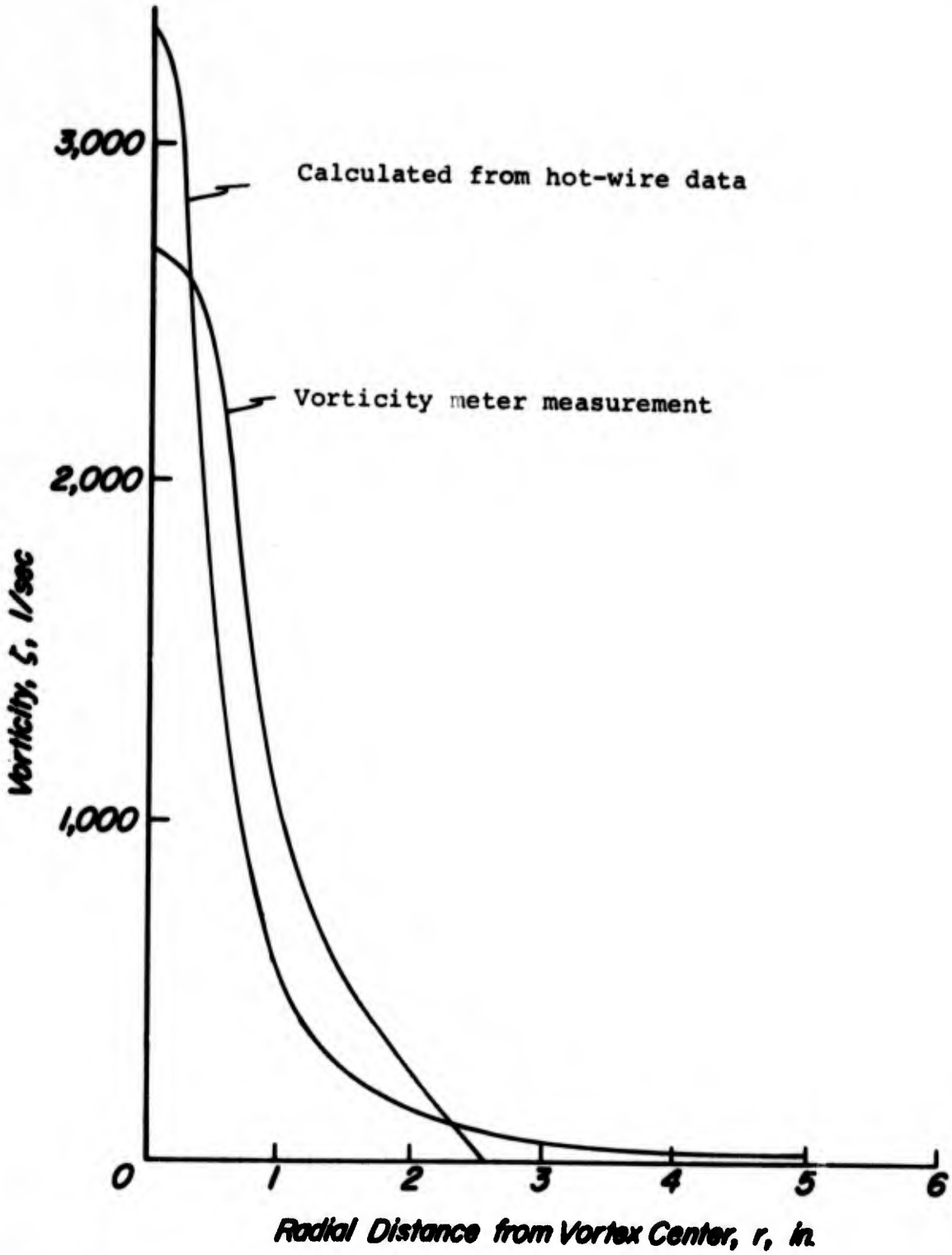

Fig. 42. Comparison of the trailing vortex vorticity distribution as measured by the vorticity meter and as calculated from hot-wire data for the unmodified 21-inch chord model, $z/c = 5.5$, $U_\infty = 150$ ft/sec, $\alpha_R = 8.5^0$

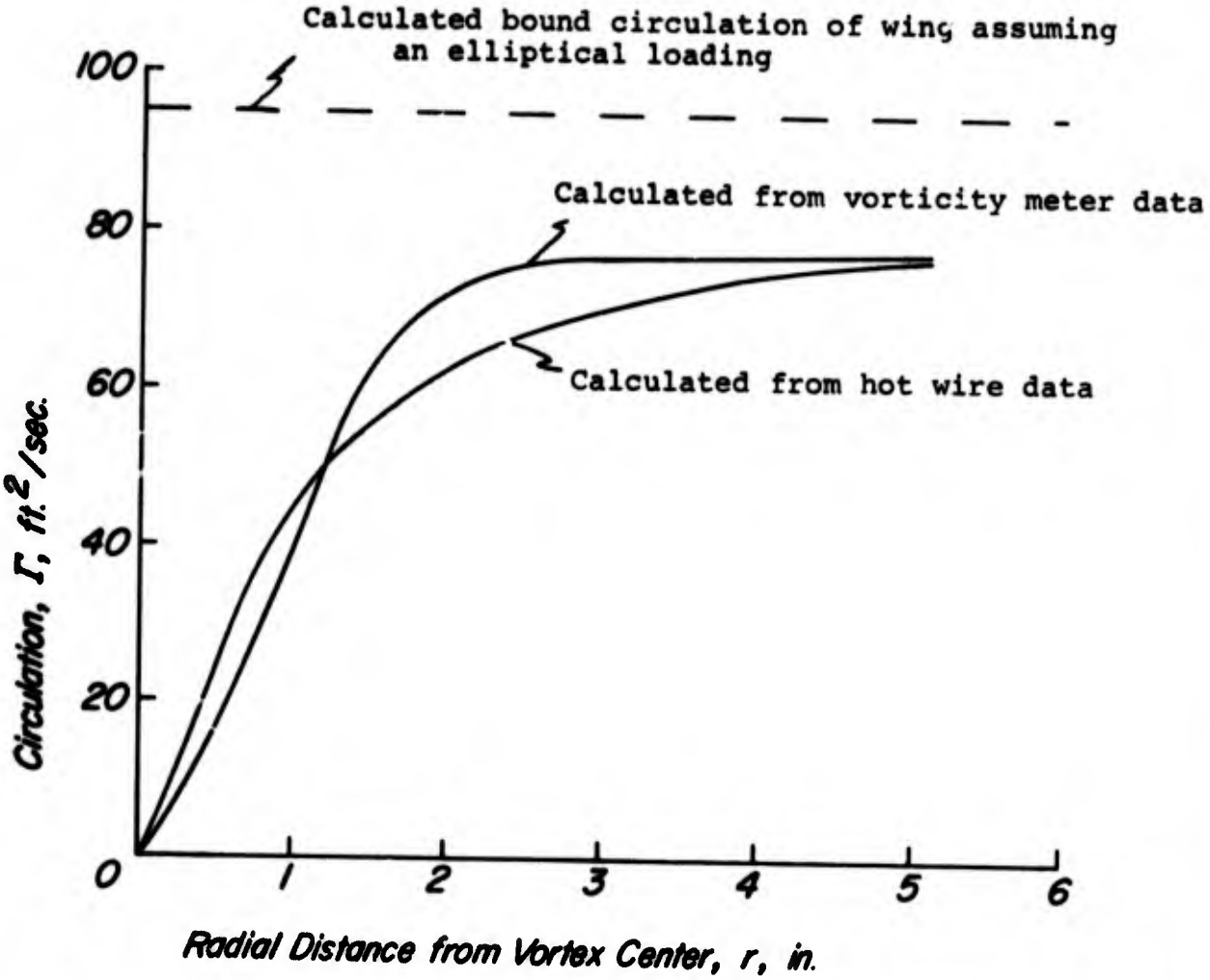

Fig. 43 Comparison of trailing vortex circulation distribution as calculated from hot-wire and vorticity meter measurements for the unmodified 21-inch chord model z/c = 6.5, U_∞ = 150 ft/sec, α_R = 8.5°

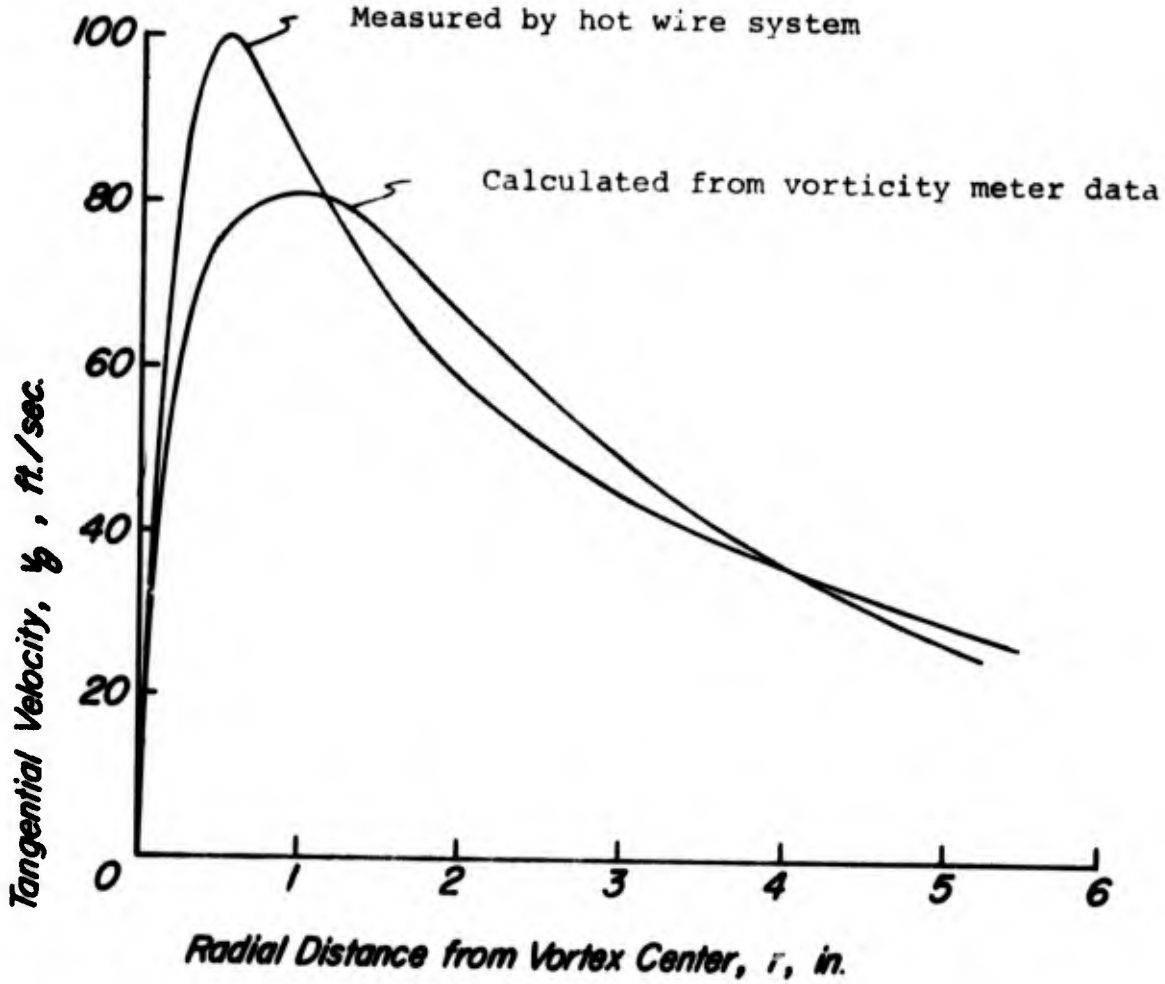

Fig. 44. Comparison of trailing vortex tangential velocity distribution as measured by hot-wire system and as calculated from the vorticity meter data for the unmodified 21-inch chord model, z/c = 6.5, U_∞ = 150 ft/sec, α_R = 8.5°

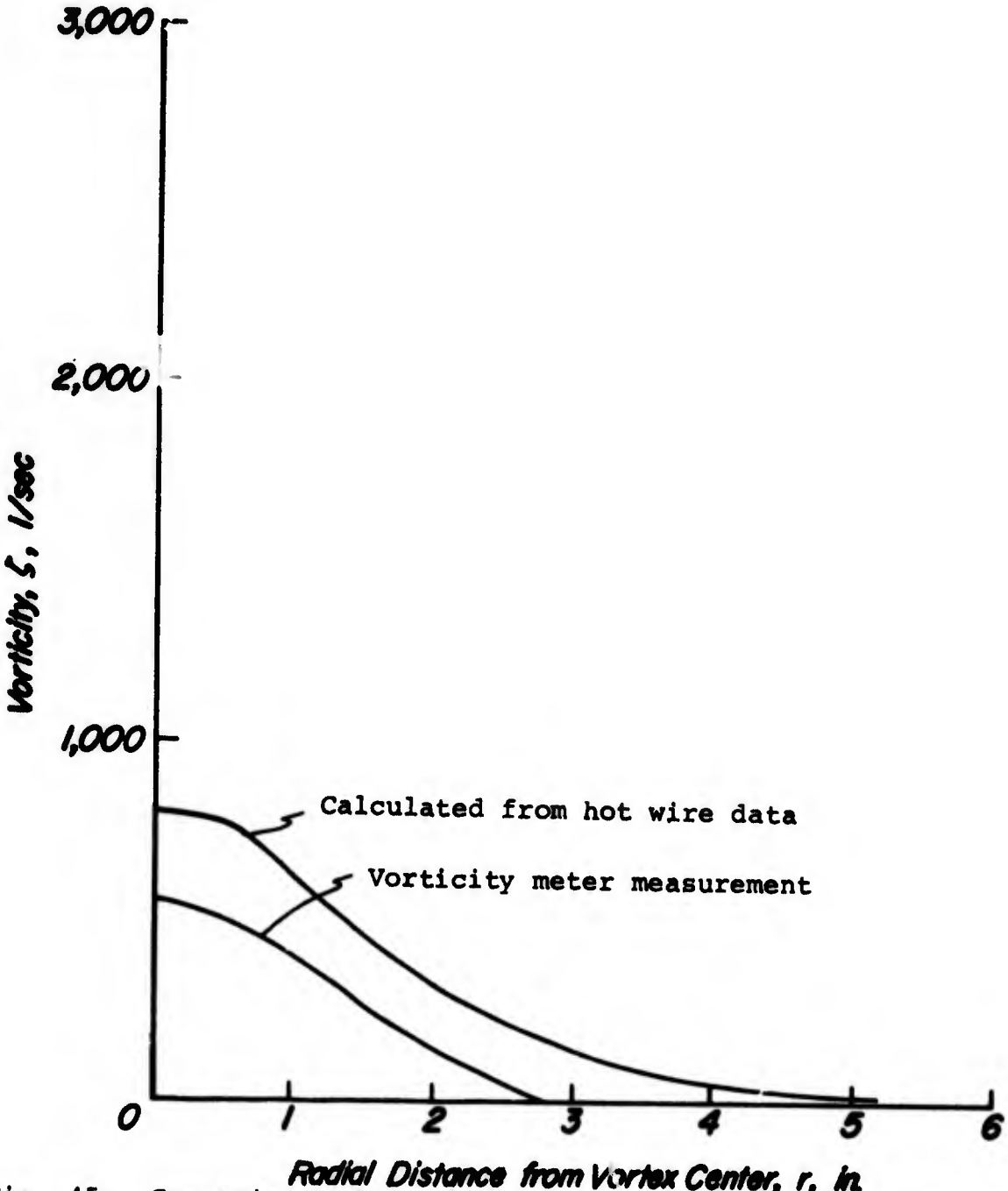

Fig. 45. Comparison of trailing vortex vorticity distribution as measured by vorticity meter and as calculated from hot-wire data for the 21-inch chord model with the 1/2-inch diameter sonic nozzle, $\dot{m}$ = 0.12 lb/sec, z/c = 6.5, U_∞ = 150 ft/sec, $\alpha_R = 8.5^\circ$

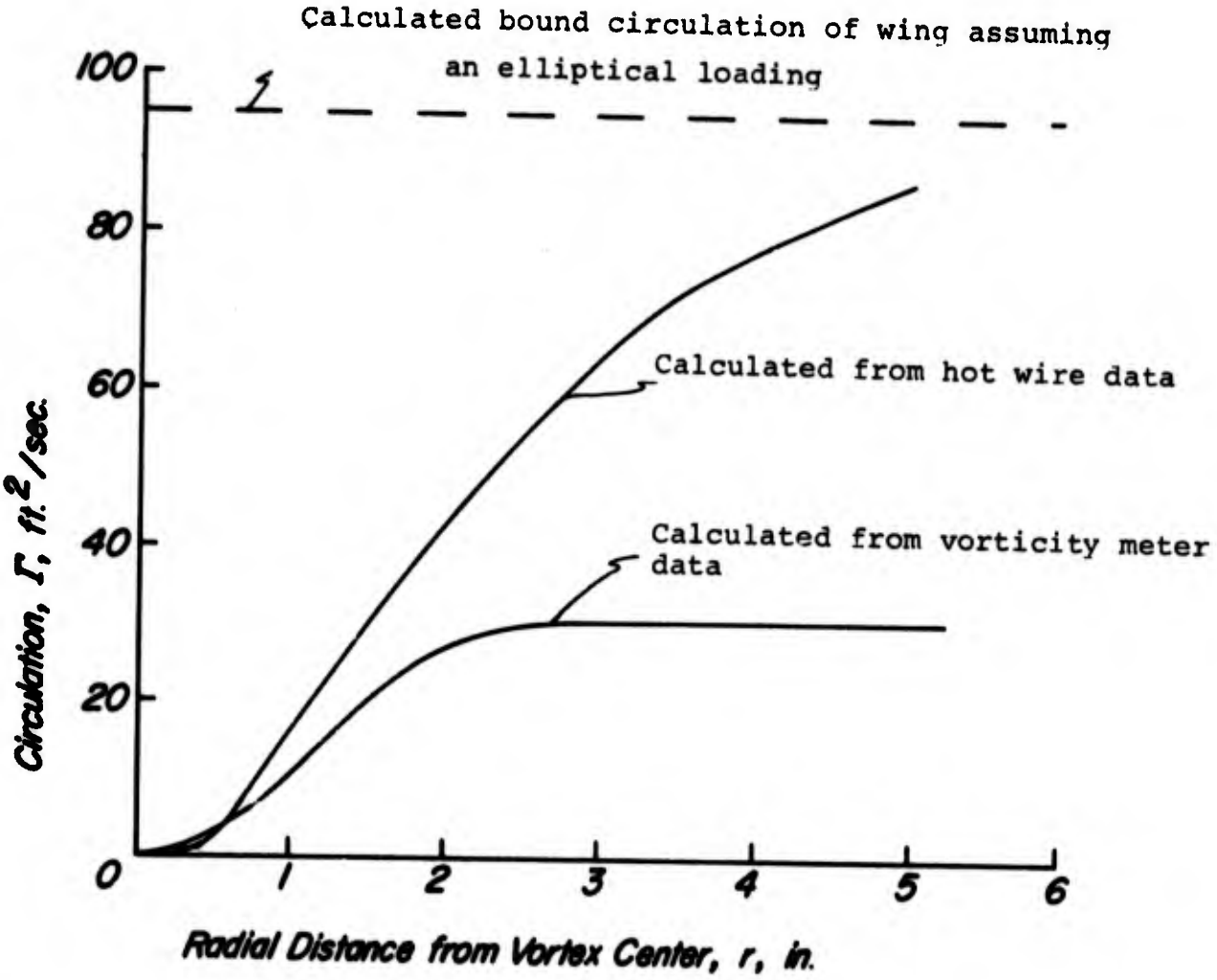

Fig. 46. Comparison of trailing vortex circulation distribution as calculated from hot-wire and vorticity meter measurements for the 21-inch chord model with the 1/2-inch diameter sonic nozzle $\dot{m} = 0.12$ lb/sec, z/c = 6.5, U_∞ = 150 ft/sec, $\alpha_R = 8.5^\circ$

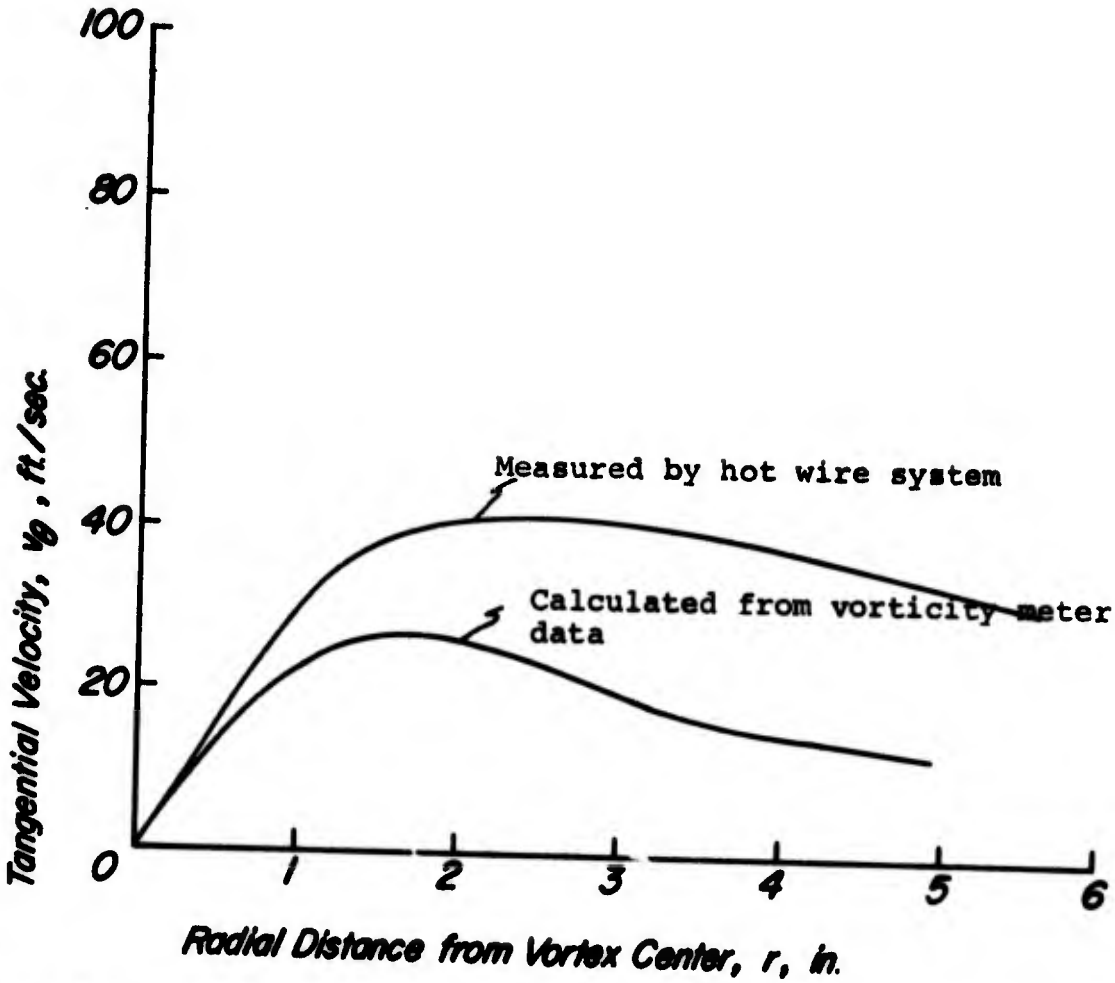

Fig. 47. Comparison of trailing vortex tangential velocity distribution as measured by hot-wire system and as calculated from the vorticity meter data for the 21-inch chord model with the 1/2-inch diameter sonic nozzle, $\dot{m}$ = 0.12 lb/sec, z/c = 6.5, U_∞ = 150 ft/sec, $\alpha_R = 8.5^0$

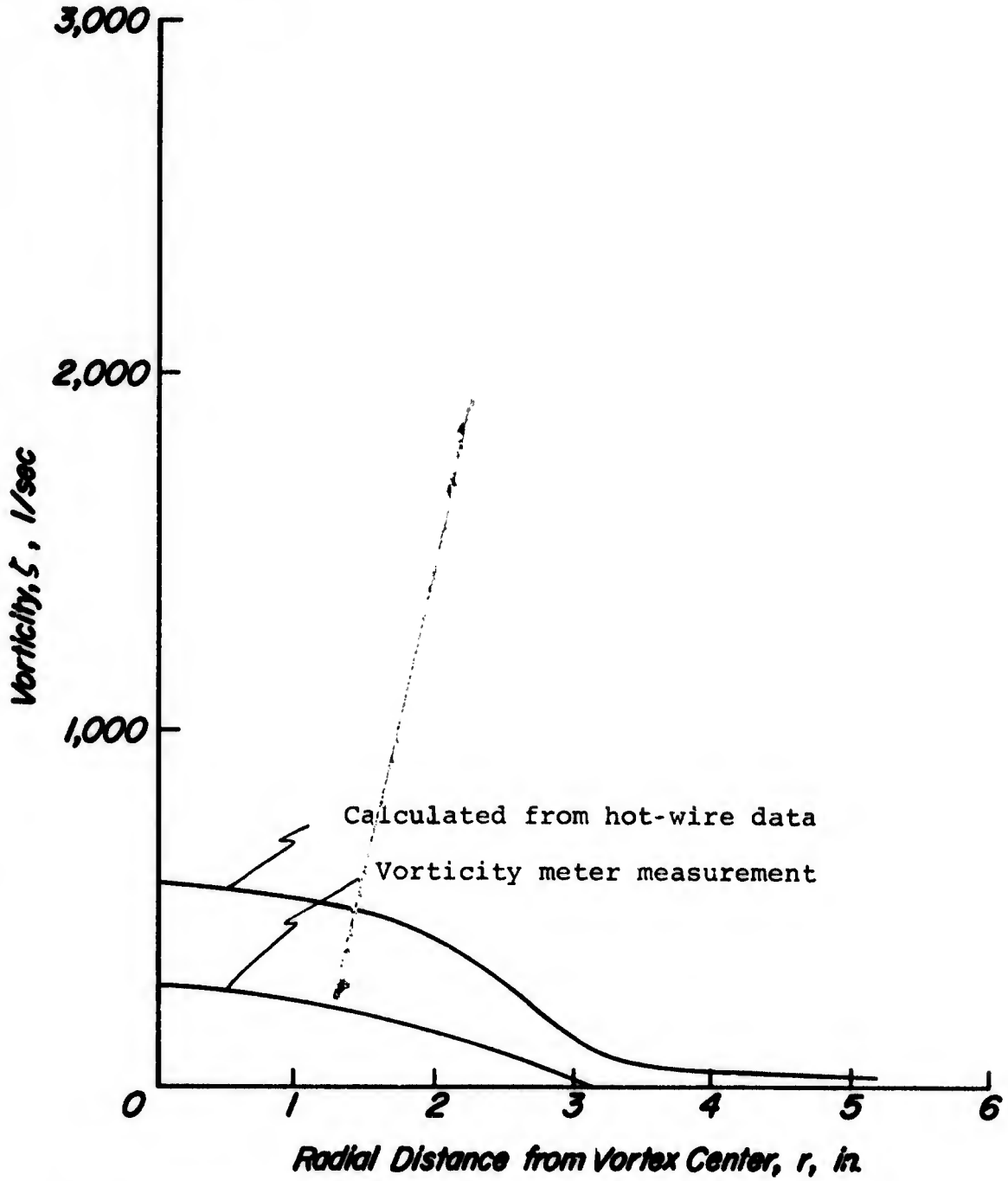

Fig. 48. Comparison of trailing vortex vorticity distribution as measured by vorticity meter and as calculated from hot-wire data for the 21-inch chord model with the 5/8-inch diameter sonic nozzle $\dot{m}_o$ = 0.18 lb/sec, z/c = 6.5, U_∞ = 150 ft/sec, α_R = 8.5°

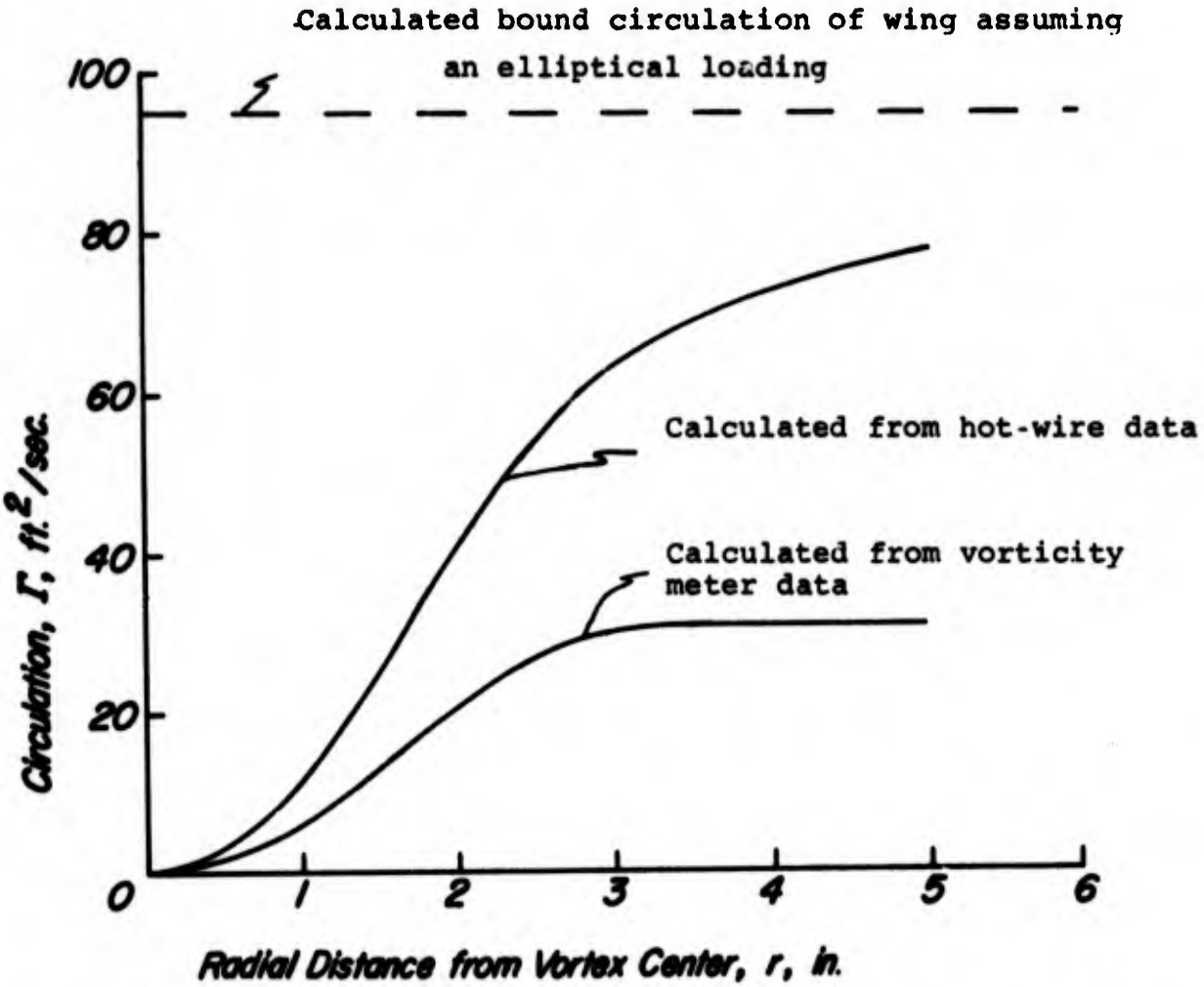

Fig. 49. Comparison of trailing vortex circulation distribution as calculated from hot-wire and vorticity meter measurements for the 21-inch chord model with the 5/8-inch diameter sonic nozzle, $\dot{m} = 0.18$ lb/sec, z/c = 6.5 $U_\infty = 150$ ft/sec, $\alpha_R = 8.5^\circ$

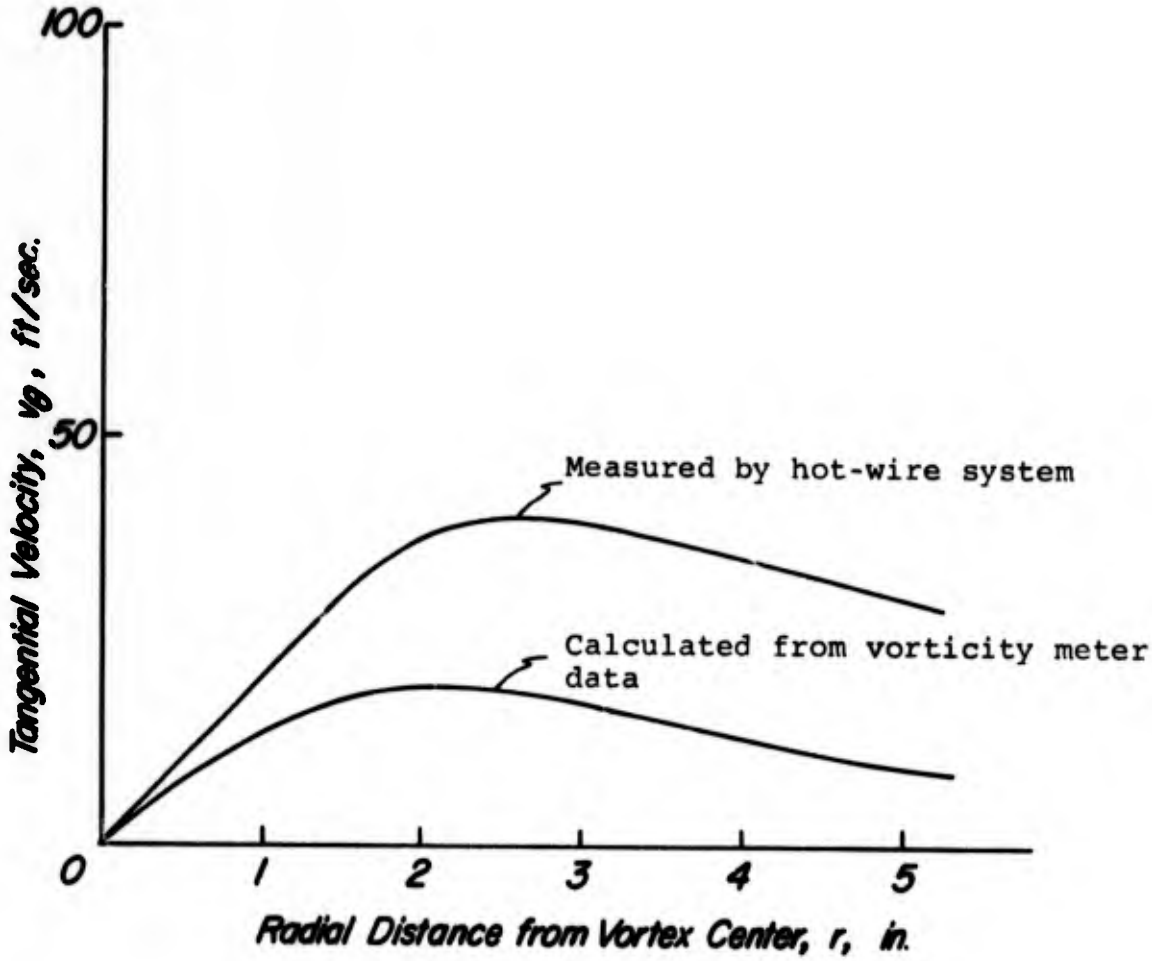

Fig. 50. Comparison of trailing vortex tangential velocity distribution as measured by hot-wire system and as calculated from the vorticity meter data for the 21-inch chord model with the 5/8-inch diameter sonic nozzle, $\dot{m}$ = 0.18 lb/sec, z/c = 6.5, U_∞ = 150 ft/sec, $\alpha_R = 8.5^0$

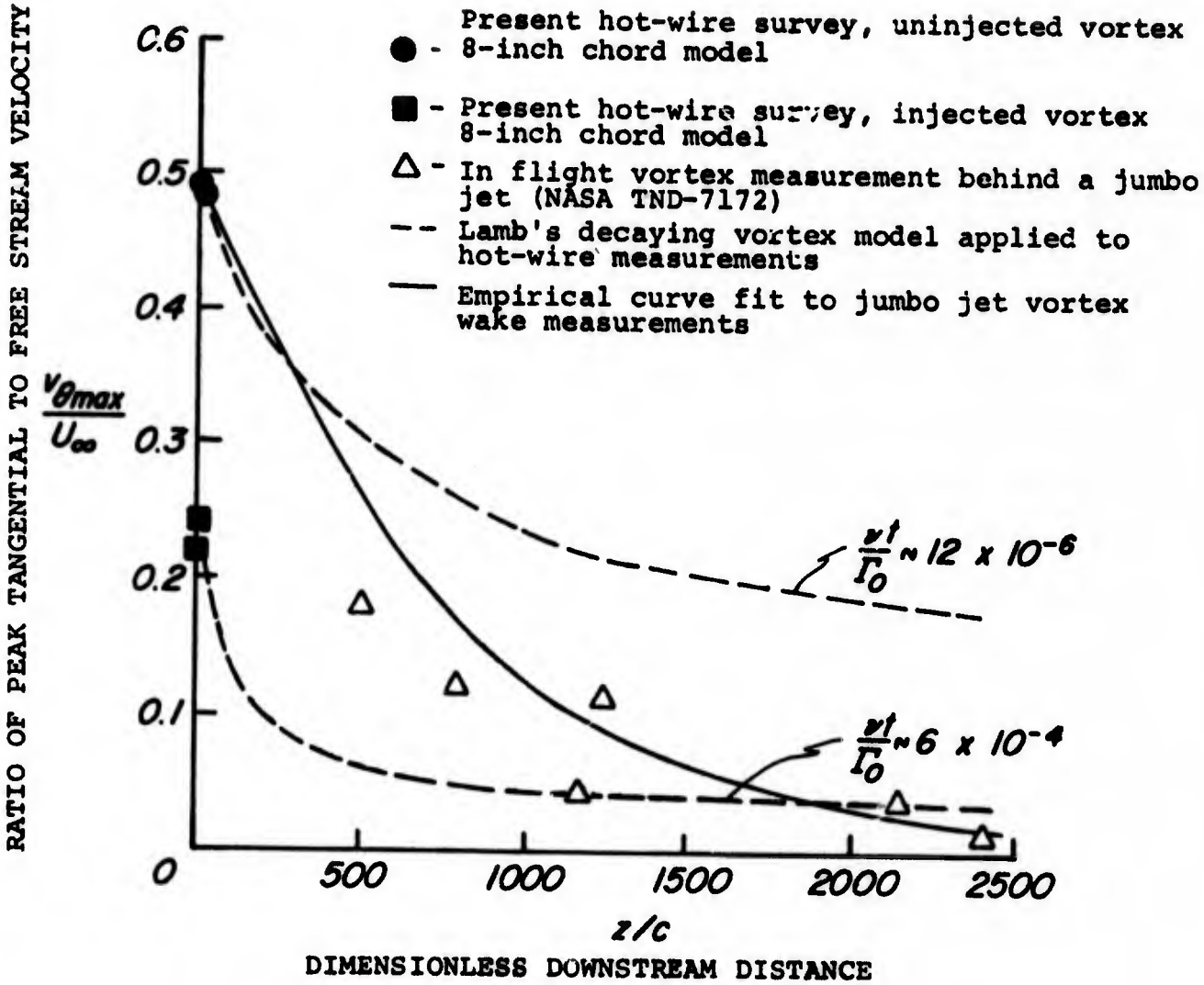

Fig. 51. Effect of turbulent mass injection on the vortex hazard behind fixed-wing aircraft

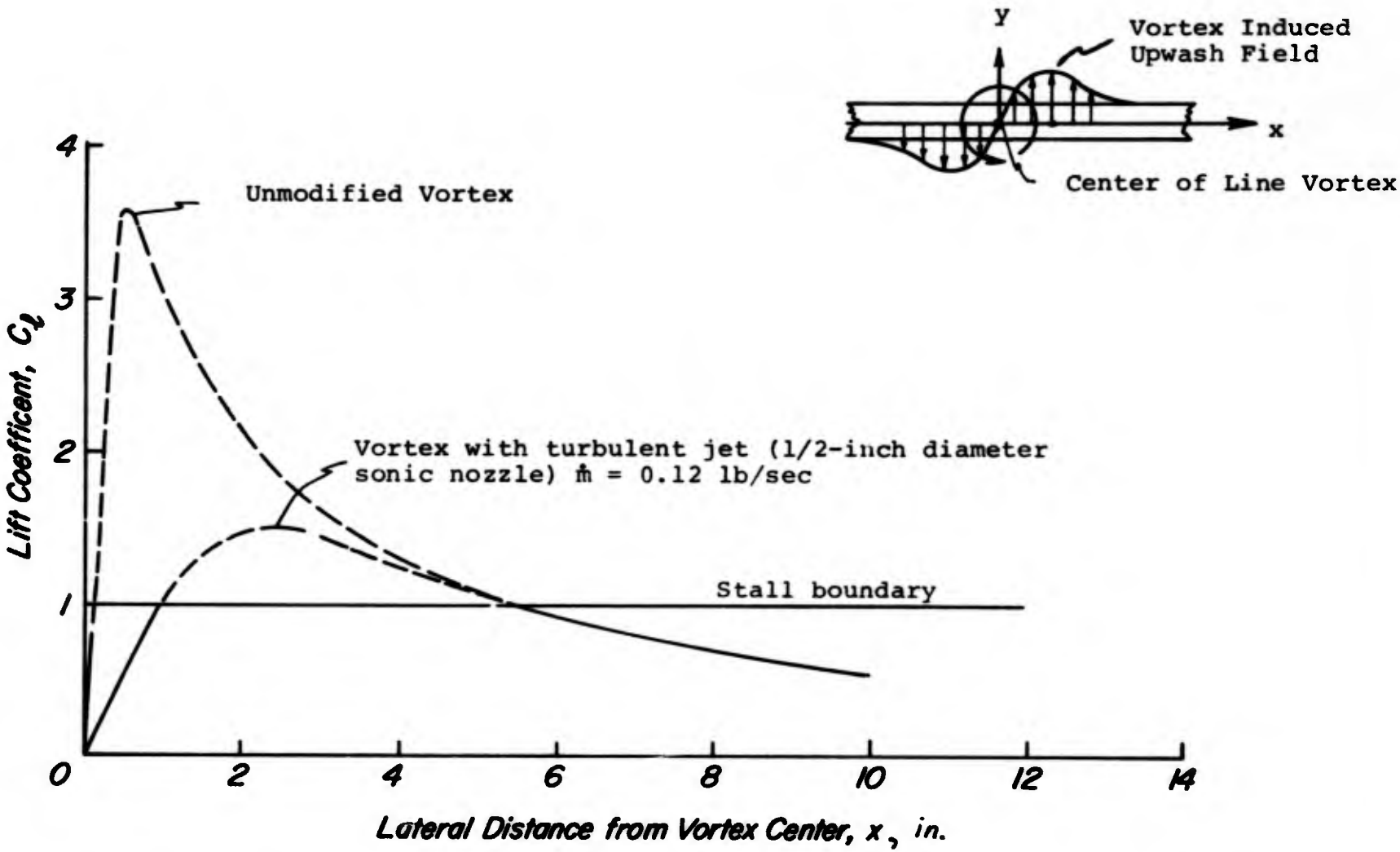

Fig. 52. Interaction of the trailing vortex from the 21-inch chord semispan model with a two-dimensional airfoil at z/c = 6.5, U_∞ = 150 ft/sec, $\alpha = 0^\circ$

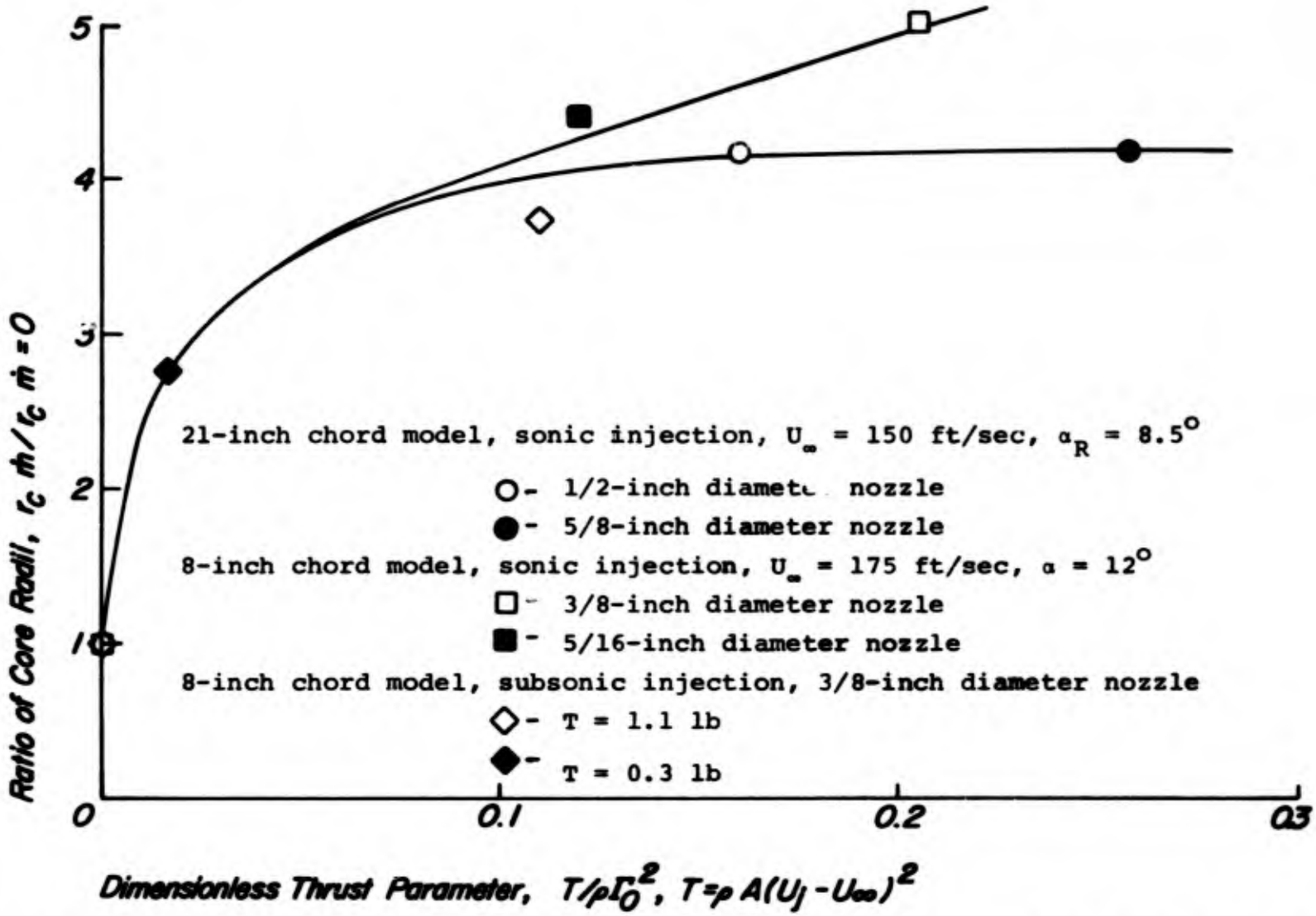

Fig. 53. Core radius of the trailing vortex for the 21-inch and the 8-inch chord semispan models at z/c = 6.5 as a function of jet thrust.

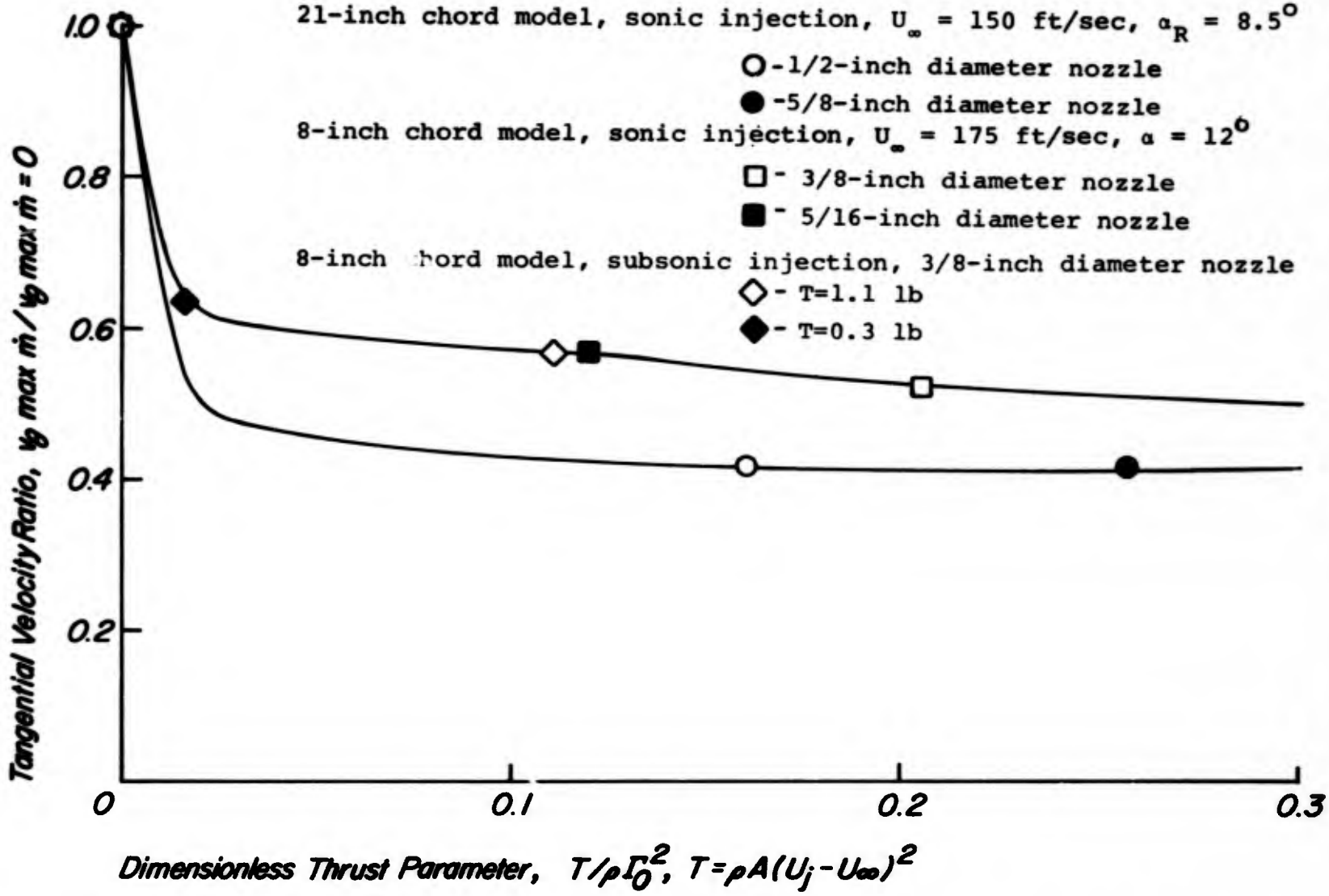

Fig. 54. Peak tangential velocity of the trailing vortex for the 21-inch and the 8-inch chord semispan models at z/c = 6.5 as a function of jet thrust

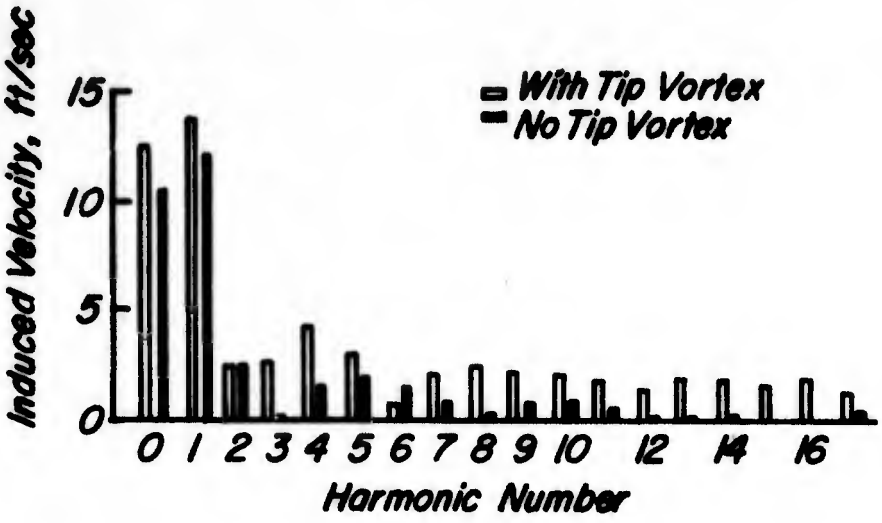

Harmonics of Induced Velocity for UH-1, r/R = 0.87

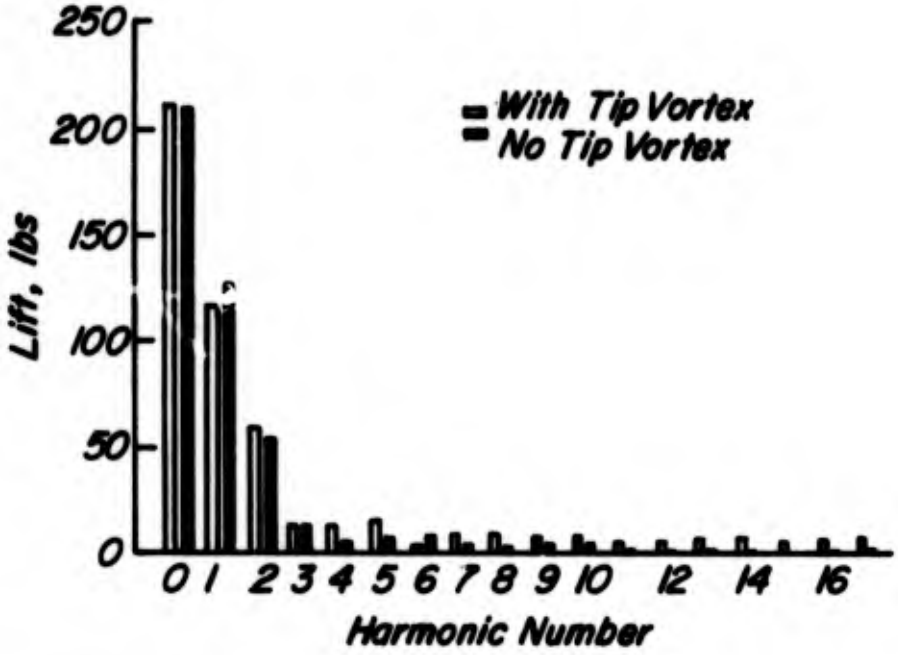

Harmonics of Section Lift for UH-1, r/R = 0.87

Fig. 55. Effect of blade vortex interaction on helicopter blade loads (Ref. 34)

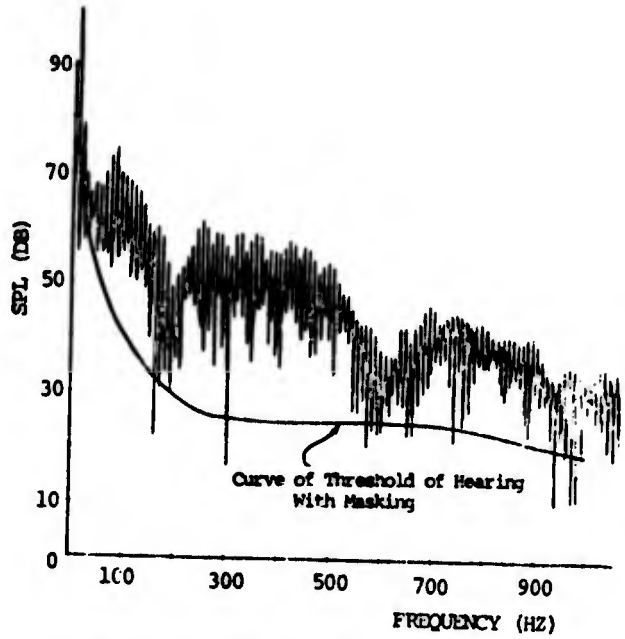

Spectrum of Rotational Noise with Blade Vortex Interaction

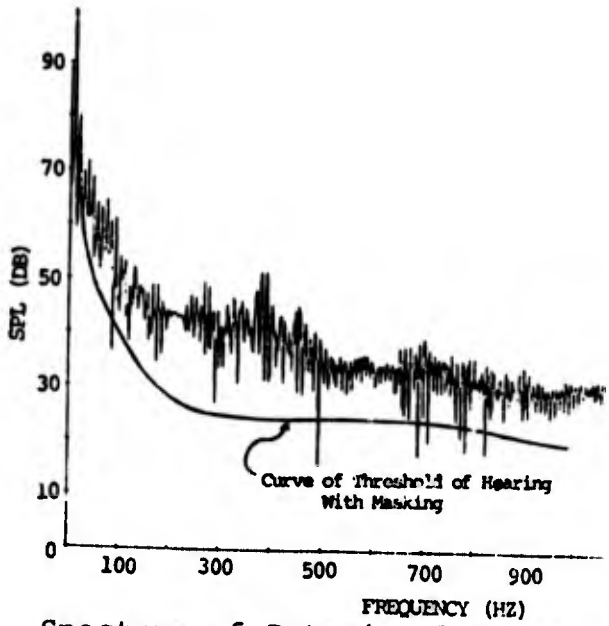

Spectrum of Rotational Noise with Tip Vortex Eliminated

Figure 56. Effect of blade vortex interaction on helicopter acoustic signature (Ref. 34)

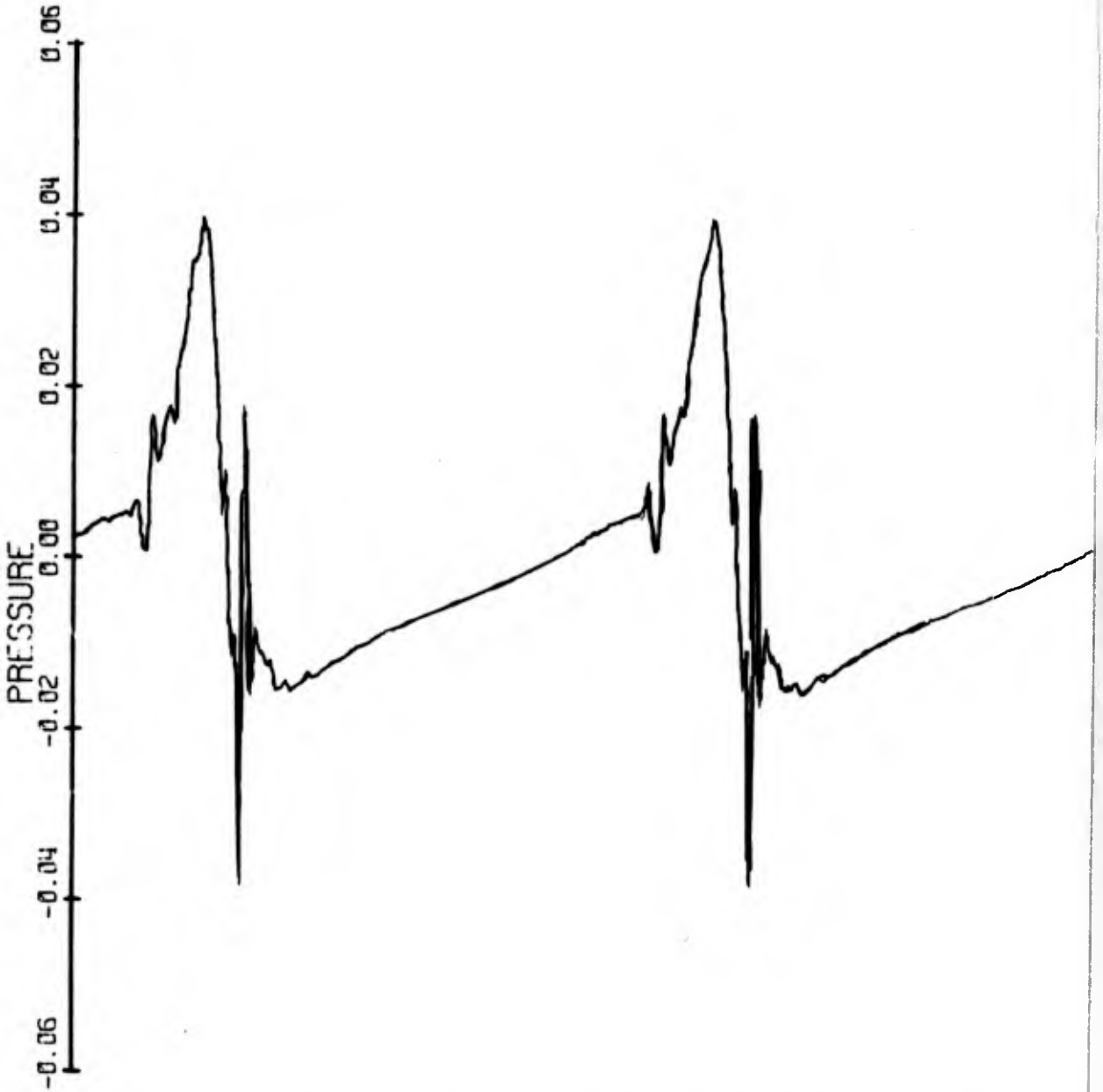

Fig. 57. Pressure time history of predicted rotational noise for a UH-1D rotor system, Γ_o=550 ft^2/sec. (Ref. 34)

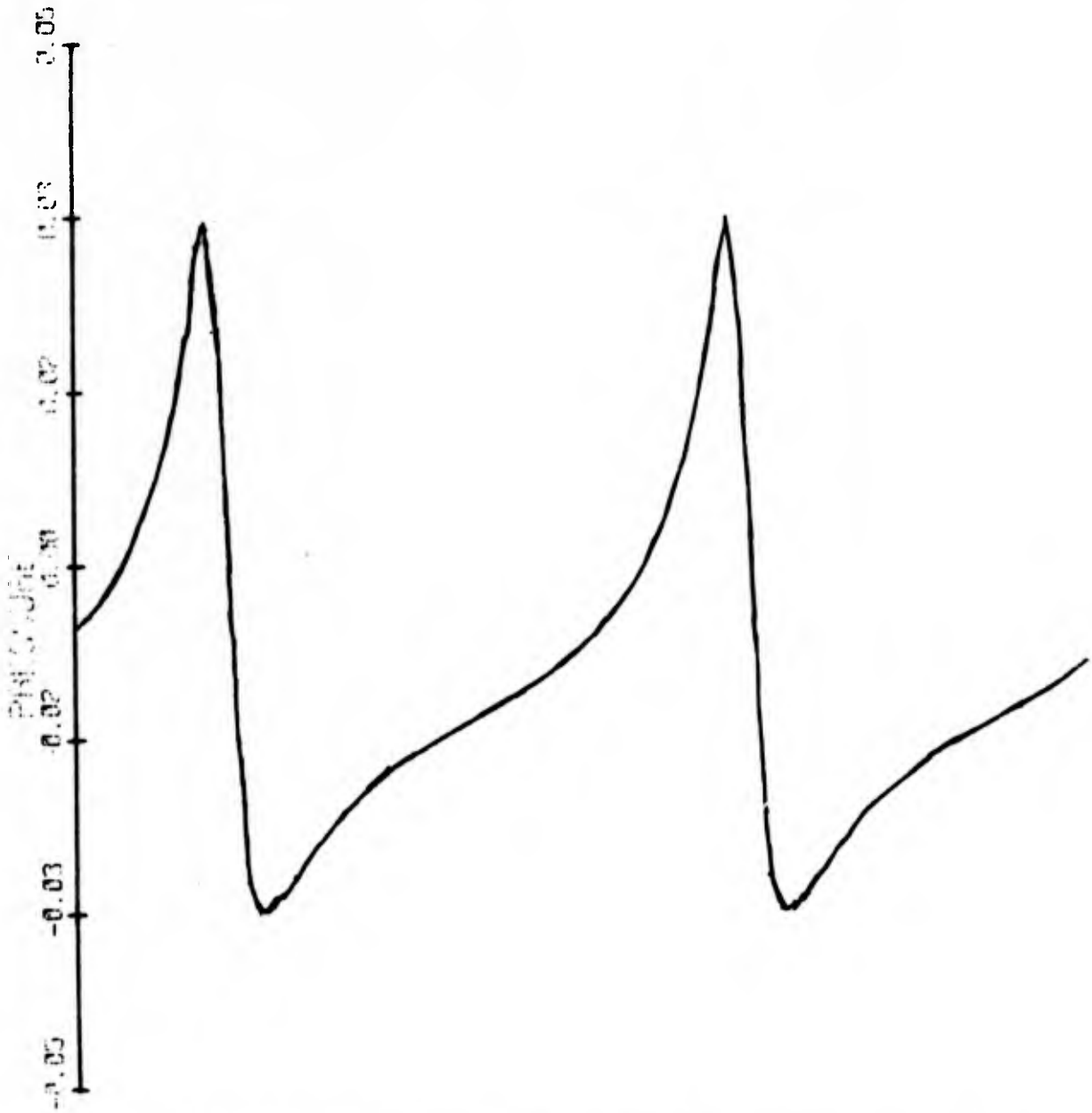

Fig. 58. Pressure time history of predicted rotational noise for a UH-1D rotor system, Γ_o=225 ft^2/sec. (Ref. 34)

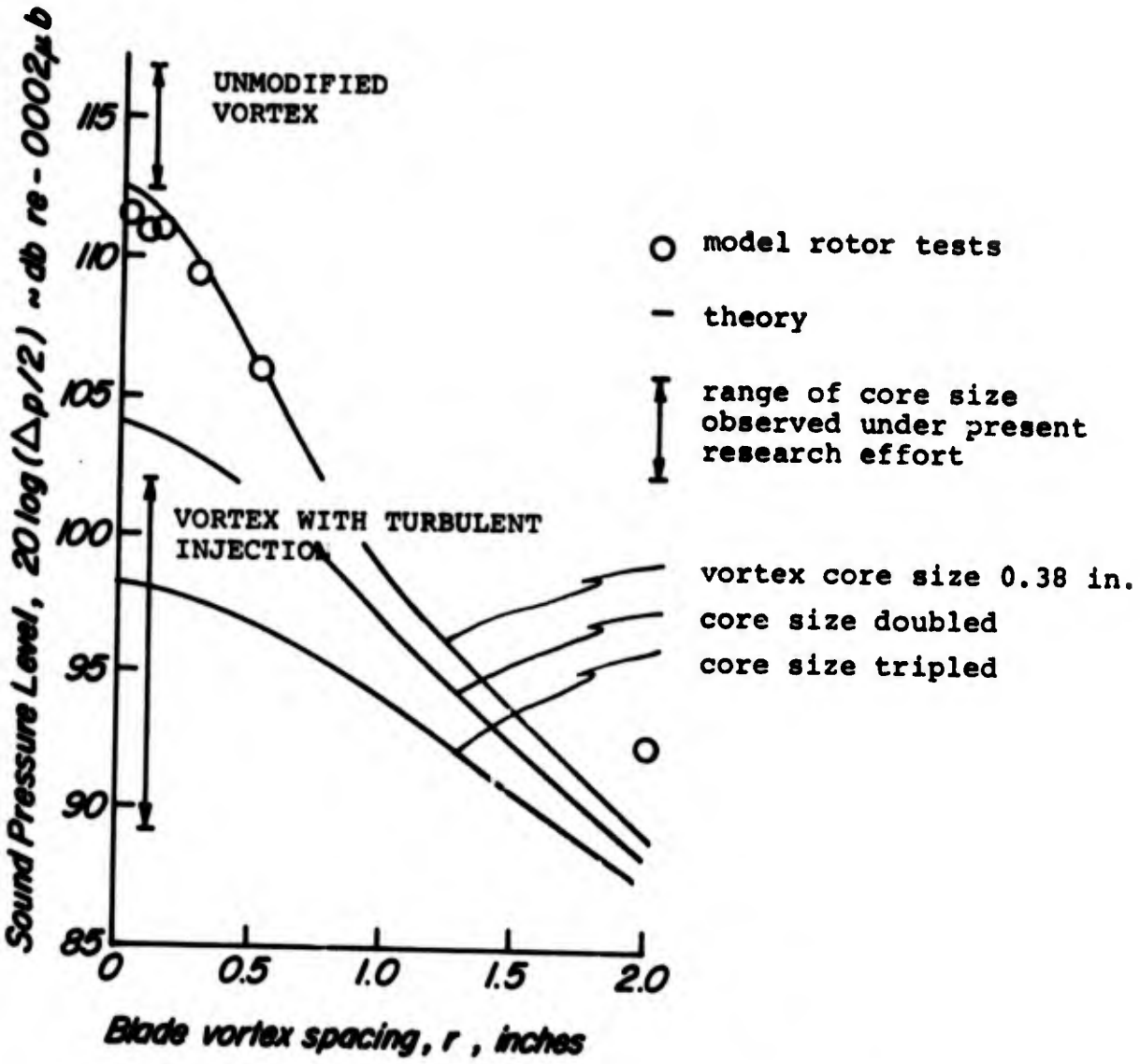

Fig. 59. Effect of tip vortex core size on helicopter noise due to blade/vortex interaction (from Ref. 35)

APPENDIX

Coordinate Transformation from Hot-Wire Coordinate System to Wind Tunnel Coordinate System

The velocity in a coordinate system oriented normal to the hot-wire elements in the x", y", z" direction can be related to linearized signal from the x, y, and z linearizers according to the relationship

$$v_x" = C_1 V_{x_2}$$

$$v_y" = C_2 V_{y_2}$$

$$v_z" = C_z V_{z_2}$$

In order to facilitate the transform process, the signals were matched for equal sensitivity so that

$$C_1 = C_2 = C_3 = C$$

The velocity in a coordinate system oriented along the hot-wire elements in the x', y', z' direction is given by the relationship

$$v_x' = [1/2\ (v_y"^2 + v_z"^2 - v_x"^2)]^{1/2}$$

$$v_y' = [1/2\ (v_x"^2 + v_z"^2 - v_y"^2)]^{1/2}$$

$$v_z' = [1/2\ (v_x"^2 + v_y"^2 - v_z"^2)]^{1/2}$$

The velocity in a coordinate system oriented along the hot-wire elements in the wind tunnel x, y, z coordinate direction is summarized as

$$v_x = -(1/2)^{1/2} v_x' + (1/2)^{1/2} v'_y$$

$$v_y = -(1/6)^{1/2} v_x' - (1/6)^{1/2} v_y' + (6)^{1/2}/3\ v_z'$$

$$v_z = (1/3)^{1/2} v_x' + (1/3)^{1/2} v_y' + (1/3)^{1/2} v_z'$$